Part IV

ANNEX

A. Taula de Fotosensibilitzadors

Porficens

Nom	*Estructura molecular*	*Línia cel·lular*	*Mètode de detecció*	*Vehiculització*	*Localització*	*Predicció***	*ID*	*Referència*
9-capronyloxytetrakis(methoxy-ethyl)porphycene **CPO**	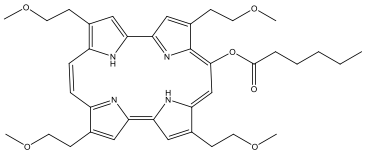	L1210	FRET	-	**RE**(MIT)	LIS	**S1**	235,342
		P388	FM	-	**MIT**			343
		L1210	FM	-	**RE**			344
		HaCaT SCL1	FM	-	**LIS**			345
		SCL2	FM	-	**LIS**			345
		1c1c7	FM	-	**MIT**			346
tetra-*n*-propylporphycene **TPrPo**	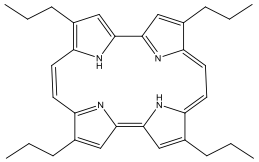	SSK2	FC	DPPC DOPC	**MEM**	OTH	**S2**	167
hydroxyethyl-tri(propyl)porphycene	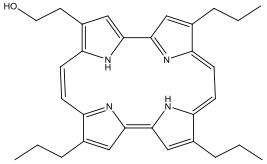	SSK2	FC	DPPC DOPC	**MEM**	OTH	**S3**	167
9-acetoxy tetra-*n*-propyl porphycene **9-ATPrPo**	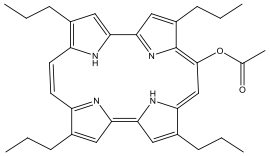	SSK2	FC	DPPC DOPC	**MEM**	OTH	**S4**	167
9-acetoxy-2,7,12,17-tetra(β-methoxyethyl)-porphycene **ATMPo**	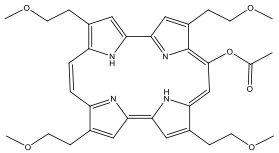	HaCaT	FM	-	**LIS** (MIT)	LIS	**S5**	347
		SCL1 SCL2	FM	-	**LIS** (MIT)			347
		N1	FM	-	**LIS** (MIT)			347
		HaCaT	CLSM	-	MIT			307

Nom	*Estructura molecular*	*Línia cel·lular*	*Mètode de detecció*	*Vehiculització*	*Localització*	*Predicció***	*ID*	*Referència*
2^3-carboxy-2^4-(methoxycarbonyl)benzo[2,3]-7,12,17-tris(methoxyethyl)porphycene	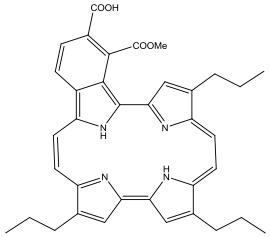	SSK2	FC	DPPC DOPC	**MEM**	OTH	**S6**	167
Tetraphenylporphycene **TPPo**	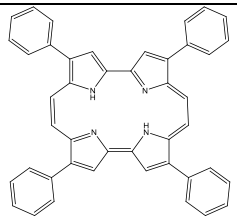	HeLa A-549	FM	DPPC	**LIS**	LIS	**S7**	118, 348
		HeLa	FM	DPPC	**LIS**, MC			349
9-hexyl-2,7,12,17-tetra(methoxyethyl)porphycene **HTMPo**	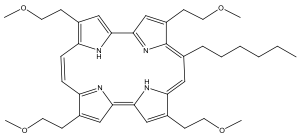	HaCaTSCL1 SCL2	FM	-	**LIS**	MIT	**S8**	345
9-nonaoyloxy-2,7,12,17-tetra(methoxyethyl)porphycene **NTMPo**	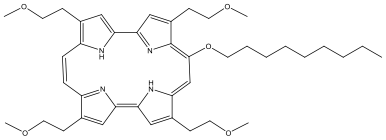	HaCaTSCL1 SCL2	FM	-	**LIS**	LIS	**S9**	345
3-sulfonamide-N-methyl-1,6-hexyl-N'-trimethyl-ammonium-2,7,12,17-tetra-*n*-propylporphycene **PS6A**	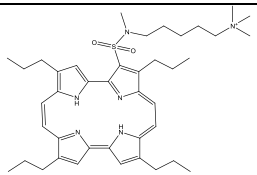	NPC/CNE-2	CM	-	**MIT**	LIS	**S10**	342
3-sulfonamide-N-methyl-1,6-hexyl-N'methylamine-2,7,12,17-tetra-*n*-propylporphycene **PS6**	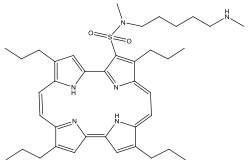	NPC/CNE-2	CM	-	**DIF**	MIT	**S11**	342

Nom	*Estructura molecular*	*Línia cel·lular*	*Mètode de detecció*	*Vehiculització*	*Localització*	*Predicció***	*ID*	*Referència*
N,N'-methylene-4-morpholine-2,7,12,17-tetra-*n*-propylporphycene **PcM**	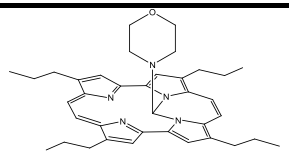	P388	FM	-	**MIT**	MIT	**S12**	350
N,N'-methylene-1,4-piperazine-bis-(2,7,12,17-tetra-*n*-propylporphycene) **PcD**	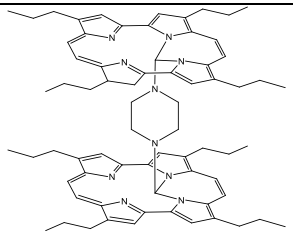	P388	FM	-	**MIT**	MIT	**S13**	350

Porfirines

Nom	*Estructura molecular*	*Línia cel·lular*	*Mètode de detecció*	*Vehiculització*	*Localització*	*Predicció***	*ID*	*Referència*
Hematoporphyrin **Hp**	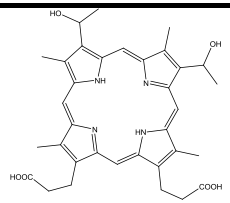	C_6	CLSM	-	**DIF**, LIS	LIS	**S14**	195
		V79	CLSM	-	**DIF**, LIS			195
		MGH-Ul	FM	-	**DIF**			351
Hematoporphyrin Derivative **HpD**	*estructura desconeguda*	V79	SF	-	**MIT** (LIS)	*indefinit*	**S15**	233
		L-cells	SSE	-	**LIS**			233
		RB230AC	SSE	-	**RE** (MIT)			233
Polyhematoporphyrin **PHp**	*estructura desconeguda*	RIF-1	FM	-	**DIF**	*indefinit*	**S16**	290
$3^1,8^1$-bis[3-amino-3-carboxypropylthio]mesoporphyrin	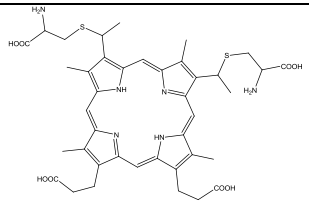	C_6	CLSM	-	**DIF**	OTH	**S17**	293
13,17-bis[3-(2-(dimethylamino)ethylamino)-3-oxopropyl]-2,7,12,18-tetramethyl-3,8-divinylporphyrin	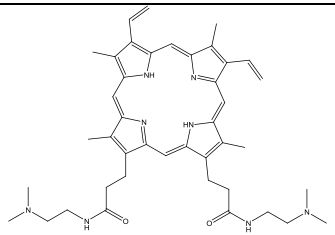	C_6	CLSM	-	**MIT**	MIT	**S18**	195, 293
		V79	CLSM	-	**MIT**			195

Nom	*Estructura molecular*	*Línia cel·lular*	*Mètode de detecció*	*Vehiculització*	*Localització*	*Predicció***	*ID*	*Referència*
13,17-bis[3-(2-(diethylamino)ethylamino)-3-oxopropyl]-2,7,12,18-tetramethyl-3,8-divinylporphyrin	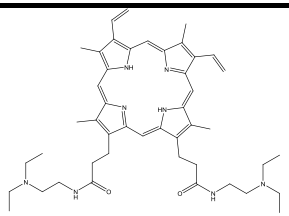	C_6	CLSM	-	**MIT**	MIT	**S19**	293
Protoporphyrin IX **PPIX**	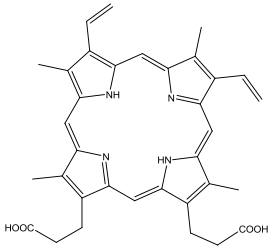	Gf	SF	-	**MIT**	OTH	**S20**	233
		NCTC 2544	FM	-	**MEM, LIS,** MC			352
		B16	FTMS	-	**MIT**, **RE**, MC			353
		RIF-1	FM	- MePEG500 PCL4100	**MC**			354
Hematoporphyrin diethylether	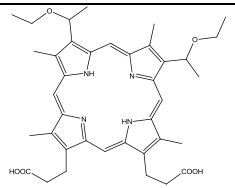	C_6	CLSM	-	**DIF**	OTH	**S21**	293
3,8-bis[2-ethoxyethyl]-13,17-bis[3-(2-(diethylamino)ethylamino)-3-oxopropyl]-2,7,12,18-tetramethylporphyrin	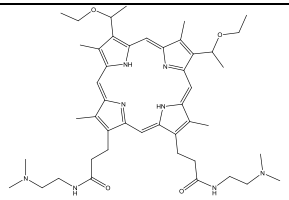	C_6	CLSM	-	**MIT**	MIT	**S22**	293

Nom	*Estructura molecular*	*Línia cel·lular*	*Mètode de detecció*	*Vehiculització*	*Localització*	*Predicció***	*ID*	*Referència*
$3^1,8^1$-bis(2-morpholinoethylthio)mesoporphyrin	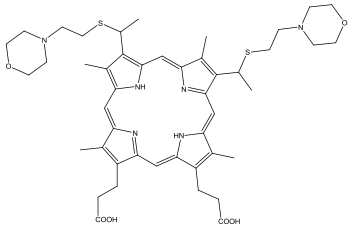	C_6	CLSM	-	**CIT**(LIS)	LIS	**S23**	293
		POVD	N.D.	-	**LIS**			128
13,17-bis[3-(2-(dimethylamino)ethylamino)-3-oxopropyl]-2,8,12,18-tetramethyl-3,7-bis[1-(2-morpholinoethylthio)ethyl]porphyrin	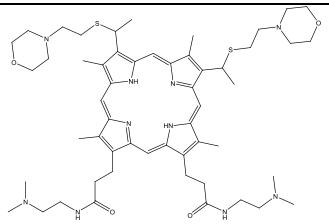	C_6	CLSM	-	**MIT**(LIS)	MIT	**S24**	293
		POVD	N.D.	-	**CIT**			128
$3^1,8^1$-bis(carboxymethylthio)mesoporphyrin	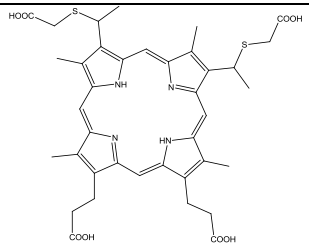	C_6	CLSM	-	**DIF**	OTH	**S25**	293
3,8-bis[1-(3-(2-(dimethylamino)ethylamino)-3-oxopropylthio)ethyl]-13,17-bis[3-(2-(dimethylamino)ethylamino)-3-oxopropyl]-2,7,12,18-tetramethylporphyrin	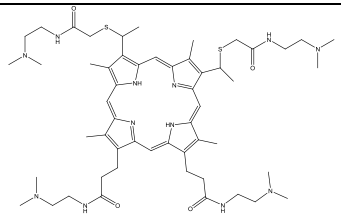	C_6	CLSM	-	**MIT**	MIT	**S26**	195
		V79	CLSM	-	**MIT**			195

Nom	*Estructura molecular*	*Línia cel·lular*	*Mètode de detecció*	*Vehiculització*	*Localització*	*Predicció***	*ID*	*Referència*
3,8-bis[2-pentyloxyethyl]-13,17-bis[3-(2-(diethylamino)ethylamino)-3-oxopropyl]-2,7,12,18-tetramethylporphyrin	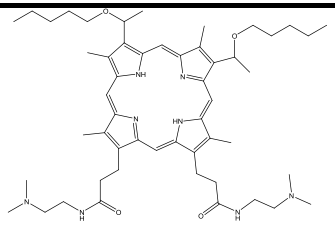	C_6	CLSM	-	**LIS**	MIT	**S27**	293
$3^1,8^1$-dimethoxymesoporphyrin dimethylester	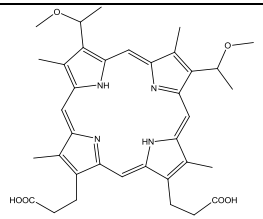	C_6	CLSM	-	**DIF**, LIS	MIT	**S28**	195
		V79	CLSM	-	**DIF**, LIS			195
$3^1,8^1$-(2-ethoxyethoxy)mesoporphyrin	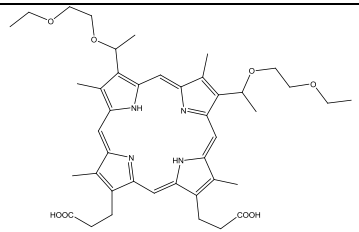	C_6	CLSM	-	**DIF**	OTH	**S29**	195
		V79	CLSM	-	**DIF**			195
3,8-bis[1-(ethoxyethoxy)ethyl]-13,17-bis[3-(2-(dimethylamino)ethylamino)-3-oxopropyl]-2,7,12,18-tetramethylporphyrin	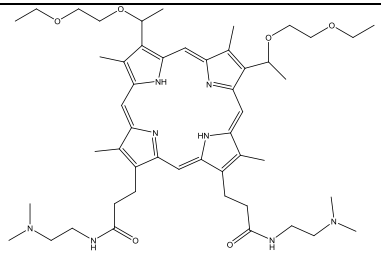	C_6	CLSM	-	**MIT**(LIS)	MIT	**S30**	195
		V79	CLSM	-	**MIT**			195

Nom	*Estructura molecular*	*Línia cel·lular*	*Mètode de detecció*	*Vehiculització*	*Localització*	*Predicció***	*ID*	*Referència*
$3^1,8^1$-bis(2-nitrosoethylthio)-mesoporphyrin	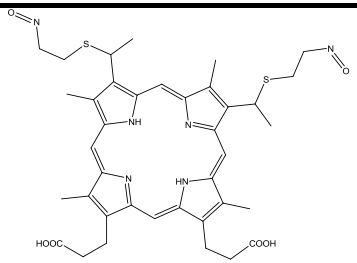	C_6	CLSM	-	**CIT**	MIT	**S31**	195
		V79	CLSM	-	**CIT**			195
3,8-bis[1-(2-nitrosoethylthio)ethyl]-13,17-bis[3-(2-(dimethylamino)ethylamino)-3-oxopropyl]-2,7,12,18-tetramethylporphyrin	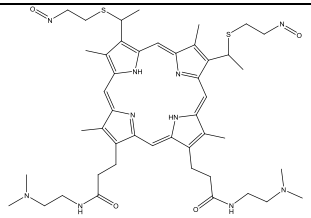	C_6	CLSM	-	**MIT**	MIT	**S32**	195
		V79	CLSM	-	**MIT**			195
2,4-(α,β-dihydroxyethyl)deuteroporphyrin IX tetrakiscarborane carboxylate ester **BOPP**	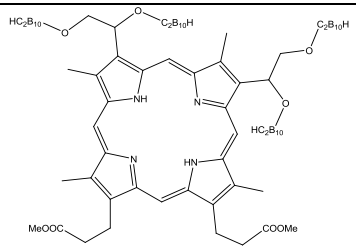	C6	CLSM	-	**MIT**	MIT	**S33**	355
5,10,15,20-tetrakis(1-decylpyridinium-4-yl)-21H.23H-porphine tetra-bromide	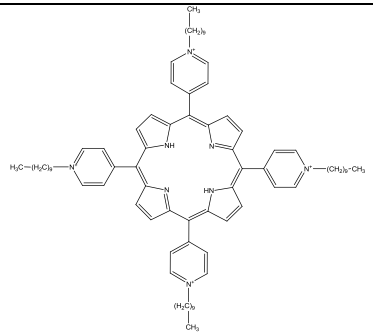	HeLa	EM	-	**MIT**	MIT	**S34**	356

Nom	*Estructura molecular*	*Línia cel·lular*	*Mètode de detecció*	*Vehiculització*	*Localització*	*Predicció***	*ID*	*Referència*
meso-tetra(4-*N*-methylpyridyl)porphyrin **TMPyP**	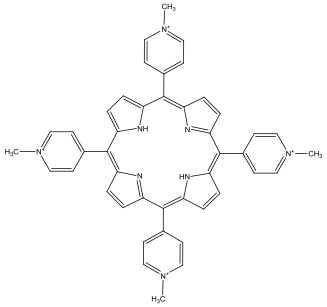	HeLa	EM	-	**MC**	OTH	**S35**	356
		HeLa Murine carcinoma	FM	-	**LIS**			357, 358
		HeLa D532 H2T	FM	-	**NUC**			291, 359, 360, 361, 313
		HeLa	FM	-	**LIS**			358
meso-tetra(1-sulfopyridinum-4-yl)porphyrin **TPPS**	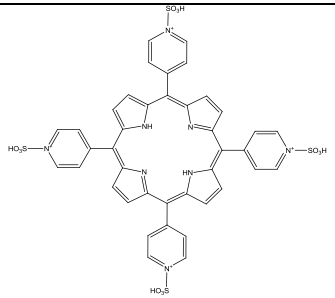	HeLa	EM	-	**DIF**	OTH	**S36**	356
Tetraphenyl([4-aminobutyl]7-chloroquinoline) propioamidoporphyrin **TPPQ**	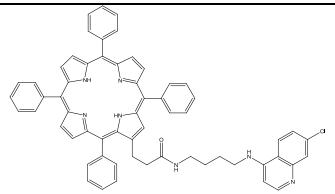	Human fibroblasts	FM	LDL	**LIS**	LIS	**S37**	362

Nom	*Estructura molecular*	*Línia cel·lular*	*Mètode de detecció*	*Vehiculització*	*Localització*	*Predicció***	*ID*	*Referència*
3,1-*meso*-tetrakis(*o*-propionamidophenyl)porphyrin **3,1-Tpro**	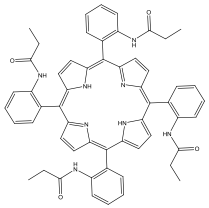	R3230AC	ENZ	Cremophor EL	**MIT**	MIT	**S38**	291, 363
meso-tetra-hexylpyridyl porphyrin	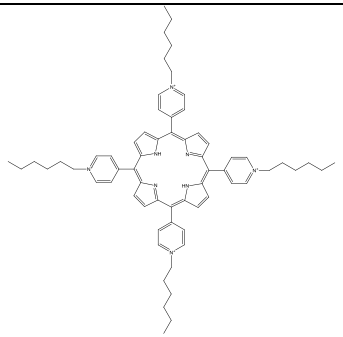	D532	MSF	-	**CIT**, LIS	MIT	**S39**	291, 360
$3^1,8^1$-bis[2-(dimethylamino)ethoxy]mesoprophyrin	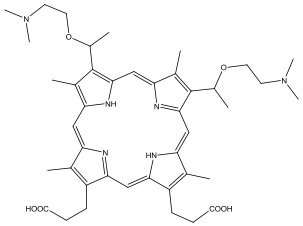	C_6	CLSM	-	**CIT**	MIT	**S40**	195
		V79	CLSM	-	**CIT**			195
Uroporphyrin I **Uro**	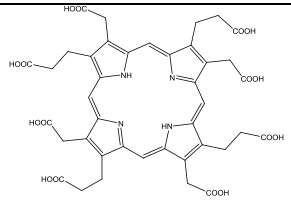	Hex	SF	-	**LIS**	OTH	**S41**	233

Nom	*Estructura molecular*	*Línia cel·lular*	*Mètode de detecció*	*Vehiculització*	*Localització*	*Predicció***	*ID*	*Referència*
Mococationic porphyrin **MCP**	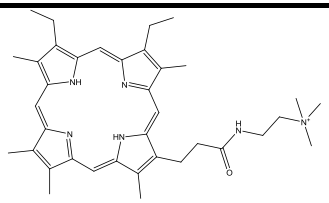	L1210	FM	-	**MEM** (CIT)	MIT	**S42**	350, 364, 365
		P388	FM		**MEM**			350, 364
		RIF	FM		**MEM**			317
meso-tetra(3-hydroxyphenyl)porphyrin **3-THPP**	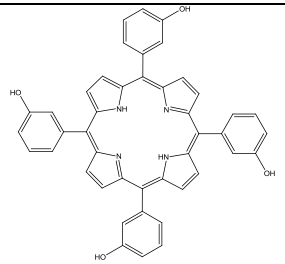	V79	FM	-	**LIS**	OTH	**S43**	366
Diphenyl-di(4-sulfonatophenyl)porphine **TPPS$_{2a}$**	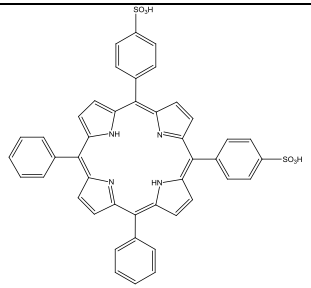	V79	SF FM	-	**LIS**	OTH	**S44**	366
		NHIK 3025	EM	-	**LIS**(CIT)			308
meso-tetra(4-sulfonatophenyl)porphine **TPPS$_4$**	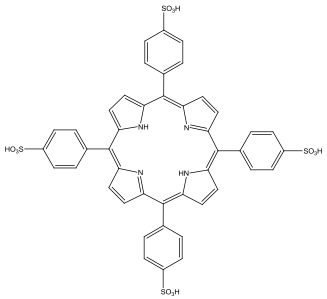	NHIK 3025	FM	-	**LIS**(NUC)	OTH	**S45**	308
		NHIK 3025	EM	-	**NUC**			233
		V79	SF FM	-	**CIT**			366
		CT26	SRI FM	-	**LIS**			367

Nom	*Estructura molecular*	*Línia cel·lular*	*Mètode de detecció*	*Vehiculització*	*Localització*	*Predicció***	*ID*	*Referència*
Triphenyl-mono(4-sulfonatophenyl)porphine **TPPS$_1$**	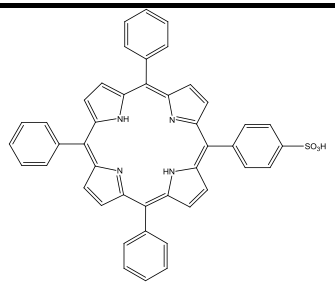	CT26	SRI FM	-	**AG**	LIS	**S46**	367
		NHIK (3025)	FM	-	**DIF**			252, 308
		NHIK (3025)	EM	-	**DIF**			233
20-(2-carboxyethoxy)-5,10,15-triphenyl-21,23-dithiaporphyrin	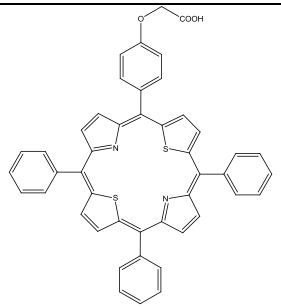	R3230AC	CLSM	-	**DIF**(MIT)	OTH	**S47**	179
5,20-(2-carboxyethoxy)-10,15-triphenyl-21,23-dithiaporphyrin	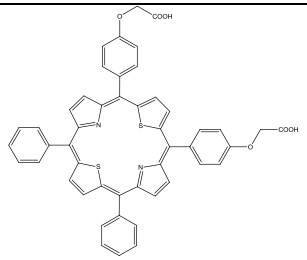	R3230AC	CLSM	-	**MIT**	OTH	**S48**	179
5-(4-PEGphenyl)-10,15,20-triphenylporphyrin	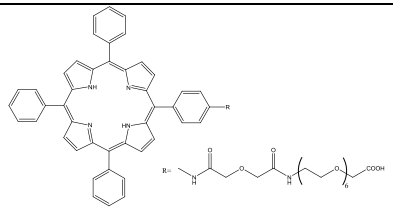	HEp2	FM	-	**RE, MIT**	MIT	**S49**	177

Nom	*Estructura molecular*	*Línia cel·lular*	*Mètode de detecció*	*Vehiculització*	*Localització*	*Predicció***	*ID*	*Referència*
5,10-di(4-PEGphenyl)-15,20-triphenylporphyrin	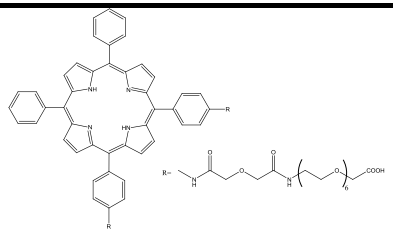	HEp2	FM	-	**RE, MIT**	LIS	**S50**	177
5,10,15-tri(4-PEGphenyl)-20-triphenylporphyrin	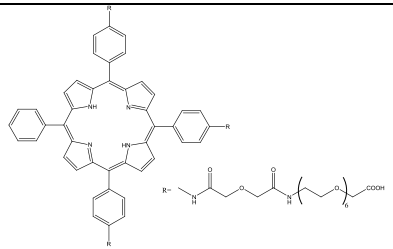	HEp2	FM	-	**LIS**	LIS	**S51**	177
5,10,15,20-tetra(4-PEGphenyl) porphyrin	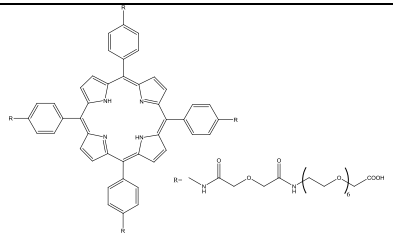	HEp2	FM	-	**LIS**	LIS	**S52**	177
Benzoporphyrin derivative monoacid **BPD**	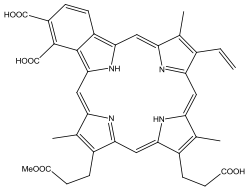	L1210	N.D.	-	**MIT**, RE	MIT	**S53**	235

Nom	*Estructura molecular*	*Línia cel·lular*	*Mètode de detecció*	*Vehiculització*	*Localització*	*Predicció***	*ID*	*Referència*
Benzoporphyrin derivative monoacid ring A **BPD-MA**	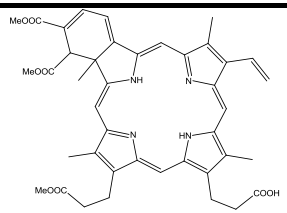	NHIK 3025	N.D.	-	**CIT**	MIT	**S54**	234, 252
Lutetium texaphyrin **Lutex**	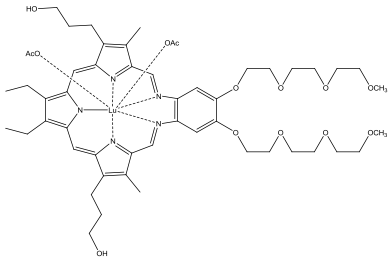	L1210			**LIS**			235
		EMT6	CLSM	-	**LIS**			368
		1c1c7	FM	-	**LIS**	OTH	**S55**	346
		HaCaT	FM	DPPC	**LIS**			346

Ftalocianines

Nom	*Estructura molecular*	*Línia cel·lular*	*Mètode de detecció*	*Vehiculització*	*Localització*	*Predicció***	*ID*	*Referència*
Aluminium phthalocyanine tetrasulfonate **$AlPcS_4$**	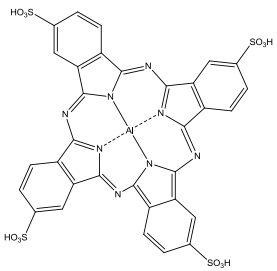	NHIK (3025)	FM	-	**LIS**, MEM	LIS	**S56**	252, 371, 369
		V79	FM	-	**LIS**, MEM			252, 305, 369
		LOX	CLSM	-	**LIS**			291
		KB	FM		**LIS**			136
		KB	FM	POPC	**LIS**			136
		KB	FM	DPPIsC	**LIS**, **CIT**			136
		RR 1022	CLSM	PBS	**MEM**			370
Aluminum phthalocyanine trisulfonate **$AlPcS_3$**	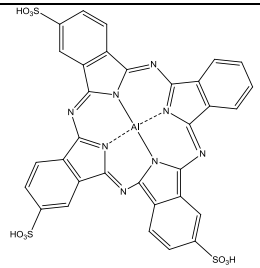	LOX	CLSM	-	**LIS**	LIS	**S57**	291
		KB	FM	-	**LIS**			136
Aluminum phthalocyanine disulfonate **$AlPcS_2$**	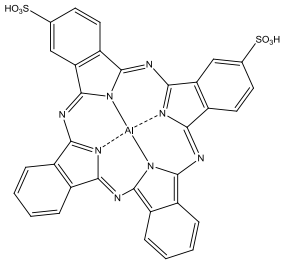	NHIK (3025)	FM	-	**LIS**, MEM	LIS	**S58**	371
		V79	FM	-	**LIS**, MEM			371
		LOX	CLSM	-	**DIF**, LIS			371
		KB	FM	-	**MC**			136

Nom	*Estructura molecular*	*Línia cel·lular*	*Mètode de detecció*	*Vehiculització*	*Localització*	*Predicció***	*ID*	*Referència*
Chloroaluminium phthalocyanine disulfonate **$AlPcS_{2b}$**	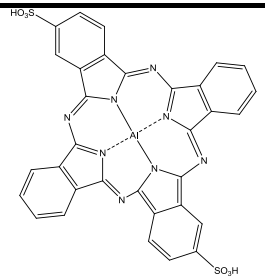	KB	FM	-	**MC**	OTH	**S59**	136
Aluminum phthalocyanine monosulphonate **$AlPcS_1$**	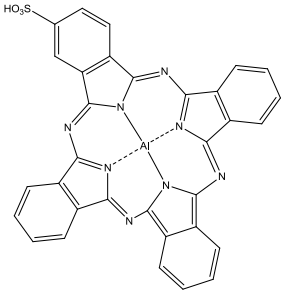	NHIK (3025)	FM	-	**CIT**	OTH	**S60**	371
		V79	FM	-	**CIT**			371
		LOX	CLSM	-	**CIT**			291
		KB	FM	-	**MC**			136
Zinc(II) phthalocyanine **ZnPc**	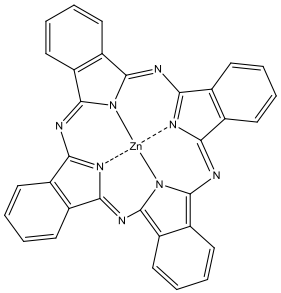	4R	FM	-	**AG**(MIT)	MIT	**S61**	372
		Pam212	FM	DPPC	**MIT**			373
		A-549	FM	DPPC	**AG**			118, 331, 374
		MS-2		DPPC	**AG**			291
		p 53-deficient HeLa	FM	DPPC	**AG**			375
		HeLa	FM	DPPC	**AG**			376

Nom	*Estructura molecular*	*Línia cel·lular*	*Mètode de detecció*	*Vehiculització*	*Localització*	*Predicció***	*ID*	*Referència*
Phthalocynine Pc4 **Pc4**	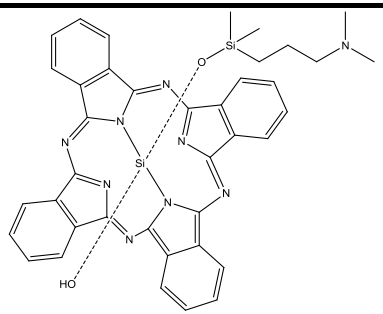	L1210			**MIT**, **RE**	MIT	**S62**	235
		L5178Y-R	CLSM	-	**MIT, AG,** LIS (LIS)			377
		PC-3	CLSM	-	**MIT**			378
		A431	CLSM	-	**MIT**, RE, AG			379
Pyridinium zinc [II] phtalocyanine **Zn-PPC**	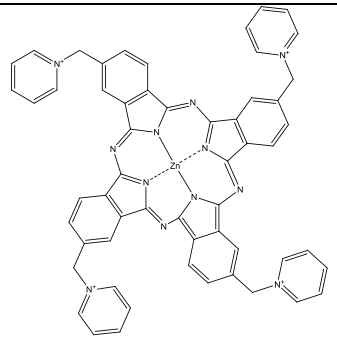	RIF-1	FM	-	**LIS**	LIS	**S63**	290
		RIF-1	FM	-	**LIS**(NUC)			380
Tetraglycine zinc [II] phtalocyanine **TGly**	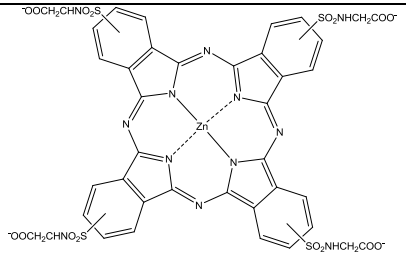	RIF-1	FM	-	**LIS**	LIS	**S64**	290

Nom	*Estructura molecular*	*Línia cel·lular*	*Mètode de detecció*	*Vehiculització*	*Localització*	*Predicció***	*ID*	*Referència*
Tetradioctylamine zinc [II] phthalocyanine **TDOPc**	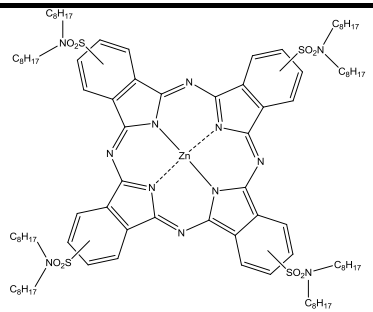	RIF-1	FM	-	**LIS**	LIS	**S65**	290
Ethynyl-trisulfonated zinc phthalocyanine **$ZnPcS_3C_2$**	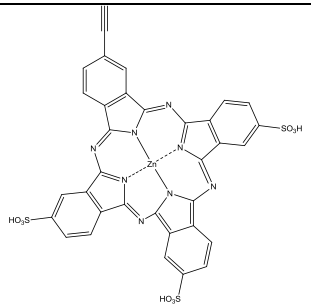	EMT-6	CLSM	-	**MC**	MIT	**S66**	381
Hexynyl-trisulfonated zinc phthalocyanine **$ZnPcS_3C_6$**	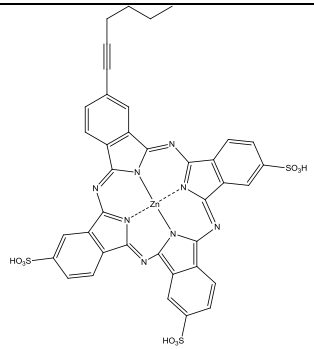	EMT-6	CLSM	-	**MIT**	MIT	**S67**	381

Nom	*Estructura molecular*	*Línia cel·lular*	*Mètode de detecció*	*Vehiculització*	*Localització*	*Predicció***	*ID*	*Referència*
Nonynyl-trisulfonated zinc phthalocyanine **$ZnPcS_3C_9$**	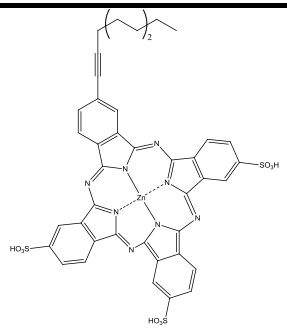	EMT-6	CLSM	-	**MIT**	MIT	**S68**	381
Dodecynyl-trisulfonated zinc phthalocyanine **$ZnPcS_3C_{12}$**	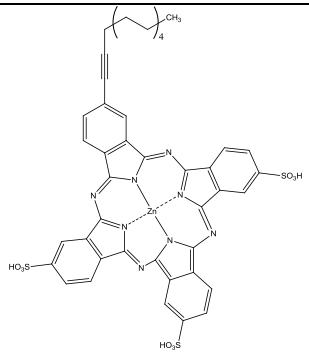	EMT-6	CLSM	-	**MC**	MIT	**S69**	381
Hexadecynyl-trisulfonated zinc phthalocyanine **$ZnPcS_3C_{16}$**	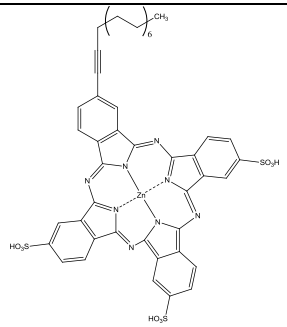	EMT-6	CLSM	-	**MIT**	LIS	**S70**	381

Nom	*Estructura molecular*	*Línia cel·lular*	*Mètode de detecció*	*Vehiculització*	*Localització*	*Predicció***	*ID*	*Referència*
Trisulfonated zinc phthalocyanine **$ZnPcS_3$**	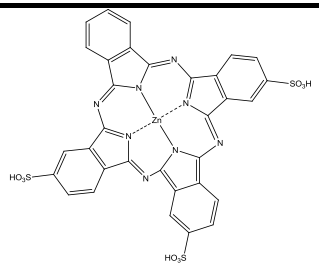	EMT-6	CLSM	-	**MIT**	MIT	**S71**	381
Zinc 2,10,16,24-tetra(trimethylammonio)phthalocyanine **ZnPcA1**	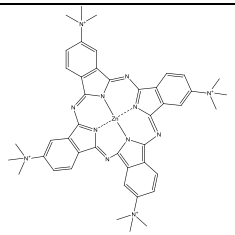	HeLa	FM EM	-	**MIT**	MIT	**S72**	320
Zinc 2,10,16,24-tetra(hexyldimethylammonio)phthalocyanine **ZnPcA6**	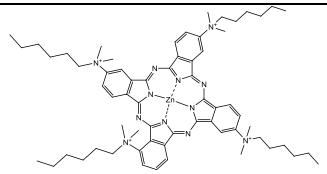	HeLa	FM EM	-	**MIT**	MIT	**S73**	320
Zinc 2,10,16,24-tetra[(trimethylammonio)methoxy]phthalocyanine **ZnPcE1**	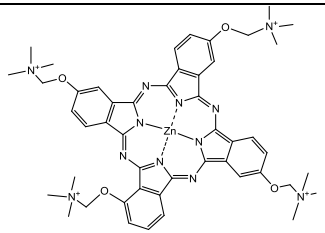	HeLa	FM EM	-	**MIT**	MIT	**S74**	320

Nom	*Estructura molecular*	*Línia cel·lular*	*Mètode de detecció*	*Vehiculització*	*Localització*	*Predicció***	*ID*	*Referència*
Zinc 2,10,16,24-tetra[3-(hexyldimethylammonio)propoxy]phthalocyanine **ZnPcE6**	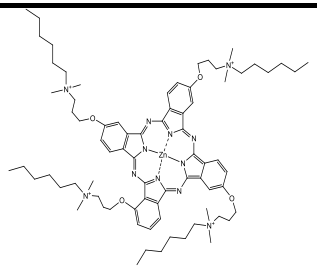	HeLa	FM EM	-	**MIT**	MIT	**S75**	320
2,10,16,24-tetrasulfonatephthalocyanine **TSPC**	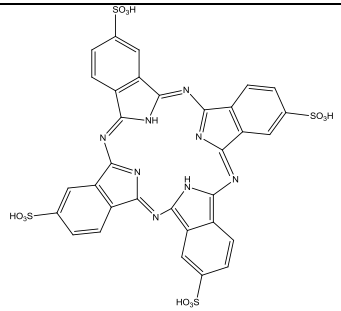	RIF-1	FM	-	**LIS**(NUC)	MIT	**S76**	380
meso-tetra(N,N-bis(2-hydroxyethyl)sulfamoyl)phthalocyanine **TDEPC**	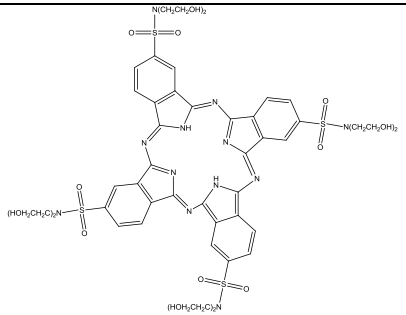	RIF-1	FM	-	**AG**, CIT	OTH	**S77**	380

Clorines

Nom	*Estructura molecular*	*Línia cel·lular*	*Mètode de detecció*	*Vehiculització*	*Localització*	*Predicció***	*ID*	*Referència*
Etiobenzochlorin monosulfonate **EBCS**	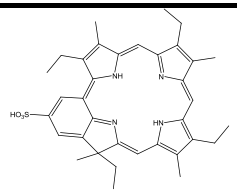	L1210	FM	-	**MEM**	OTH	**S78**	382
Etiobenzochlorin **EBC**	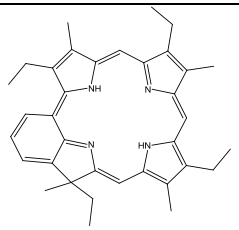	L1210	FM	-	**LIS**	MIT	**S79**	382
Tin etiobenzochlorin monosulfonate **SnEBCS**	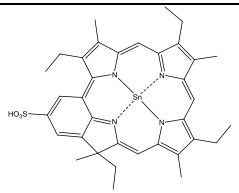	L1210	FM	-	**MEM**	OTH	**S80**	382
Tin etiobenzochlorin **SnEBC**	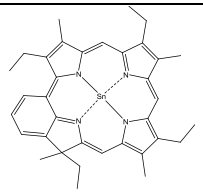	L1210	FM	-	**LIS**	MIT	**S81**	382

Nom	*Estructura molecular*	*Línia cel·lular*	*Mètode de detecció*	*Vehiculització*	*Localització*	*Predicció***	*ID*	*Referència*
Mono-*L*-aspartyl chlorin **NPe6**	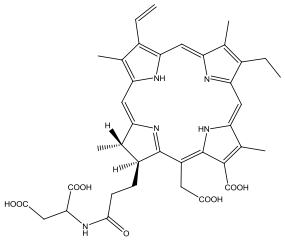	L1210 CHO-K1	FM	-	**LIS**	LIS	**S82**	344, 383
		1c1c7	FM	-	**LIS**			346
Ethylene diamine chlorin e_6 **EDA-e_6**	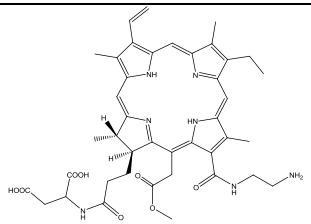	HeLa	SFM	-	**MEM**	OTH	**S83**	384
LISyl Chlorin p6 **LCP**	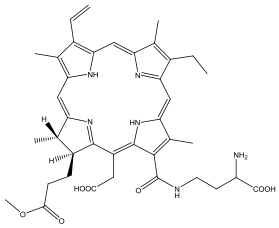	1c1c7	FM	-	**LIS**	MIT	**S84**	346
		P388	FM	-	**LIS**			350
		L1210	FM	-	**LIS**			330
		9L	FM	-	**MIT, AG, RE** (CIT)			392
Lysyl Chlorin p6 triester **LCP2**	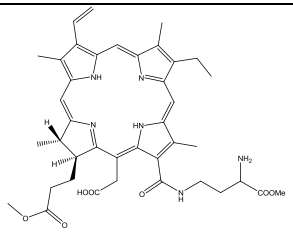	L1210	FM	-	**LIS**	MIT	**S85**	330

Nom	*Estructura molecular*	*Línia cel·lular*	*Mètode de detecció*	*Vehiculització*	*Localització*	*Predicció***	*ID*	*Referència*
5,10,15,20-tetra(m-hydroxyphenil)chlorin **m-THPC** (foscan)	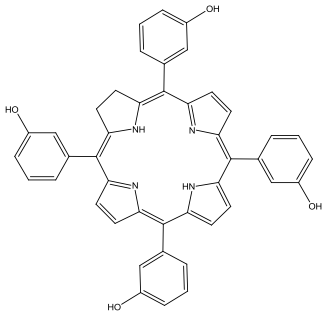	L1210	FM	-	**RE**	OTH	**S86**	235, 385
		HT29	FM	PBS	**MC**			387
		NPC/HK1 NPC/CNE2	CLSM	DMF	**MIT**			386
		P388			**MIT**			343
		M1	CLSM	-	**MIT**			388
		JCS	CLSM	-	**MIT**			388
		Colo 201	CLSM	-	**LIS**			389
		RIF-1	FM	-	**DIF**			290
		HT29	FM	-	**DIF**			387
		MCF-7	CLSM	-	**RE**, **AG**			390
Lysyl chlorin imide **LCI**	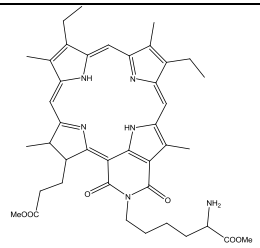	L1210	FM	-	**MIT**, MC	MIT	**S87**	330
Dicationic ketochlorin **DCKC**	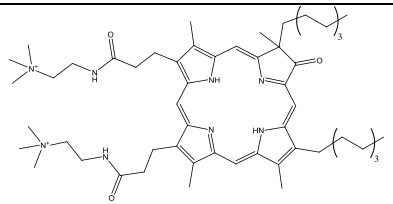	P388	FM	-	**MEM**	OTH	**S88**	364

Nom	*Estructura molecular*	*Línia cel·lular*	*Mètode de detecció*	*Vehiculització*	*Localització*	*Predicció***	*ID*	*Referència*
Chlorin e_6 **Ce_6**	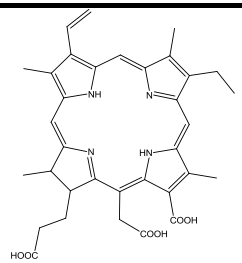	MGH-U1	CLSM		**MEM**, **MIT, NUC**	OTH	**S89**	391
Chlorin e_6 polystyrene	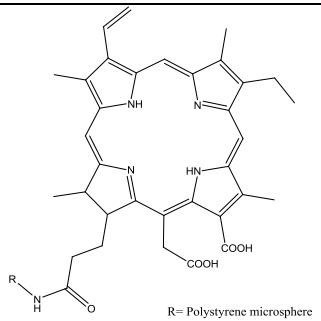	MGH-U1	CLSM	Polystyrene microspheres	**LYS**	MIT	**S90**	391
Benzobacteriochlorin_16	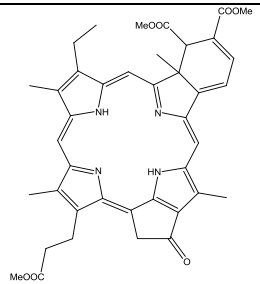	*RIF* C3H/HeJ	FM	-	**MIT**	MIT	**S91**	173
Benzobacteriochlorin_17	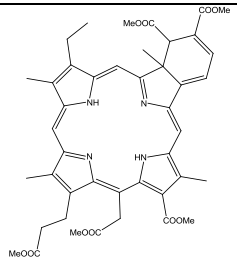	*RIF* C3H/HeJ	FM	-	**MIT**	MIT	**S92**	173

Nom	*Estructura molecular*	*Línia cel·lular*	*Mètode de detecció*	*Vehiculització*	*Localització*	*Predicció***	*ID*	*Referència*
Benzobacteriochlorin_18	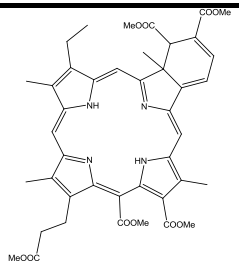	*RIF* C3H/HeJ	FM	-	**MIT**	MIT	**S93**	173
Benzobacteriochlorin_19	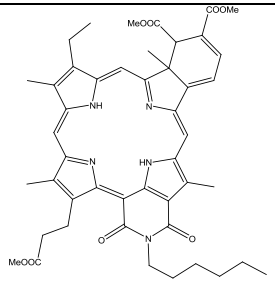	*RIF* C3H/HeJ	FM	-	**MIT**	MIT	**S94**	173
Benzobacteriochlorin_20	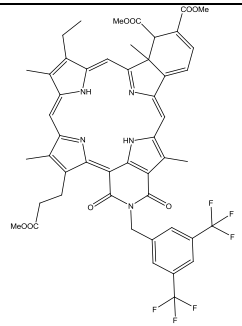	*RIF* C3H/HeJ	FM	-	**MIT**	MIT	**S95**	173

Purpurines

Nom	*Estructura molecular*	*Línia cel·lular*	*Mètode de detecció*	*Vehiculització*	*Localització*	*Predicció***	*ID*	*Referència*
Tin etiopurpurin **SnET2**	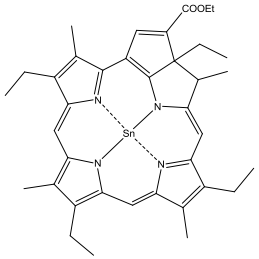	P388	FM	-	**MIT, LIS**	MIT	**S96**	350
		L1210	FM	-	**LIS**, **RE**			384
Tin octaethylpurpurin amadine **SnOPA**	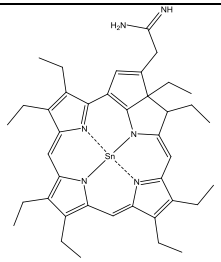	P388	FM	-	**CIT**, MEM, LIS, MIT	OTH	**S97**	237

Feofòrbids

Nom	*Estructura molecular*	*Línia cel·lular*	*Mètode de detecció*	*Vehiculització*	*Localització*	*Predicció***	*ID*	*Referència*
2-(1-hexyloxyethyl)-2-devinyl pyropheophorbide-a **HPPH**	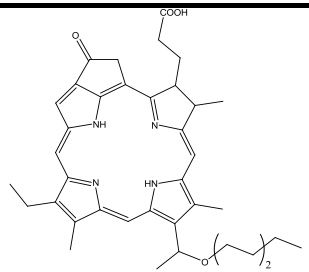	L1210			**RE**	OTH	**S98**	235
2-[1-propyloxyethyl]-2-devinylpyropheophorbide-a **Pyropheophorbide C3**	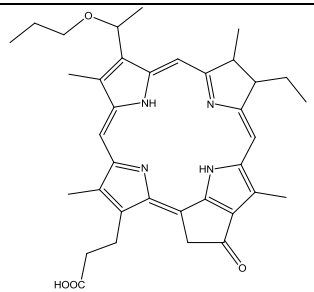	FaDu	FM	-	**MIT**	MIT	**S99**	305
2-[1-pentyloxyethyl]-2-devinylpyropheophorbide-a **Pyropheophorbide C5**	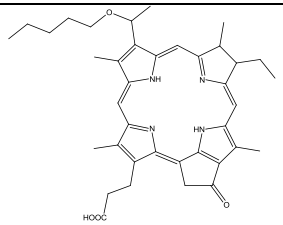	FaDu	FM	-	**MIT**	MIT	**S100**	305
2-[1-hexyloxyethyl]-2-devinylpyro-pheophorbide-a **Pyropheophorbide C6**	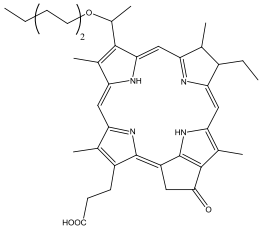	FaDu	FM	-	**MIT**	MIT	**S101**	305
		RIF	FM	-	**LIS**			305

Nom	*Estructura molecular*	*Línia cel·lular*	*Mètode de detecció*	*Vehiculització*	*Localització*	*Predicció***	*ID*	*Referència*
Aggregated 2-[1-hexyloxyethyl]-2-devinylpyropheophorbide-a **Pyropheophorbide C6**	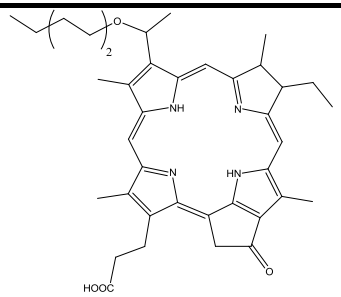	RIF	FM	-	**MIT**	*indefinit*	**S102**	305
2-[1-heptyloxyethyl]-2-devinylpyropheophorbide-a **Pyropheophorbide C7**	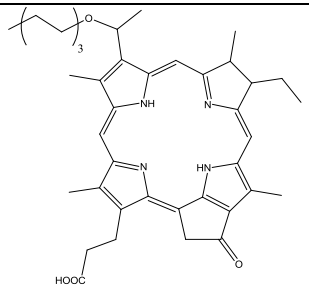	FaDu	FM	-	**MIT**	MIT	**S103**	305
2-[1-octyloxyethyl]-2-devinylpyropheophorbide-a **Pyropheophorbide C8**	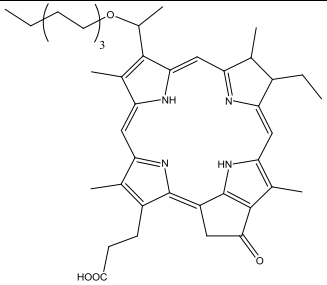	FaDu	FM	-	**LIS**	LIS	**S104**	305
Aggregated 2-[1-octyloxyethyl]-2-devinylpyropheophorbide-a **Pyropheophorbide C8**	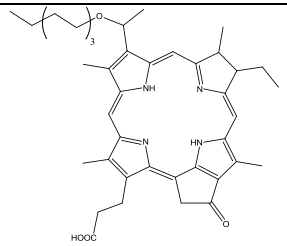	FaDu	FM	-	**MIT**	*indefinit*	**S105**	305

Nom	*Estructura molecular*	*Línia cel·lular*	*Mètode de detecció*	*Vehiculització*	*Localització*	*Predicció***	*ID*	*Referència*
2-[1-decyloxyethyl]-2-devinylpyropheophorbide-a **Pyropheophorbide C10**	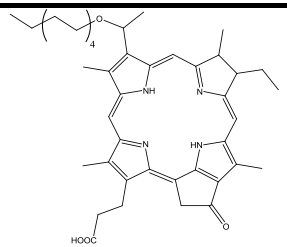	FaDu	FM	-	**LIS**	LIS	**S106**	305
Aggregated 2-[1-decyloxyethyl]-2-devinylpyropheophorbide-a **Pyropheophorbide C10**	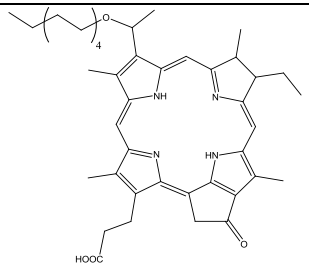	FaDu	FM	-	**MIT**	*indefinit*	**S107**	305
2-[1-dodecyloxyethyl]-2-devinylpyropheophorbide-a **Pyropheophorbide C12**	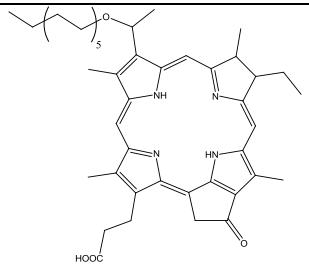	FaDu	FM	-	**LIS**	LIS	**S108**	305
Aggregated 2-[1-dodecyloxyethyl]-2-devinylpyropheophorbide-a **Pyropheophorbide C12**	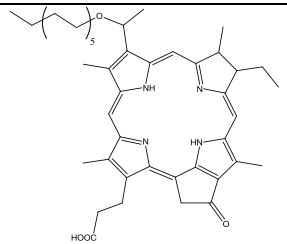	FaDu	FM	-	**MIT**	*indefinit*	**S109**	350

Nom	*Estructura molecular*	*Línia cel·lular*	*Mètode de detecció*	*Vehiculització*	*Localització*	*Predicció***	*ID*	*Referència*
Pyropheophorbide-a methyl ester **MPPa**	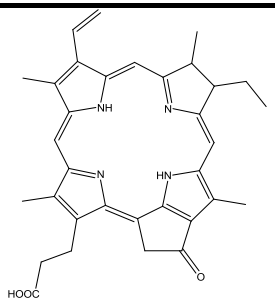	NCI-h446	CLSM	-	**MC**	OTH	**S110**	311

* Les localitzacions principals s'indiquen en negreta, seguida de les localitzacions secundàries. En cas de produir-se relocalització, s'indica l'orgànul destí entre parèntesis.
** Els FS sobre els quals no s'ha pogut aplicar el mètode de classificació es mostren amb com *indefinit.*

Nomenclatura emprada:

AG	aparell de Golgy
CIT	citoplasma
DIF	localització difosa
LIS	lisosomes
MC	membranes nuclears
MEM	membrana cel·lular
MIT	mitocondri
NUC	nucli
OTH	altres localitzacions subcel·lulars
RE	reticle endoplasmàtic

DOPC	dioleoyl phosphatidylcholine liposome
DPPC	dipalmitoyl phosphatidylcholine liposome
DPPIsC	1,2-di-O-(Z-1'-hexadecenyl)-sn-glycero-3-phosphocholine liposome
ENZ	Inhibition of mitochondrial enzymes
LDL	low density lipoprotein, lipoproteïna de baixa densitat
PC/Chol	phosphatidylcholine and cholesterol
PLA	poly(D,L-lactide) nanoparticle
PLGA	poly(D,L-lactide-coglycolide) nanoparticle
POPC	palmitoyl-oleoyl phosphatidylcholine liposome

CLSM	Confocal Laser Scanning Microscopy
CM	Confocal Microscopy
EM	Electron Microscopy
FC	Flow Cytometry
FM	Fluorescent Microscopy
FRET	Fluorescence resonance Energy Transfer
FTMS	Fourier Transform Multipixel Spectroscopy
MSF	Microspectrofluorometry
SF	Subcellular Fractionation
SSE	Studies of Sensitizing Effects

1c1c7	Murine hepatoma
4R	Rats embryo fibroblasts
9L	Brain tumor
A431	Human epidermoid carcinoma
A-549	Human lung adenocarcinoma
B16	Mouse melanoma
C6	Mice glioma
chok1	Chinese hamster ovary K1
CNE2	Nasopharyngeal carcinoma
colo201	Human colon carcinoma
CT26	Colon carcinoma
D532	Human skin fibroblast
EMT6	Mammary tumor
FaDu	Human hypopharyngeal carcinoma
H2T	Hamster pancreatic tumor
HaCaT	Human keratinocyte
HCT-116	Human colon carcinoma
HeLa	Human epithelial carcinoma
HEp2	Human epidermoid carcinoma
Hex	Rats hexachlorobenzene-fed
HT29	Human colon adenocarcinoma
JCS	Myeloid leukemia
KB	Human nasopharyngeal cancer
L1210	Murine leukemia
L5178Y-R	Mice lymphoma
LLC	Lewis Lung Carcinoma
LOX	Human melanoma
M1	Mouse myeloid leukemia
MCF7	Human breast cancer
MGH-U1	Human bladder cancer
MS-2	Fibrosarcoma
NCI-h446	Human lung carcinoma
NCTC-2544	Human keratinocyte
NHIK	Human cervical carcinoma
NPC/CNE-2	Human squamous cell carcinoma
OAC	Human oesophageal adenocarcinoma
P388	Murine leukemia
Pam 212	Murine keratinocyte
PC-3	Human prostate cancer
POVD	Human lung cancer
R323AC	Rats adenocarcinoma
RB230	Mammary adenocarcinoma
RIF-1	Fibrosarcoma
RIF-SA	Fibrosarcoma with induced resistance to photofrin
RR1022	Rat sarcoma
SC1	Human squamous cell carcinoma
SC2	Human squamous cell carcinoma
SSK2	Murine fibrosarcoma
V79	Chinese Hamster lung fibroblast
Gf	Mice griseofulvin-fed
Colo-26	Murine colon carcinoma
CHO	Chinese Hamster ovary

B. Formulacions químiques

International Journal of
Cosmetic Science

International Journal of Cosmetic Science, 2010, 1–11 doi: 10.1111/j.1468-2494.2009.00565.x

Comparative study of neural networks and least mean square algorithm applied to the optimization of cosmetic formulations

A. C. Balfagón*, A. Serrano-Hernanz*, J. Teixido†[1] and R. Tejedor-Estrada†

*Chemical Formulation Laboratory, Industrial Engineering Department, Institut Químic de Sarrià (IQS), Barcelona and †Molecular Design Laboratory, Organic Department, Institut Químic de Sarrià (IQS), Barcelona, Spain

Received 27 July 2009, Accepted 25 September 2009

Keywords: cosmetic formulations, design of experiments, neural networks

Synopsis

In this work, a comparative study between two methods to acquire relevant information about a cosmetic formulation has been carried out. A Design of Experiments (DOE) has been applied in two stages to a capillary cosmetic cream: first, a Plackett–Burman (PB) design has been used to reduce the number of variables to be studied; second, a complete factorial design has been implemented.

With the experimental data collected from the DOE, a Least Mean Square (LMS) algorithm and Artificial Neural Networks (ANN) have been utilized to obtain an equation (or model) that could explain cream viscosity. Calculations have shown that ANN are the best prediction method to fit a model to experimental data, within the interval of concentrations defined by the whole set of experiments.

Résumé

Dans cet article on compare deux méthodes d'acquisition d'information remarquable sur une formulation cosmétique. On a appliqué un plan d'expérience (Design Of Experiments, DOE) en deux étages sur une crème cosmétique capillaire: on a utilisé un dessin Plackett–Burman afin de réduire le nombre de variables à étudier, suivi d'un plan factoriel complet.

Avec les données obtenues du DOE, on a confronté les algorithmes des moindres carrés (Least Mean Square, LMS) et des réseaux de neurones artificiels (Artificial Neural Networks, ANN) pour obtenir une équation (ou modèle) qui puisse justifier la viscosité de la crème. Les calculs out démontré que les ANN sont la meilleure méthode pour ajuster un modèle aux données expérimentales, afin de prédire la propriété dans l'intervalle de concentrations utilisé dans l'ensemble des essais.

Correspondence: Alberto C. Balfagón, Chemical Formulation Laboratory, Industrial Engineering Department, Institut Químic de Sarrià (IQS), Barcelona, Spain. Tel.: +34 932 672000; fax: +34 932 056266; e-mail: albert.balfagon@iqs.edu

[1]Current address: Fundació TecnoCampus Mataró-Maresme.

Introduction

The influence of formulation's components over some of its properties has been traditionally studied by performing a large number of experiments. The successive variation of a component's concentrations represented a waste of time and money and even worse, results did not make improvement of the formulation always possible.

The first goal of this study was to perform a Design of Experiments (DOE) to reduce the number of tests needed to improve the viscosity of a capillary cosmetic cream by maintaining all the relevant information. For this, two DOE are implemented; the first one is suitable for dealing with a large number of variables (the Plackett–Burman DOE, PB–DOE) and the second one

(a complete factorial DOE, CF–DOE) to obtain all possible information of a set of experiments carried out with a small set of components.

The second goal of this work was to study and compare two different methods of modelling the cosmetic formulation: Least Mean Square (LMS) and the Artificial Neural Networks (ANN).

This study is divided into four main sections: in the first one, the formulation to be studied and the property to be modelled are described, clearing the way to a brief explanation of PB–DOE, CF–DOE and LMS methods. The next section is dedicated to ANN's description. Finally, in the last section, all results are shown.

Cosmetic capillary creams

Formulation

A cosmetic o/w emulsion vehicle for a permanent hair dye was studied. The oily phase was composed of consistence factors such as cetostearyl alcohol, ceteareth-23, stearilic alcohol, cocamide MEA and stearic acid. Alcohols, in addition to other characteristics, also exhibit an autoemulsification function; MEA is commonly used as a viscosity regulator and stearic acid provides pearl effects. The aqueous phase carried preservatives such as ascorbic acid, sodium sulphite and quelation agents in a very low concentration.

Furthermore, ammonia was used to increase the absorption of the dye in the hair, thus the resultant pH was quite basic. The strong odour was masked with the addition of a coconut perfume. Suitable conditioning properties were provided at such high pH by adding an amphoteric polymer (Merquat®, Nalco company, Leiden, The Netherlands). The high pH causes skin irritation, which was relieved with Shootex, tridecyl salicilate (Cosmacol ESI) and quaternary protein (Gluadin WQ), all of them with emollient properties.

Table I Components of the fundamental formulation

Component	Percentage (%)
Cetostearyl alcohol	15
Stearilic alcohol	15
Cocamide MEA	15
Ceteareth-23	1
Stearic acid	1.5
Cosmacol	0.2
Shootex	0.5
NH_3 (25%)	20
Deionized water	20
Minor components	11.8

The fundamental formulation is shown in Table I.

Only percentages of the first eight components were changed to study their effect on the viscosity of the cream. Some minor components were considered as a group and their percentage was kept constant in all experiments. Water was used to maintain the overall percentage at 100.

After preparing each formulation and before the rheological test (see Rheological test), each cream was mixed (one to one) with hydrogen peroxide.

Rheological test

The viscosity of each formulation was measured using a rheometer (AR550) (TA Instruments, New Castle, DE, U.S.A.). The experimental test consisted of two steps, each one lasting 1 min:

- First step: an increasing linear stress ramp, starting from 0 Pa up to 150 Pa.
- Second step: a constant stress of 150 Pa.

The viscosity used in subsequent mathematical analysis was the one that the formulation attained in the last point sampled in the second step [hereafter called η (100%)].

The homogeneity of the emulsion is critical in the study; therefore, the emulsion must be stirred properly. Once the emulsion was prepared, it was left to rest for 5 days. The test was carried out at room temperature.

DOE and LMS method

Plackett–Burman DOE

As seen before, when there are several variables that could affect one or several properties, the classical approach to study their effect would be to perform a large number of experiments with different values for each variable.

The DOE is a statistical tool that allows obtaining useful information from a system performing the minimum number of experiments [1]. There are several ways to carry out a DOE depending on the kind of information to be obtained, the number of variables that could affect the system and limitations on the number of experiments that can be performed.

In this study, a PB–DOE [2, 3] was undertaken followed by a 2-level CF–DOE to reduce the number of experimental tests, keeping the fundamental information intact.

The purpose of a PB–DOE is to identify the variables that are mainly responsible for the property under study, with as few experimental tests as possible.

The first step in applying this method consists of identifying the variables that could affect the property. The second step fixes the number of levels, and their values, for each variable. For example, if the concentration of one compound is a variable under study, then the number of different concentrations that will be taken into account and their values must be established. In this work, all variables studied had two levels (+high level, −low level) and their values have been proposed according to professionals' criteria (see Table II). The last step, before starting the experiments, is the choice of the best type of PB–DOE that fulfils all the requirements of the research.

The selected DOE uses a generator of experiments that, when rotating, gives the levels of each variable for a given experiment [2]. According to the number of variables, we used the generator related to a PB design in 16 runs:

+, +, +, +, −, +, −, +, +, −, −, +, −, −, −, −

The rotation of this generator (with the last sign fixed) determines the level of each variable for the 16 possible experiments.

The first eight columns of Table III are representative of the different levels of the variables used, whereas the other columns are used to set a significance level to determine whether or not a variable affects the studied property.

Table II Variable list for the Plackett–Burman design of experiments (DOE)

Var. number	Variable	Low level (−)	High level (+)
1	Cetostearyl alcohol	5	15
2	Stearilic alcohol	5	15
3	Cocamide MEA	5	15
4	Ceteareth-23	0.2	1
5	Stearic acid	1.5	8
6	Cosmacol	0.2	2
7	Shootex	0.5	2
8	NH_3 (25%)	6	20

The procedure to set the relevance of one variable, after carrying out the formulations and the measurement of the property, is described below: the process starts with the product between the column of signs associated with the variable and the results obtained for each experiment (see Table IV). The second step consists in summing up the values obtained in the previous step. The numerical result obtained is finally divided by the number of experiments (16, for the generator used in this study), obtaining the 'effect' of the variable. These operations are applied for each variable studied, including the 'dummy' variables (E1–E7 in Table III).

The third step fixes the cut-off level of significance to discriminate relevant from irrelevant variables using Equation 1.

$$\left(\sqrt{\sum_{i=1}^{n} val(E_i)^2/n}\right)t \qquad (1)$$

Equation 1 depends only on calculated values of 'dummy' variables: t is the 't' of Student value (generally fixed at 95% of certainty), $val(E_i)$ is the effect for the 'dummy' variable i and n is the number of 'dummy' variables.

A variable will be relevant if the absolute value of its effect is equal or greater than the value given by Equation 1 (cut-off level).

Complete factorial DOE and LMS method

In a CF–DOE it is possible to study all the interactions between variables. The number of experiments to be performed will be: $levels^{variables}$.

In this study, a CF–DOE for two variables with two levels was studied because of the results obtained during the experimental process (see Plackett–Burman DOE Results), requiring a total of four experiments (see Table V).

A and B are the variables under study, and the level of each one is shown in the columns (+high concentration level and −low concentration level). The heading AB stands for the column to be used to study the effect of the interaction of both variables in the property studied. Percentages of the rest of components are reported in Table VIII (see Results).

The effect of each variable is obtained in the same way as in PB–DOE, including the effect for the interaction AB. It is then possible to eliminate a variable if its effect is clearly not significant (i.e. the values obtained should be one or more order

Table III Plackett–Burman (PB) design for 16 runs

	Variable number								Dummy variables						
Experiment	1	2	3	4	5	6	7	8	E1	E2	E3	E4	E5	E6	E7
1	+	−	−	−	+	−	−	+	+	−	+	−	+	+	+
2	+	+	−	−	−	+	−	−	+	+	−	+	−	+	+
3	+	+	+	−	−	−	+	−	−	+	+	−	+	−	+
4	+	+	+	+	−	−	−	+	−	−	+	+	−	+	−
5	−	+	+	+	+	−	−	−	+	−	−	+	+	−	+
6	+	−	+	+	+	+	−	−	−	+	−	−	+	+	−
7	−	+	−	+	+	+	+	−	−	−	+	−	−	+	+
8	+	−	+	−	+	+	+	+	−	−	−	+	−	−	+
9	+	+	−	+	−	+	+	+	+	−	−	−	+	−	−
10	−	+	+	−	+	−	+	+	+	+	−	−	−	+	−
11	−	−	+	+	−	+	−	+	+	+	+	−	−	−	+
12	+	−	−	+	+	−	+	−	+	+	+	+	−	−	−
13	−	+	−	−	+	+	−	+	−	+	+	+	+	−	−
14	−	−	+	−	−	+	+	−	+	−	+	+	+	+	−
15	−	−	−	+	−	−	+	+	−	+	−	+	+	+	+
16	−	−	−	−	−	−	−	−	−	−	−	−	−	−	−

of magnitude higher), but this point is not always very clear and it is advisable to be sure that one variable can be erased.

The final stage in all experiments consists in generating a prediction model (in terms of an equation, if possible), to predict property values without performing any kind of experiment. The model must be validated by applying it over inputs not belonging to the set used to build it, to guarantee its prediction capacity and to avoid over-fitting and over-training results.

An easy way to generate the model is by using the LMS algorithm [4] which generates a polynomial expression. Using the CF–DOE generator described above (Table V), the polynomial obtained would be:

$$Y = a_0 + a_1 A + a_2 B + a_3 AB \quad (2)$$

Here, Y is the predicted property; and A, B and AB are the normalized concentrations (between −1 and +1) for the variables A, B and its product AB. The coefficients a_i have to be fixed using the LMS algorithm.

An alternative way to LMS to find out these coefficients is that they can be interpreted as the effect of each variable:

a_1 is the effect of variable A.

a_2 is the effect of variable B.

Table IV Signs for each experiment for input 5

Experiment	Input 5	Property	(Sign level)*Property
1	+	Y1	+Y1
2	−	Y2	−Y2
3	−	Y3	−Y3
4	−	Y4	−Y4
5	+	Y5	+Y5
6	+	Y6	+Y6
7	+	Y7	+Y7
8	+	Y8	+Y8
9	−	Y9	−Y9
10	+	Y10	+Y10
11	−	Y11	−Y11
12	+	Y12	+Y12
13	+	Y13	+Y13
14	−	Y14	−Y14
15	−	Y15	−Y15
16	−	Y16	−Y16

Table V Complete factorial design of experiments (DOE) for two variables with two levels

Experiment	A	B	AB
1	−	−	+
2	+	−	−
3	−	+	−
4	+	+	+

a_3 is the effect of variable AB (the interaction of A and B).

a_4 is the mean value of the property.

Artificial neural networks

Linear regression models such as LMS provide only linear relationships, whereas ANN belong to artificial intelligence methods and appear to be an alternative methodology to adjust non-linear correlations, mimicking human brain behaviour.

The complex neural design of the brain is thought to be responsible for its ability to remember, think and learn. Most of our daily life tasks could not be carried out without a previous learning process based on our personal experiences, which are often acquired through a trial-and-error process. The combination of these characteristics allows a human being to be faster than a computer in facial recognition problems, although a PC can solve more difficult numerical calculations.

In an attempt to transfer the learning ability to computers, ANN permit simulating neural processes in a mathematical way. As a result of their similarity with biological systems, most of the terms involved in ANN receive the name of their biological analogues.

Artificial neural networks were first developed in the middle 20th century by McCullogh and Pitts. However, their development has been continuous and extended until today and they offer a huge range of applications from image recognition to drug discovery in medicinal chemistry [5–7].

In this study, multi-layered feed-forward neural networks have been used. This type of ANN is made up of processing units called neurons, which can be considered as nodes arranged in layers. There are three main types of layers: (1) the input layer, where each neuron receives an input signal that will be used as starting point to obtain a desired output; (2) the output layer, which includes the neurons whose output signal becomes the ANN's result and (3) one or more hidden layers that help in finding the input interactions. The manner in which neurons of different layers are connected defines the net's architecture and each connection is ruled by weights. These values define how one connection affects the other, and could be interpreted as synapse strength. The number of neurons in every layer forms the ANN's topology.

Neurons can be mathematically defined as a summing function over all inputs modified by its synaptic weight, acting like a linear combiner (Equation 3).

$$u_k = \sum_{j}^{N} \omega_{jk} x_j + b_k \tag{3}$$

Here, N is the number of neurons that fires to the kth neuron, b_k is the bias term, an external parameter acting as an affine transformation of the neural response, which is treated like any other neural input, with an input value fixed at 1 and an associated weight equal to b_k.

One of the advantages of ANN over other regression methods is their ability to establish non-linear relationships among inputs. This is because of the introduction of a non-linear operator (called activation function) in output's processing (Fig. 1), which usually corresponds to a sigmoid function (Equation 4).

$$y_k = \frac{1}{1 + e^{-u_k}} \tag{4}$$

Thus, defining input values and setting initial weights, neural network propagates the information right to the output neurons. The final result will be interpreted according to the problem to be solved: classification methods usually have one neuron per class with binary output values, whereas predictive ones have only one output neuron with a real number as a result.

To obtain reliable results, ANN must be trained using a learning method. The attention is focused on supervised learning methods in which the network training optimizes not only connection weights but also the weight associated with the bias term to obtain the minimum error between the expected value and ANN's result. This learning method assumes having a training set of inputs with known expected output values for all of them. Following a trial-and-error process, weights are slowly optimized to the best situation to predict

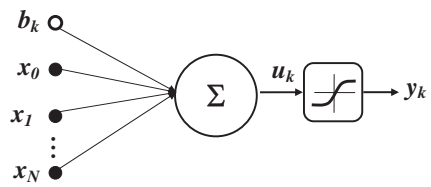

Figure 1 Block diagram of a neuron.

training set values. In this study, the results obtained are described using a back-propagation (BP) algorithm in batch mode (all inputs are presented to the net before weight updating) as a supervised learning method for training ANN. Commonly, BP uses the error between expected value and ANN's output to calculate a correction factor to be applied on weights to improve ANN's efficacy [5, 6, 8]. The way learning algorithm moves overall response surface is determined by the learning rate parameter which, applied over weight's correction factor, controls the convergence speed; low values mean small changes between weights of different iterations, ensuring a solution finding, but increasing the number of iterations. High learning rate values help to speed convergence, but run the risk of losing a solution.

Results

Plackett–Burman DOE

The values of rheological tests performed for each formulation are shown in Table VI.

The effects of each variable (calculated using the method explained in previous sections) and the cut-off levels, calculated using Equation 1, are shown in Table VII.

Considering the results, it can be noticed that the most relevant variables are the concentration of MEA and stearic acid. Both components showed a value of the same magnitude as the cut-off level. Thus, the concentrations of these two compounds are the ones chosen to implement the CF–DOE. Obviously, some information will be lost in this simplification, but we assume this in favour of making final results easier to use.

Table VI Experimental results

Experiment	η (100%)	Experiment	η (100%)
PB 1	1.43	PB 9	0.68
PB 2	6.92	PB 10	28.3
PB 3	1.56	PB 11	8.58
PB 4	3.63	PB 12	3.27
PB 5	28.47	PB 13	1.42
PB 6	19.92	PB 14	0.70
PB 7	2.56	PB 15	0.34
PB 8	4.42	PB 16	0.06

PB, Plackett–Burman.

Table VII Effects for each variable

Variable	100%
Cetostearyl alcohol	−1.79
Stearilic alcohol.	2.18
Cocamide MEA	**4.93**
Ceteareth-23	1.42
Stearic acid	**4.21**
Cosmacol	−1.37
Shootex	−1.79
NH_3 (25%)	−0.92
Cut-off level	**4.86**

Values in bold indicate the variables with effects similar to the cut-off level.

Complete factorial DOE

The concentration values of the fixed components over all the experiments are presented in Table - VIII. Note that although some values do not correspond to low or high concentration level, all of them are included in PB–DOE's percentage range.

The variables studied were the concentration level of cocamide MEA and stearic acid. The two levels studied for each product are shown in Table IX.

Table VIII Concentration percentages of the fixed components

Component	Percentage (%)
Cetostearyl alcohol	15
Stearílic alcohol	10
Ceteareth-23	0.8
Cosmacol	1
Shootex	1
NH_3 (25%)	16
Cadesol	3.75
Merquat	1.25
Amisol trio	1
Perfume	0.8
Ascorbate	0.3
Sodium sulphite	0.3
Dissolvine	0.1
Sequion	0.1
WQ Gluadin	0.05

Table IX Concentration level of cocamide MEA and stearic acid

Variable	Low level (−)	High level (+)
(A) Cocamide MEA	5	15
(B) Stearic acid	1.5	8

Table X Complete factorial design of experiments (DOE) (two variables with two levels) including experimental values

Formulation	A	B	AB	η (100%)
CF 1	−	−	+	0.60
CF 2	+	−	−	2.08
CF 3	−	+	−	1.10
CF 4	+	+	+	2.54

CF, complete factorial.

Table XI Effect of components A and B, and their interaction

Effect (variable)	100%
A	0.73
B	0.24
AB	−0.01

The property values for each formulation are shown in Table X.

The effects of each component and their interactions are shown in Table XI.

The equation obtained for theoretical prediction of η (100%) was:

$$\eta(100\%) = 1.58 + 0.73 \cdot A + 0.24 \cdot B \qquad (5)$$

The interaction between A and B (AB) was suppressed because the effect is one order lower than that of the others.

An external validation was performed to verify the utility of the prediction method, proposing three new experiments which were not included when establishing the model (training set). The codified values and the experimental and predicted η (100%) results, obtained using Equation 5, are summarized in Table XII.

It is easy to note that the error increases when the values of the variables A, B and AB drift apart from the points of the training set (whose codified values are ±1).

At this point, ANN seem to be a good method to solve this problem, finding a better prediction model.

Artificial neural networks

Computational study

This study was focused on the application of ANN as a regression method for experimental data, and its comparison with LMS.

The experimental results obtained in both PB–DOE (16 formulations) and CF–DOE (seven formulations) were used as a data set. In all studies, internal Leave-One Out validation (LOO) was performed to obtain better models with higher predictive power. The LOO error was calculated at the end of each epoch of training and contributed to the estimation of a global prediction error for the resulting model.

Artificial neural networks implemented in ArIS software tool developed at Molecular Design Laboratory at Organic Department of Institut Químic de Sarrià (IQS) was used in this study. These networks had already incorporated back-propagation

Table XII Codified values and experimental and predicted data for the external validation set

Experiment	A	B	AB	Predicted	Experimental	Relative error (%)
CF5	0.7	−0.2	−0.14	2.04	2.31	11.74
CF6	0.5	0.5	0.25	2.07	2.20	5.91
CF7	0	0	0	1.58	1.02	54.90

CF, complete factorial.

learning modes. Some modifications were carried out in internal ArIS's source code to fulfil specific requirements that arose during the calculations.

Initial random weights were delimited between −0.5 and 0.5, and a sigmoid function was used as an activation function. Learning rate was also optimized in each run because its value highly depends on topology, numerical range of input values and the internal error definition.

A feed-forward neural network with eight input neurons corresponding to the eight components of the chemical formulation (Table II) was defined for all runs. One output neuron was used to obtain a real number for associating its value with the formulation's viscosity. The effect of varying the number of hidden layers and hidden neurons was studied, to identify the best topology to solve problems raised in each part of the study.

The number of hidden layers was limited to a maximum of two because there are evidences that this is enough to adjust continuous functions, according to Kolmogorov's theorem [9]. Regarding the number of hidden neurons, the number of hidden units was kept below the number of descriptors [10], to prevent over-fitting problems [11]. Taking these limitations into account, a trial-and-error methodology was followed to find the best net topology.

Results and discussions

The first results obtained showed that ANN with only one hidden layer yield better results than the ones obtained with two hidden layers.

The first viscosity prediction model (Model 1A) (derived from PB–DOE's data as training set and CF–DOE's data as external validation set) was deduced with an 8-5-1 net topology; the results obtained are shown in Fig. 2. Quite good agreements with experimental training set (R^2 = 1.0) and external validation set (R^2 = 0.78) were obtained. The relative error of the validation set was still too high for prediction purposes. Nevertheless, the results presented at this point are in accordance with those reported by Trenn [12], who considers that five hidden neurons should be enough to adjust an approximation order of two functions in a system with eight inputs.

To improve the prediction capacity of the model, points with viscosities below 0.7 were removed from the training set, assuming that low values

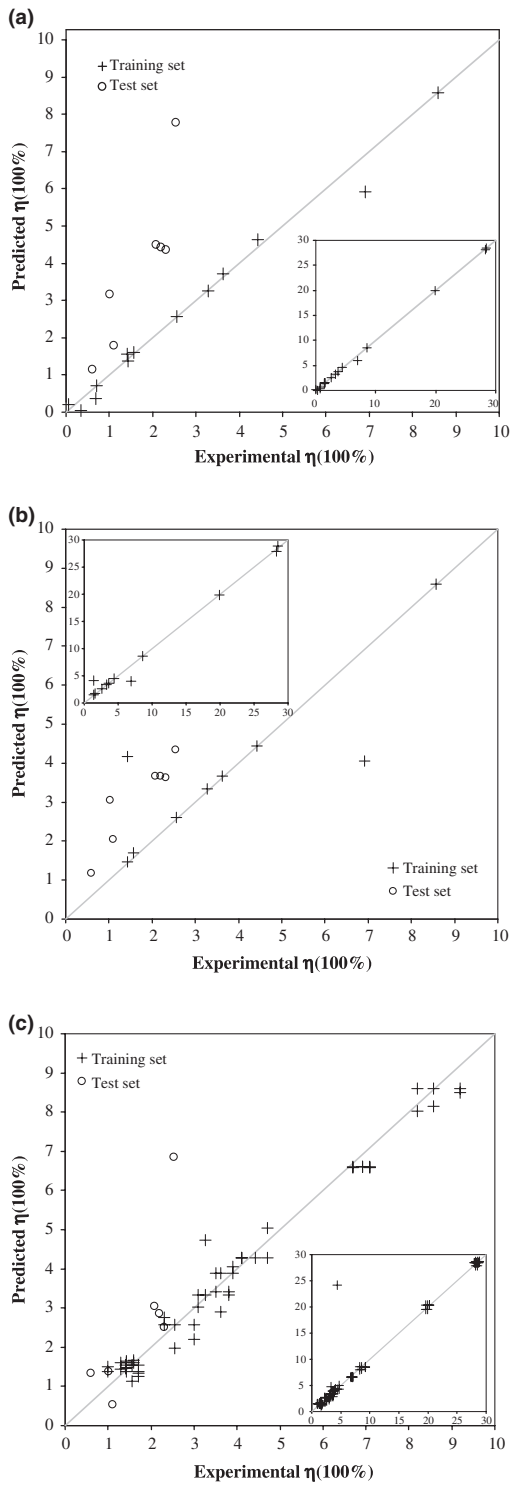

Figure 2 Predicted η (100%) values calculated by 8-5-1 ANN vs. experimental results for the first three proposed models (1a–1c). Inset shows the whole range of results for the training set, maintaining the same axis units as in the main figure.

were affected by experimental error. Artificial neural networks were re-trained under these conditions, obtaining a better model (Model 1B). Note that points above 10 were not removed to maintain the margin of interest in which the model would be applied.

Although recognition of the training set was maintained ($R^2 = 0.99$), prediction power was increased in external validation set ($R^2 = 0.85$).

Finally, in an attempt to increase the prediction capacity of the model, the first experimental training data set was duplicated by including small random changes to mimic experimental error [5, 13], obtaining Model 1C. Given the small data set size, duplication must be carried out assuring that new points are different from the test set, otherwise it would no longer be considered as external, unseen data. If more experiments were available, the splitting of the test set into two subsets could be used to study the benefit of data duplication (first subset) and as external validation (second subset).

The results for the different models are shown in Table XIII.

All models derived from this first study were capable of adjusting data set values (Fig. 2). Although Model 1C fits better with experimental values, Model 1B maintains the viscosity order between them: Spearman's rank correlation coefficient (ρ) is quite higher in Model 1B (0.82) than in Model 1C (0.75).

To identify the most important components of formulations in this study, the number of inputs was diminished. Considering this issue, two different approaches could be used:

(a) Attending to the value of resulting connection weights on models 1A–1C, identifying the inputs with lower synapse strength [14, 15].
(b) Using a genetic neural network (GNN), discarding inputs with less importance in ANN performance. This method applies a genetic algorithm (GA) to find the best set of descriptors to use as input [16].

Inspection of synapse strength for ANN on models 1A–1C shows that variables 2, 4 and 7 (Table II) could be removed from training data set (Model 2A), as their weights are, in average, two to four times lower than the rest of the variables. This result partially agrees with that of the GNN, where different runs found that inputs 5 and 7 (Table II) could be omitted (Model 2B). Each calculation was followed by parameter optimization. The results are shown in Table XIV.

Note that the input suppression is only carried out in the mathematical treatment of data, and not in the experimental formulation. The suppressed inputs do not have a significant influence on formulation's viscosity within the studied range of experimental concentrations.

Considering both results obtained, the model with the best performance was Model 2B trained without inputs 5 and 7 (Fig. 3).

Results presented until this point do not agree with the variable selection made with CF–DOE (which discards all inputs except for 3 and 5). In the attempt to obtain a prediction model under the same conditions as in LMS linear regression (using only CF–DOE data as the training set), we realized that ANN is not able to adjust a valid model with this restriction. However, a prediction model was obtained by setting aside one value to use as an external validation. The entire PB data set was useless because of the fact that some of its points are far away from training set values.

Unfortunately, the resulting model is still not satisfactory enough because of its lack of applicability for high viscosity values.

Conclusions

In this work, the comparison between two fitting methods applied to cosmetic formulations was investigated. For this reason, two DOEs were applied according to the number of variables. The first one was a Plackett–Burman DOE adapted to

Table XIII Comparative results for models A, B and C

Model	RMSE (train)	RMSE (validation)
1A (n = 16)	0.071	0.988
1B (n = 12)	0.333	0.554
1C (n = 12)	0.061	0.655

Table XIV Results for models 2A and 2B

Model	Excluded inputs	RMSE (train)	RMSE (validation)
2A (n = 12)	2, 4, 7	0.867	0.842
2B (n = 12)	5, 7	0.125	0.232

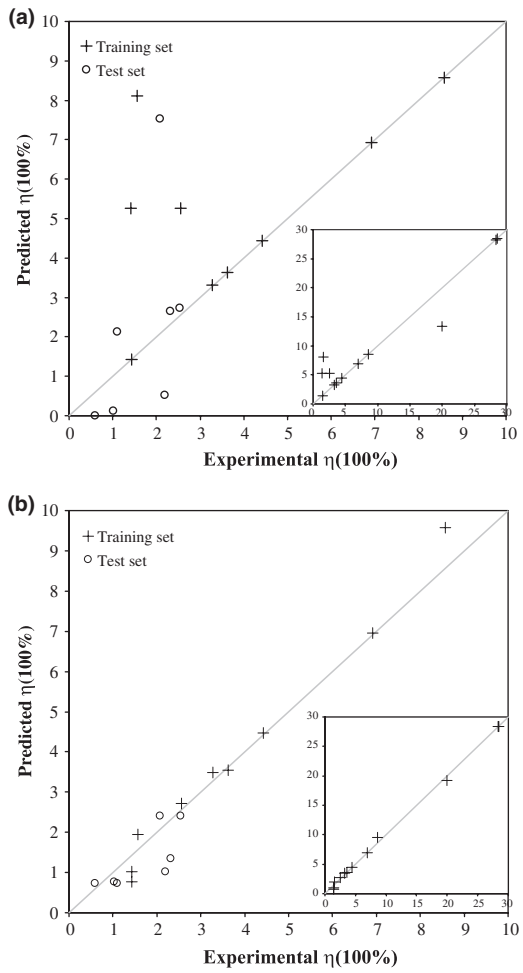

Figure 3 Predicted η (100%) values vs. experimental results for Model 2a (calculated by 5-4-1 ANN) and Model 2b (calculated via GNN by 6-4-1 ANN). Inside figure shows the whole range of results for the training set, maintaining the same axis units as in the main figure.

work with a large number of variables, which helps in identifying the variables that are mainly responsible for the formulation's viscosity. The second one was a complete factorial DOE which, using the result of previous stage, is an ideal method to obtain the maximum information from a reduced set of variables.

The LMS method is very easy to apply to statistical results of the complete factorial DOE and permits obtaining a preliminary prediction method. The problem appears in points which drift apart from those used as training set, where the prediction error increases significantly. It becomes more important when the set of data is reduced, as has been shown in the experiments carried out.

Artificial neural networks are a more complex methodology to fit a model, although they appear to be more suitable to obtain predictions from a reduced data set. A useful theoretical model has been established for the prediction of η (100%) value in capillary cosmetic creams.

Artificial neural networks also permit improvement in the identification of components related to formulation's viscosity calculated using DOE. Results are valid within the range of concentrations under study and its generalization cannot be argued according to the nature of removed components. As we would expect from a chemical point of view, both models find cocamide MEA to be an important factor to describe formulation's viscosity, but the suppression of one component does not mean that it is always negligible: it can only be removed in this formulation within the studied range of experimental concentrations.

Acknowledgement

R. Tejedor thanks the Comissionat per a Universitats i Recerca del Departament, d'Innovació, Universitats i Empresa de la Generalitat de Catalunya and the European Social Fund for a FI2009 grant.

References

1. Montgomery, D.C. *Diseño y análisis de experimentos*. Limusa Wiley, Mexico (2002).
2. Plackett, R.L. and Burman, J.P. The design of optimum multifactorial experiments. *Biometrika* **33**, 305–25 (1946).
3. Fisher, R. The arrangement of field experiments. *J. Minist. Agric. (Great Britain)* **33**, 503–513 (1926).
4. Navidi, W. *Estadística para ingenieros y científicos*. MacGraw Hill, Mexico (2006).
5. Haykin, S. *Neural Networks, A Comprehensive Foundation*. Prentice Hall, New Jersey (1999).
6. Zupan, J. and Gasteiger, J. Neural networks: a new method for solving chemical problems or just a passing phase? *Anal. Chim. Acta.* **248**, 1–30 (1991).
7. Terfloth, L. and Gasteiger, J. Neural networks and genetic algorithms in drug design. *DDT* **6**, S102–S108 (2001).
8. Freeman, J.A. and Skapura, D. *Neural Networks: Algorithms, Applications and Programming Techniques*. Addison-Wesley, Reading (1992).
9. Poggio, T. and Girosi, F. *A Theory of Networks for Approximation and Learning, Technical Report*. Massachusetts Institute of Technology, Cambridge (1989).
10. Blum, A. *Neural Networks in C++*. Wiley, New York (1992).

11. Aizenberg, I. Multilayer feedforward neural network based on multi-valued neurons (MLMVN) and back-propagation learning algorithm. *Soft. Comput.* **11**, 169–183 (2007).
12. Trenn, S. Multilayer perceptrons: approximation order and necessary number of hidden units. *IEEE Trans. Neural Netw.* **19**, 836–844 (2008).
13. Burns, J. and Whitesides, G.M. Feed-forward neural networks in chemistry: mathematical systems for classification and pattern recognition. *Chem. Rev.* **93**, 2583–2601 (1993).
14. Caballero, J., Tundidor-Camba, A. and Fernández, M. Modeling of the inhibition constant (Ki) of some Cruzain ketone-based inhibitors using 2D spatial autocorrelation vectors and data-diverse ensembles of Bayesian-regularized genetic neural networks. *QSAR Comb. Sci.* **26**, 27–40 (2007).
15. Hemmateenejad, B., Safarpour, M.A., Miri, R. and Nesari, N. Toward an optimal procedure for PC-ANN Model building: prediction of the carcinogenic activity of a large set of drugs. *J. Chem. Inf. Model.* **45**, 190–199 (2005).
16. Gedeon, T. Indicators of hidden neuron functionality: the weight matrix versus neuron behaviour. *Proceedings of the 2nd New Zealand Two-Stream International Conference on Artificial Neural Networks and Expert Systems*. IEEE, Dunedin (1995).

C. Estudi de la tautomeria del 9ATPPo

PCCP

Dynamic Article Links

Cite this: *Phys. Chem. Chem. Phys.*, 2011, **13**, 10326–10332

www.rsc.org/pccp

PAPER

Dual fluorescence in 9-amino-2,7,12,17-tetraphenylporphycene†

Miquel Duran-Frigola, Roger Tejedor-Estrada, David Sánchez-García and Santi Nonell*

Received 24th November 2010, Accepted 31st March 2011
DOI: 10.1039/c0cp02654a

The absorption spectrum of the asymmetric 9-amino-2,7,12,17-tetraphenylporphycene shows new, strongly red-shifted bands compared to the symmetric parental 2,7,12,17-tetraphenylporphycene and to the also asymmetric 9-acetoxy-2,7,12,17-tetraphenylporphycene. Dual emission is also observed with relative contributions that depend strongly on the excitation wavelength and temperature. The gap between the two fluorescence bands is 84 nm. Tautomerization in both the ground and excited states is shown to account for these observations, the 9-amino group being particularly able to selectively lower the energy of the first excited singlet state of just one of the *trans* tautomers. Introduction of amino groups in porphycenes may be a convenient way to gain a deeper insight into the tautomerization mechanisms in this macrocyclic core.

1. Introduction

Porphycenes are prominent isomers of porphyrins in terms of fundamentals and applications, particularly in light-mediated processes. Their photophysics have been widely studied[1] and proposed as attractive second-generation agents for photodynamic therapies (PDT).[2] This is due to their ability to absorb red light and photosensitize singlet oxygen.[3] Our group has focused on 2,7,12,17-tetraphenylporphycenes (TPPos)[4] that are endowed with excellent *in vitro* PDT photosensitizing properties.[5] In order to improve the biological compatibility and selectivity of the parental TPPo, some combinatorial approaches[6] and 9-regioselective insertions of functionalities[7] have been achieved. Our previous works showed that the fluorescence quantum yield and the ability to produce singlet oxygen were substantially decreased in 9-amino-2,7,12,17-tetraphenylporphycene (9-ATPPo), but not in 9-acetoxy or 9-nitro derivatives. Moreover, the fluorescence decay kinetics of 9-ATPPo were biexponential, suggesting the presence of two emitting forms.[6] The amino derivatives are of special interest because they contain a linking point for further conjugation to biological vectors that would enhance the intrinsic selectivity of PDT. Therefore, a better understanding of the abnormal photophysics of the model 9-ATPPo is crucial to overcome these drawbacks for future photosensitizer designs.

On the other hand, porphycenes' particularly well-defined inner cavity, with migrating hydrogen atoms isolated from the environment, has provided a unique framework to probe tautomerism, coupling between vibrations, cooperativity, and other basic chemical processes.[8] Since porphycenes undergo sensitive dimensional changes of the inner cavity depending on the peripheral substitution, they offer the chance to establish correlations between NH···H distances and tautomerization mechanisms inside the macrocycle.[9] Interestingly, the difference between tautomerism in porphycene and in the parental isomer porphyrin is caused by geometry perturbations rather than by electronic structure factors,[8] and a major understanding of the hydrogen migration processes in porphyrins can thus be approached by systematically modulating the geometry of porphycenes. It is noteworthy that, among all porphycenic systems, the symmetric ones are the most extensively characterized. The general trend is the observation of a low-barrier tunneling equilibrium in the ground state and a high-barrier distance-dependent hydrogen movement in the first excited state.[8,9] However, studies of symmetric porphycenes deal with just three different tautomers, because opposite tautomers have the same properties. This is not the case of 9-ATPPo and other 9-substituted porphycenes, in which opposite tautomers are no longer equivalent (Fig. 1).

Even though previous studies of asymmetric porphycenes reported significant spectral perturbations and gave convincing evidence of relative energy changes in the excited states,[10,11] 9-ATPPo shows an abnormal absorption spectrum shape[6] and a striking two-band emission that cannot be explained just by taking into account bulky asymmetric effects. The present work provides spectroscopic insight into the problem and gives evidence of a high electronic stabilization of just one tautomer in its excited state. Therefore, 9-amino derivatives of porphycenes can provide useful experimental proof of the effects and relevance of the relative positions of inner hydrogen atoms in terms of energy and electronic structure.

Grup d'Enginyeria Molecular, Institut Químic de Sarrià, Universitat Ramon Llull, Via Augusta 390, E-08017, Barcelona, Spain. E-mail: santi.nonell@iqs.url.edu; Fax: +34 93 205 6266; Tel: +34 93 267 2000

† Electronic supplementary information (ESI) available. See DOI: 10.1039/c0cp02654a

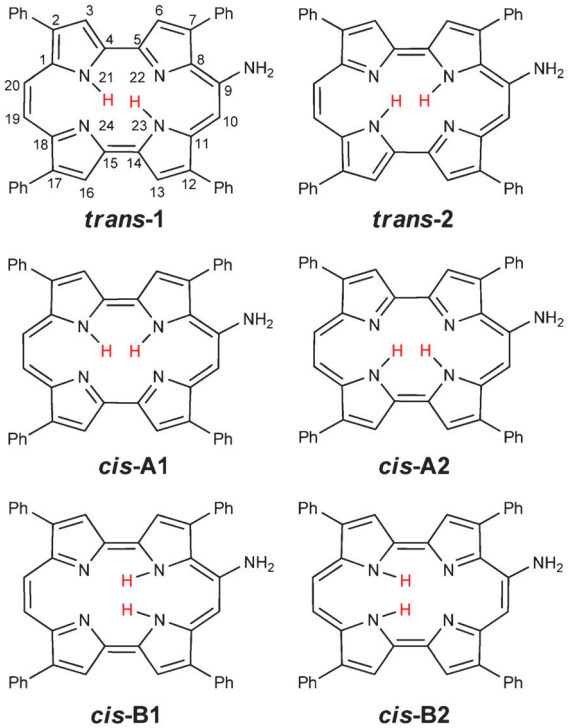

Fig. 1 The six possible tautomers of 9-ATPPo named according to Gil *et al.*[10]

2. Experimental

2.1 Chemicals

9-ATPPo and 9-acetoxy-2,7,12,17-tetraphenylporphycene (9-AcOTPPo) were synthesized as described previously and found to be of purity >99% by HPLC.[6] Spectroscopic quality solvents were purchased from Aldrich and were used as received.

2.2 Photophysical techniques and methods

All photophysical measurements were carried out in spectroscopic grade solvents. Absorption spectra were recorded using a Varian Cary 4E dual-beam UV/vis spectrophotometer. Corrected fluorescence excitation and emission spectra were recorded on a JobinYvon-Spex Fluoromax-2 spectrofluorometer with optically-thin solutions (absorbance below 0.1 at the Q-bands maxima). Fluorescence decays were recorded using a Pico-Quant Fluotime 200 time-correlated single photon counting system equipped with a red-sensitive photomultiplier. Picosecond diode lasers working at a 40 MHz repetition rate were used for excitation at 654, 596 and 375 nm. All spectroscopic measurements were carried out in 1-cm quartz cuvettes (Hellma, Germany) in air-saturated solutions at room temperature unless otherwise stated.

2.3 Computational methods

Ground state geometry optimizations were performed using the B3LYP method at 6-31G(d) level of theory. This method was validated by optimizing the parent porphycene (Po) geometry and comparing the results with the energy values and natural orbital topologies calculated elsewhere with HF and DFT methods.[12,13] Frequency calculations to predict zero point energies (ZPE) were considered necessary for the comparison between energies of the tautomers. TD-DFTB3LYP/6-31G(d) calculations were carried out to estimate the energies of the first excited state of 9-ATPPo tautomers. Gaussian03 software was used for all calculations.[14]

3. Results

3.1 Absorption spectra

The room-temperature absorption spectrum of 9-ATPPo is compared in Fig. 2 with that of 9-AcOTPPo, an asymmetric porphycene with an electronically neutral substituent at the *meso* position. The main differences between both spectra are (i) a more pronounced splitting of the Soret band in the case of 9-ATPPo, (ii) lower absorption coefficients in the Soret region as a result of band splitting, and (iii) a 110-nm red shift of the lowest-energy Q band, which appears at 755 nm for 9-ATPPo.

3.2 Emission spectra

The emission spectrum of 9-ATPPo is shown in Fig. 2. Two well resolved bands F_1 and F_2 can be observed, with maxima at 780 and 696 nm, respectively. Such a large gap of 84 nm is unprecedented for the porphycenes and largely exceeds the separation between vibrational energy levels. More strikingly, the 696-nm emission band appears at a *shorter* wavelength than the lowest-energy absorption band (755 nm). Finally, we found that the ratio of the F_2/F_1 intensities is strongly excitation wavelength dependent (Fig. 3b).

3.3 Excitation spectra

The excitation spectra monitored at different emission wavelengths are shown in Fig. 3a. The shape of the spectra depends strongly on the observed emission wavelength and almost matches the absorption spectrum when the F_1 emission is monitored. A total number of 6 bands, Q_1–Q_6 can be identified, Q_3 and Q_4 being strongly overlapped at room temperature. Interestingly, the Q_3 band is significantly enhanced when the F_2 emission is monitored.

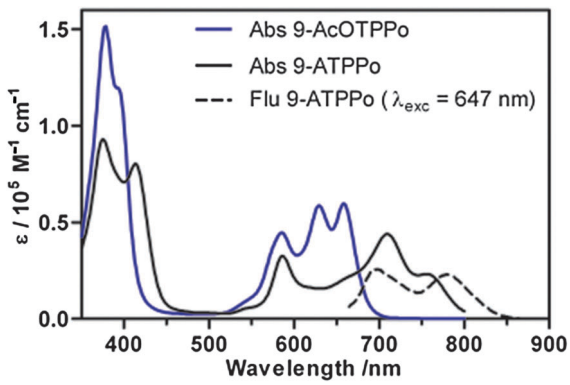

Fig. 2 Absorption and fluorescence spectra of 9-ATPPo in toluene. The absorption spectrum of 9-AcOTPPo is shown for comparison.

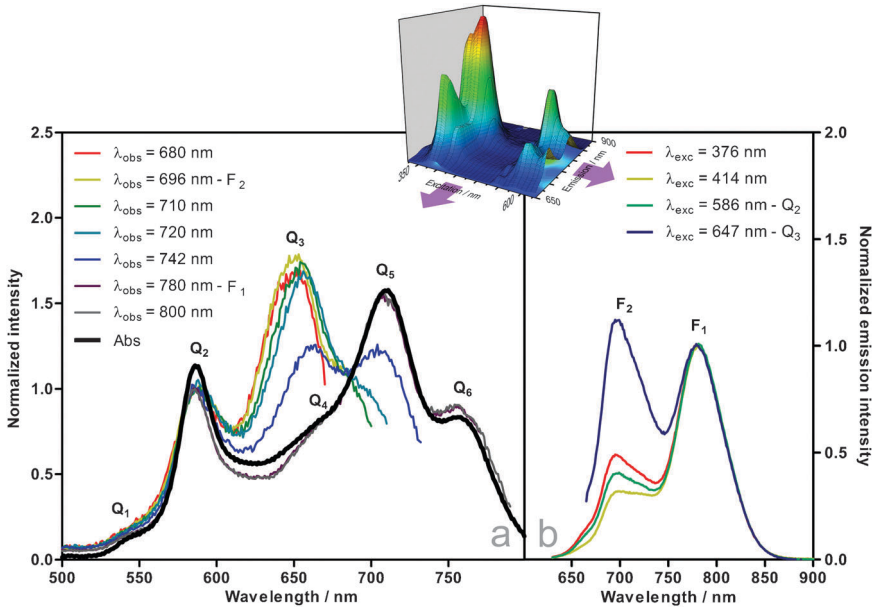

Fig. 3 (a) Normalized excitation and absorption spectra of 9-ATPPo. (b) Emission spectra of 9-ATPPo at different excitation wavelengths. Toluene was used as solvent.

3.4 Fluorescence kinetics

Time-resolved emission spectra (TRES) provide an opportunity to ascertain the decay kinetics of the two emissions observed in the steady state spectra. Global analysis of the decays excited at 375 nm reveals that the F_1 and F_2 emissions are mono-exponential (Fig. 4), F_2 decaying more slowly than F_1 (1.90 *vs.* 0.83 ns). Changing the excitation wavelength from 375 to 596 nm or 654 nm did not affect the kinetics of the components.

3.5 Temperature effects

Absorption spectra remain essentially constant in shape, bandwidths and relative intensities over the temperature range 10–80 °C. However, the relative intensities of the F_1 and F_2 fluorescence emission bands change significantly when λ_{exc} = 647 nm (Q_3). Specifically, increasing the temperature leads to *ca.* 40% decrease in F_2 while F_1 decreases only 5%. When the same experiment is carried out at 586 nm (Q_2) the two emissions behave identically and show only a modest decrease (Fig. 5).

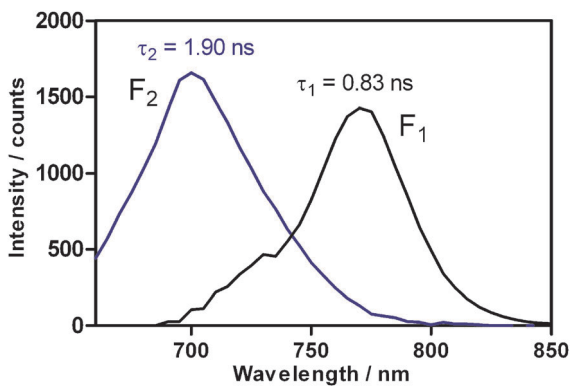

Fig. 4 Decay-associated spectra of F_1 and F_2 recovered by global analysis of the fluorescence decays (λ_{exc} = 375 nm) in toluene.

A further decrease of the temperature down to 77 K confirms the above trend (Fig. 6). Not surprisingly, excitation spectra are temperature-dependent as well (Fig. 7). Interestingly, at 77 K the ratio of Q_3/Q_2 intensities is increased and a significant shift to the red is observed for the lowest-energy bands Q_5 and Q_6 but not for the other bands.

3.6 Computational support

The ground state geometries and energies of the tautomers ***trans*-1**, ***trans*-2**, ***cis*-A1**, ***cis*-A2**, ***cis*-B1** and ***cis*-B2** (Fig. 1) were estimated using DFT/B3LYP 6-31G(d) methods. The ***trans*-1** tautomer was found to have the lowest ground state energy, but ***trans*-2** energy was only 0.9 kJ mol^{-1} higher. Significantly higher energies were obtained for the *cis* tautomers, ***cis*-A1** and ***cis*-A2** (7.8 and 10.3 kJ mol^{-1}, respectively). Electronic transitions were computed as vertical excitations from the ground state structures by using the TD DFT approach. S_1 and S_2 energies of ***trans*-1** were 178.7 and 216.2 kJ mol^{-1}, and those of ***trans*-2** were 190.4 and 207.1 kJ mol^{-1}, respectively.

4. Discussion

4.1 Existence of two absorbing tautomers in solution

The findings reported in this study illustrate the strong influence of the amino group on the absorption and fluorescence properties of tetraphenylporphycenes. Compared to the parental TPPo, an electronically neutral group such as acetoxy introduced only a marginal hypsochromic shift in all absorption and emission bands, whereas the amino-substituted analogue showed large perturbations.[6] The dependence of the fluorescence excitation spectra of 9-ATPPo on the observation wavelength clearly demonstrates that there are, at least, two absorbing species in solution. Tetrapyrroles such as porphyrins and porphycenes are well known for the tautomerism involving the exchange of two hydrogen atoms among

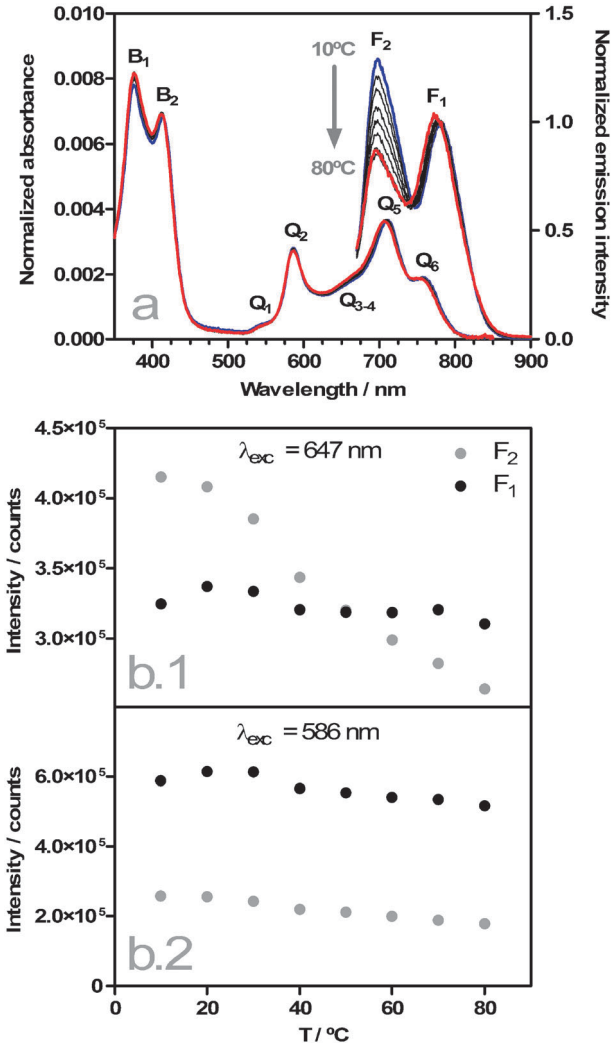

Fig. 5 (a) Absorption and emission spectra of 9-ATPPo from 10 to 80 °C in toluene. Measurements were performed every 10 °C. The absorption spectra were normalized relative to the total area of absorption. Emission spectra were recorded at λ_{exc} = 647 nm and were normalized at 780 nm (F_2). (b) Temperature variation of the absolute intensities of the F_1 and F_2 bands at λ_{exc} = 647 nm (b.1) and 586 nm (b.2).

the four nitrogens of their inner cavity.[8,15,16] In porphyrins, it has recently been shown that tautomerization can lead to dual fluorescence.[17] In porphycenes, Gil *et al.* demonstrated that substitution of 2,7,12,17-tetra-*n*-propylporphycene by an acetoxy group changes the excited state energy of the two *trans* tautomers.[10] However, while the tautomers could be distinguished by their absorption spectra, fluorescence occurred mainly from only one of them, although the authors noted a weak emission at the blue edge of the main fluorescence band and attributed it to the other tautomer. Based on these earlier works, we propose that our observations are likewise the result of tautomerization processes. With the purpose of establishing the number and identity of the 9-ATPPo tautomers existing in solution, and assigning the bands in the absorption and emission spectra, DFT/B3LYP 6-31G(d) calculations were carried out on the tautomers shown in Fig. 1. The geometry and S_1–S_0 relative energies calculated for the *trans* tautomers were in good agreement with those of a model porphycene (Po),[13]

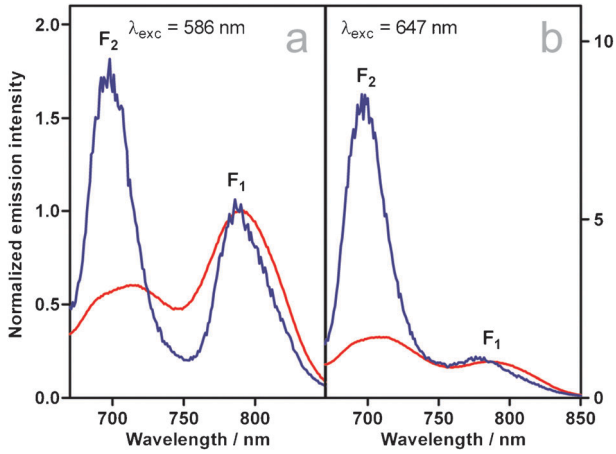

Fig. 6 Emission spectra in 2-MeTHF at room temperature and at 77 K recorded at (a) λ_{exc} = 586 nm and (b) λ_{exc} = 647 nm. The intensities are normalized at 788 nm to facilitate the comparison.

whereas for the *cis* tautomers the results were somewhat in disagreement and might need further, more accurate calculations. It was nevertheless evident that the two *trans* tautomers are much lower in energy than their *cis* counterparts and can therefore be considered the only existing ground state species in solution.[18] The similarity between the energies of the two *trans* tautomers also confirms the observations in Fig. 5 that the absorption spectra are temperature independent. Global analysis of TRES results confirms the existence of two emitting species with different emission spectra (Fig. 4), indicating that the two tautomers are no longer equivalent in energy in their singlet excited state. Using the $S_0 \rightarrow S_1$ transition calculations performed with TD-DFT methods, the fluorescence band of lowest energy (F_1) is assigned to the tautomer ***trans*-1**, and the highest-energy band (F_2) to ***trans*-2**. Thus, dual fluorescence in porphycenes occurs with an unprecedented gap of 84 nm between the spectra of the two tautomers.

4.2 Tautomerization in the excited states

Tautomerization also takes place in the excited state as revealed by the excitation spectra. As shown in Fig. 3a, excitation spectra of the F_1 band match almost perfectly the absorption spectrum of the tautomer mixture. This indicates that a population flow from ***trans*-2** to ***trans*-1** must be taking place in the excited state whenever ***trans*-2** is the primary light-absorbing tautomer. This would suggest that a rise component in the F_1 fluorescence kinetics should be observed when ***trans*-2** would be the primary photoexcited species. The following kinetic analysis shows that the situation is however more complex. Emission at 800 nm (F_1) is proportional to the concentration of ***trans*-1**, which, according to our hypothesis, can be populated both directly and from photoexcited ***trans*-2** (eqn (1)):

$$F_1 \propto [trans-1]_t = [trans-1]_0 \cdot e^{-\frac{t}{\tau_1}} + [trans-2]_0 \times f \times \left[\frac{\tau_1}{\tau_T - \tau_1}\left(e^{-\frac{t}{\tau_T}} - e^{-\frac{t}{\tau_1}}\right)\right] \quad (1)$$

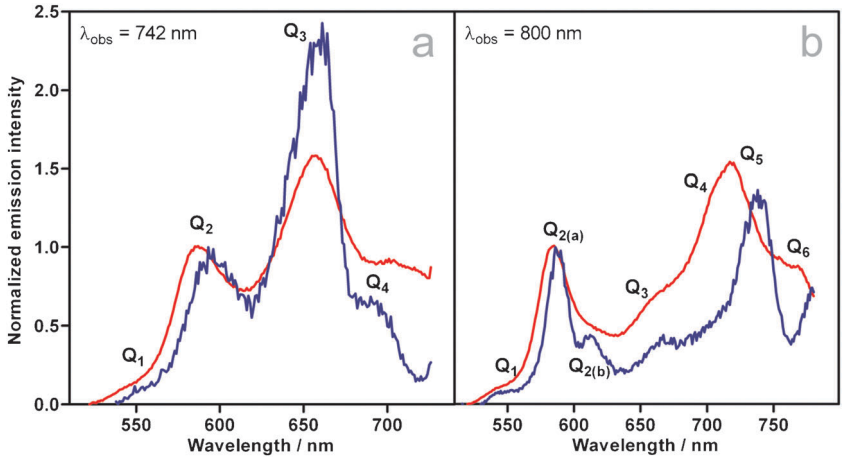

Fig. 7 Normalized excitation and emission spectra of 9-ATPPo in 2-MeTHF at 77 K and at room temperature. Spectra were recorded at (a) λ_{obs} = 742 nm and (b) λ_{obs} = 800 nm.

where τ_1 is the lifetime of ***trans*-1** (0.84 ns), τ_T is the lifetime for production of ***trans*-1** *via* ***trans*-2**, and f is the fraction of ***trans*-2** undergoing tautomerization. Rearranging terms:

$$F_1 = a_1 \cdot e^{-\frac{t}{\tau_1}} + a_2 \cdot e^{-\frac{t}{\tau_T}} \quad (2)$$

where

$$a_1 = [trans-1]_0 - [trans-2]_0 \times f \times \frac{\tau_1}{\tau_T - \tau_1} \quad (3)$$

and

$$a_2 = [trans-2]_0 \times f \times \frac{\tau_1}{\tau_T - \tau_1} \quad (4)$$

If tautomerization takes place from the S_1 level of ***trans*-2**, then it competes with radiative decay and therefore τ_T can be equated to the observed lifetime for F_2 (1.9 ns). In this case we ought to see a biexponential function with lifetimes 0.84 and 1.9 ns. This is in fact what we see when we excite at 654 nm, albeit the preexponential factor for the 1.9 ns component is very small, *ca.* 5%. We must then conclude that tautomerization occurs with a very small efficiency from S_1 of ***trans*-2**. As such, both a_1 and a_2 are positive and no growth can be observed.

On the other hand, if tautomerization takes place before the S_1 level of ***trans*-2** reaches thermal equilibrium (*i.e.*, from an upper electronic or a not fully equilibrated state in S_1)[11] then $\tau_T \ll \tau_1,\tau_2$. Under these conditions, $a_1 \approx$ [***trans*-1**]$_0$ + [***trans*-2**]$_0 \times f > 0$ and $a_2 \approx -$[***trans*-2**]$_0 \times f < 0$. Thus, we should see a rise component with lifetime τ_T. However, if such growth is faster than the resolution of our system (*ca.* 100 ps) such rise component will be undetectable. We believe that this is actually the case.

Of course a third scenario is possible, in which excited-state tautomerization would not take place at all. This is however hard to reconcile with the almost perfect match between the F_1 excitation spectra and the absorption spectra of the equilibrated tautomer mixture.

Additional insight can be obtained from the temperature effects: Fig. 5 shows that emission spectra are highly temperature- and excitation-wavelength dependent. For λ_{exc} = 647 nm (Q_3), increasing the temperature leads to a *ca.* 40% decrease of F_2 while F_1 decreases only 5%. However, when the same experiment is carried out at 586 nm (Q_2) the two emissions behave identically, showing only a very slight decrease over the whole temperature range. We must conclude that (1) a temperature-dependent non-radiative process exists for ***trans*-2** which is more efficient than for ***trans*-1**, and (2) a population flow from ***trans*-2** to ***trans*-1** occurs at the S_2 level and it is more efficient than at the S_1 level. If ***trans*-1** and ***trans*-2** would not interconvert in the excited state then the temperature behavior of their fluorescence would have been independent of the excitation wavelength. At 77 K (Fig. 6b), a further enhancement of the F_2/F_1 ratio is observed. Accordingly, the F_1 excitation spectrum recorded at 77 K (Fig. 7b) shows a very small contribution of the Q_3 and Q_4 bands. Taken together, these observations indicate that Q_3 and Q_4 belong to the ***trans*-2** tautomer, and that thermal activation is needed to reach the S_1 state of ***trans*-1** despite the fact that it lies lower in energy. Based on the similarity between the energy of Q_4 and that of F_2 we assign them to the S_0–S_1 (0,0) transition of ***trans*-2**. Thus, the higher energy absorption bands Q_5 and Q_6 must belong to ***trans*-1**, Q_6 and F_1 corresponding to the S_0–S_1 (0,0) transition.

Inspection of the F_1 excitation spectra also reveals that the Q_5/Q_2 ratio is almost insensitive to temperature, implying that either Q_2 belongs to ***trans*-1** or it belongs to ***trans*-2** but then tautomerization takes place efficiently. The observation that Q_2 involves in fact two transitions similar in energy (Fig. 7b), together with the computational TD-DFT results indicating that the S_2 states of the two isomers are close in energy, allows us to assign Q_2 to the $S_0 \rightarrow S_2$ (0, 0) electronic transition for *both* isomers. The temperature effects on the emission spectra at Q_2 (λ_{exc} = 586 nm; Fig. 6a) confirm that the two possibilities above indeed simultaneously contribute to F_1, and that the ***trans*-2** to ***trans*-1** conversion from S_2 is still uphill, although it is more efficient than from the S_1 state. As an aside, Q_1, Q_3 and Q_5 must then be assigned to vibrational overtones of the corresponding electronic transitions, as is usually observed in the electronic spectra of porphycenes.[19]

Comparison with 9-acetoxy-2,7,12,17-tetraphenylporphycene. Observation of Fig. 2 indicates only a modest energy difference between the ***trans*-2**-bands and the absorption profile

of 9-AcOTPPo, but a remarkable shift of ***trans*-1** absorption to the red. Because 9-AcOTPPo is paradigmatic of non-electronic but asymmetry effects on the spectral properties of a TPPo core, it is safe to conclude that this shift to the red must be caused by electronic stabilization of the S_1 electronic state of ***trans*-1** due to the amino group. This was further examined by exploring the effect of changing the solvent polarity. No significant absorption or emission shifts were observed for any of the bands but the steady state fluorescence intensity and the decay kinetics turned out to be highly solvent dependent (Table S1 in the ESI†). F_1 showed no significant correlation with none of the usual solvatochromic parameters α, β and π^*, while F_2 was clearly deactivated in solvents of higher polarity and H-bond accepting capacity (Table 2 in the ESI†). Similar trends can be observed in the decay lifetimes. It would thus seem that the decay of ***trans*-1**, but not of ***trans*-2**, is mediated by H-bonding with solvent molecules.

Fig. 8 summarizes our findings and attempts to provide a fairly complete picture of the Q states energies of both ***trans*-1** and ***trans*-2** tautomers and their conversions.

As a final comment, analysis of the $S_0 \rightarrow S_1$ and $S_0 \rightarrow S_2$ transitions in terms of the Gouterman's 4-orbital model[20] using the calculated LUMO + 1, LUMO, HOMO and HOMO − 1 orbitals reveals that after the 9-amino symmetry breakdown, orbital topologies are no longer governed by the relative position of the inner-cavity hydrogen atoms but by the position of the amino group. A striking consequence is that the $S_0 \rightarrow S_1$ and $S_0 \rightarrow S_2$ dipole moments do not change direction upon tautomerization (Fig. 8), the 9-amino group thus acting as an orbital-topology anchoring point. A recent report indicates that the polarity introduced by oxygen atoms in a 9-acetoxyporphycene reduces the angle between the transition dipole moment of the two tautomers from the typical *ca.* 90° of symmetric porphycenes to 50°.[21] It therefore supports our expectation that the more polar amino group further reduces this angle. It would be interesting to seek experimental confirmation of this prediction.[22–24]

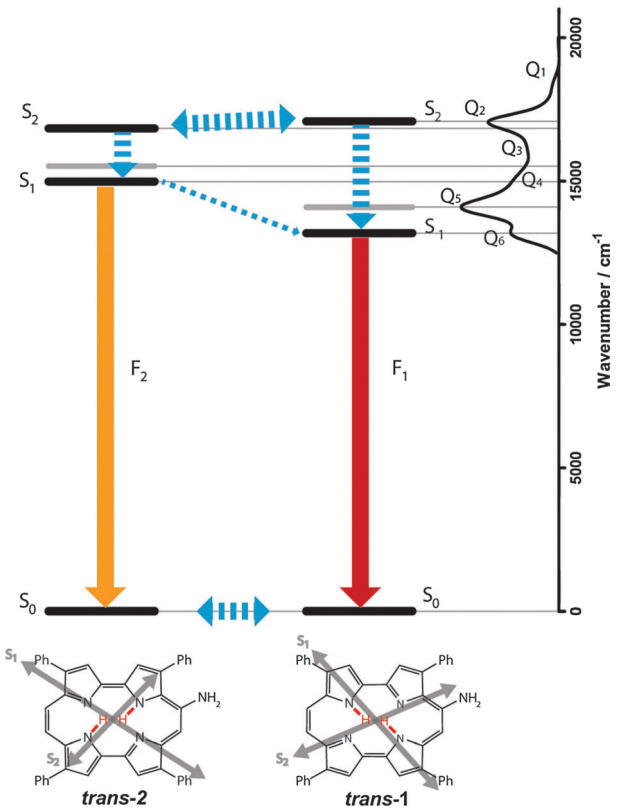

Fig. 8 Proposed diagram for the dual-emission process in 9-ATPPo in toluene. Dashed arrows represent non-radiative conversions. Continuous lines stand for fluorescence decays. The grey arrows at the bottom represent projections of the $S_0 \rightarrow S_1$ and $S_0 \rightarrow S_2$ transition dipole moments on the planes of the macrocycles.

5. Conclusions

The absorption spectrum of 9-ATPPo has been shown to be composed by overlapped absorption spectra of two equally-populated *trans* tautomers with very different energies in the first excited singlet state. The presence of the amino group is spectroscopically irrelevant for one of the tautomers while for the other it induces a remarkable shift to the red in the absorption and emission spectra owing to the selective stabilization of its singlet excited state. Temperature effects on spectra have proved that the essentially unidirectional *trans–trans* tautomerism in the excited states is not a downhill conversion but follows a thermally activated pathway. Careful observation of excitation spectra showed that such a conversion is effortlessly feasible in the S_2 state, which turned out to have similar energies in both tautomers. Overall, these findings provide good proof that introduction of amino groups in porphycenes may be a convenient way to gain a deeper insight into the tautomerization mechanisms in this macrocyclic core.

Acknowledgements

This work was supported by a grant of the Spanish Ministerio de Ciencia e Innovación (CTQ2007-67763-C03-01/BQU). M.D. and R.T. thank the Comissionat per a Universitatsi Recerca del Departamentd'Innovació, Universitats i Empresa de la Generalitat de Catalunya and the European Social Fund for their fellowships.

References

1 S. E. Braslavsky, M. Mueller, D. O. Martire, S. Poerting, S. G. Bertolotti, S. Chakravorti, G. Koc-Weier, B. Knipp and K. Schaffner, *J. Photochem. Photobiol., B*, 1997, **40**, 191–198.
2 J. C. Stockert, *Curr. Med. Chem.*, 2007, **14**, 997–1026.
3 C. Richert, J. M. Wessels, M. Mueller, M. Kisters, T. Benninghaus and A. E. Goetz, *J. Med. Chem.*, 1994, **37**, 2797–2807.
4 S. Nonell, N. Bou, J. I. Borrell, J. Teixidó, A. Villanueva, A. Juarranz and M. Cañete, *Tetrahedron Lett.*, 1995, **36**, 3405–3408.
5 D. Sánchez-García, J. I. Borrell, X. Batllori, J. Teixidó, X. Tomás and S. Nonell, *J. Porphyrins Phthalocyanines*, 2009, **13**, 528–536.
6 O. Arad, N. Rubio, D. Sánchez-García, J. I. Borrell and S. Nonell, *J. Porphyrins Phthalocyanines*, 2009, **13**, 371–381.
7 E. Vogel, M. Mueller, O. Halpern and A. D. Cross, Cytopharm, Inc. USA. 96-US4177(9631452), 30.10-10-1996. WO. 4-4-1996.
8 J. Waluk, *Acc. Chem. Res.*, 2006, **39**, 945–952.
9 M. Gil and J. Waluk, *J. Am. Chem. Soc.*, 2007, **129**, 1335–1341.
10 M. Gil, J. Jasny, E. Vogel and J. Waluk, *Chem. Phys. Lett.*, 2000, **323**, 534–541.
11 M. K. Abdel-Latif and O. Kühn, *Theor. Chem. Acc.*, 2011, **128**, 307–316.

12 J. Wan, Y. Ren, J. Wu and X. Xu, *J. Phys. Chem. A*, 2004, **108**, 9453–9460.
13 A. L. Sobolewski, M. Gil, J. Dobkowski and J. Waluk, *J. Phys. Chem. A*, 2009, **113**, 7714–7716.
14 M. J. Frisch, G. W. Trucks, H. B. Schlegel, G. E. Scuseria, M. A. Robb, J. R. Cheeseman, J. A. Montgomery, Jr., T. Vreven, K. N. Kudin, J. C. Burant, J. M. Millam, S. S. Iyengar, J. Tomasi, V. Barone, B. Mennucci, M. Cossi, G. Scalmani, N. Rega, G. A. Petersson, H. Nakatsuji, M. Hada, M. Ehara, K. Toyota, R. Fukuda, J. Hasegawa, M. Ishida, T. Nakajima, Y. Honda, O. Kitao, H. Nakai, M. Klene, X. Li, J. E. Knox, H. P. Hratchian, J. B. Cross, V. Bakken, C. Adamo, J. Jaramillo, R. Gomperts, R. E. Stratmann, O. Yazyev, A. J. Austin, R. Cammi, C. Pomelli, J. W. Ochterski, P. Y. Ayala, K. Morokuma, G. A. Voth, P. Salvador, J. J. Dannenberg, V. G. Zakrzewski, S. Dapprich, A. D. Daniels, M. C. Strain, O. Farkas, D. K. Malick, A. D. Rabuck, K. Raghavachari, J. B. Foresman, J. V. Ortiz, Q. Cui, A. G. Baboul, S. Clifford, J. Cioslowski, B. B. Stefanov, G. Liu, A. Liashenko, P. Piskorz, I. Komaromi, R. L. Martin, D. J. Fox, T. Keith, M. A. Al Laham, C. Y. Peng, A. Nanayakkara, M. Challacombe, P. M. W. Gill, B. Johnson, W. Chen, M. W. Wong, C. Gonzalez and J. A. Pople, *Gaussian 03, Revision C.02*, Gaussian, Inc.,Wallingford, CT, 2004.
15 Y.-D. Wu, K. W. K. Chan, C.-P. Yip, E. Vogel, D. A. Plattner and K. N. Houk, *J. Org. Chem.*, 1997, **62**, 9240–9250.
16 S. Völker and J. H. van der Waals, *Mol. Phys.*, 1976, **32**, 1703–1718.
17 M. Uttamlal and A. S. Holmes-Smith, *Chem. Phys. Lett.*, 2008, **454**, 223–228.
18 M. Gil, J. Dobkowski, G. Wiosna-Sałyga, N. Urbańska, P. Fita, C. Radzewicz, M. Pietraszkiewicz, P. Borowicz, D. Marks, M. Glasbeek and J. Waluk, *J. Am. Chem. Soc.*, 2010, **132**, 13472–13485.
19 J. Waluk, M. Muller, P. Swiderek, M. Kocher, E. Vogel, G. Hohlneicher and J. Michl, *J. Am. Chem. Soc.*, 1991, **113**, 5511–5527.
20 M. Gouterman, G. H. Wagnière and L. C. Snyder, *J. Mol. Spectrosc.*, 1963, **11**, 108–127.
21 P. Fita, P. Garbacz, M. Nejbauer, C. Radzewicz and J. Waluk, *Chem.–Eur. J.*, 2011, **17**, 3672–3678.
22 H. Piwoński, C. Stupperich, A. Hartschuh, J. Sepioł, A. Meixner and J. Waluk, *J. Am. Chem. Soc.*, 2005, **127**, 5302–5303.
23 H. Piwoński, A. Hartschuh, N. Urbanska, M. Pietraszkiewicz, J. Sepioł, A. J. Meixner and J. Waluk, *J. Phys. Chem. C*, 2009, **113**, 11514–11519.
24 A. M. Chizhik, R. Jäger, A. I. Chizhik, S. Bär, H.-G. Mack, M. Sackrow, C. Stanciu, A. Lyubimtsev, M. Hanack and A. J. Meixner, *Phys. Chem. Chem. Phys.*, 2011, **13**, 1722–1733.

Bibliografia

[1] D. Voet, J.G. Voet. *Bioquímica.* Ed. Médica Panamericana S.A., **2006**.

[2] J. Wang, P. Cieplak, P.A. Kollman. How well does a restrained electrostatic potential (RESP) model perform in calculating conformational energies of organic and biological molecules? *J. Comput. Chem.*, 21:1049–1074, **2000**.

[3] J. Fabricius, S.B. Engelsen, K. Rasmussen. The consistent force field. 5. PEF95SAC: Optimized potential energy function for alcohols and carbohydrates. *J. Carbo. Chem.*, 16:751–772, **1997**.

[4] L. de Broglie. The reinterpretation of wave mechanics. *Foundations of physics*, 1(1):5–15, **1970**.

[5] W.R. Hamilton. A second essay on a general method in dynamics. *Philos. Trans. R. Soc. London*, 124:247–308, **1835**.

[6] R. Carbó-Dorca. Conèixer la matèria: la química quàntica, *Desafiaments del segle XXI. La veu de la ciència*, Residència d'Investigadors, Barcelona, **2010**.

[7] R.S. Mulliken. Spectroscopy, molecular orbitals and chemical bonding. *Science*, 157(3784):13–24, **1967**.

[8] C. Moller, M. Plesset. Note on an approximation treatment for many-electron systems. *Phys. Rev.*, 46(7):618–622, **1934**.

[9] M. Häser. Moller-plesset (MP2) perturbation theory for large molecules. *Theor. Chem. Accounts: Theory, Computation and Modeling*, 87(1-2):147–173, **1993**.

[10] T. Ziegler. Approximate density functional theory as a practical tool in molecular energetics and dynamics. *Chem. Rev.*, 91(5):651–667, **1991**.

[11] P. Hohenberg, W. Kohn. Inhomogeneous electron gas. *Phys. Rev. B*, 136(3B):864–871, **1964**.

[12] P. Hohenberg, W. Kohn, L.J. Sham. The beginnings and some thoughts on the future. *Adv. Quantum Chem.*, 21:7–26, **1990**.

[13] A.D. Becke. Density-functional thermochemistry. III. The role of exact exchange. *J. Chem. Phys.*, 98(7):5648–5652, **1993**.

[14] A.D. Becke. A new mixing of Hartree-Fock and local density-functional theories. *J. Chem. Phys.*, 98(2):1372–1377, **1993**.

[15] A.F. Jalbout, F. Nazari, L. Turker. Gaussian-based computations in molecular science. *J. Mol. Structure*, 671:1–21, **2004**.

[16] A. G. Kutateladze, editor. *Computational Methods in Photochemistry*. Taylor & Francis, **2005**.

[17] J. Stewart. Optimization of parameters for semiempirical methods.II. Applications. *J. Comput. Chem.*, 10(2):221–264, **1989**.

[18] M. Dewar, E. Zoebisch, H. Eamonn, J. Stewart. Development and use of quantum mechanical molecular models. AM1: a new general purpose quantum mechanical molecular model. *J. Am. Chem. Soc.*, 115(12):5348, **1993**.

[19] J.C. Paniagua, P. Alemany. *Química Quàntica, Elements de la Química Física*, vol.3. Llíbres de l'Índex. Universitat, Barcelona, **1999**.

[20] J. Gasteiger. History and challenges of chemoinformatics, *Strasbourg Summer School on Chemoinformatics*, Obernai, France, **2008**.

[21] S. Renner, M. Hechenberger, T. Noeske, A. Böcker, C. Jatze, M. Schmuker, C.G. Parsons, T. Weil, G. Schneider. Searching for drug scaffolds with 3D pharmacophores and neural networks ensembles. *Angew. Chem. Int. Ed.*, 46:5336–5339, **2007**.

[22] C.L. Bruce, J.L. Melville, S.D. Pickett, J.D. Hirst. Contemporary QSAR classifiers compared. *J. Chem. Inf. Model.*, 47:219–227, **2007**.

[23] P. Mazzatorta, L. Tran, B. Schilter, M. Grigorov. Integration of structure-actvity relationship and artificial intelligence systems to improve in silico prediction of Ames test mutagenicity. *J. Chem. Inf. Model.*, 47:34–38, **2007**.

[24] N. Schneider, C. Jäckels, C. Andres, M.C. Hutter. Gradual in silico filtering for druglike substances. *J. Chem. Inf. Model.*, 48(3):613–628, **2008**.

[25] R. Todeschini, V. Consonni. *Molecular Descriptors for Chemoinformatics*. WILEY-VCH, Weinheim, **2009**.

[26] Inc. ChemicalComputingGroup. Molecular operating environment (MOE), v.2010.10, **2010**.

[27] L.P. Hammett. Some relations between reaction rates and equilibrium constants. *Chem. Rev.*, 17(1):125–136, **1935**.

[28] L.P. Hammett. The effect of structure upon the reactions of organic compounds. benzene derivatives. *J. Am. Chem. Soc.*, 59(1):96–103, **1937**.

[29] R.W. Taft. Linear free energy relationships from rates of esterification and hydrolysis of aliphatic and ortho-substituted benzoate esters. *J. Am. Chem. Soc.*, 74(11):2729–2732, **1952**.

[30] C. Hansch. A quantitative approach to biochemical structure-activity relationships. *Acct. Chem. Res.*, 2:232–239, **1969**.

[31] C. Hansch, A. Leo. *Exploring QSAR. Fundamentals and Applications in Chemistry and Biology*. ACS Professional Reference Book. American Chemical Society, **1995**.

[32] H. Kubinyi. Free wilson analysis. Theory, applications and its relationship to Hansch analysis. *Quantitative Structure-Activity Relationships*, 7(3):121–133, **1988**.

[33] J.J. Sutherland, L.A. O'Brien, D.F. Weaver. A comparison of methods for modeling quantitative structure-activity relationships. *J. Med. Chem.*, 47:5541–5554, **2004**.

[34] T.A. Andrea, H. Kalayeh. Applications of neural networks in quantitative structure-activity relationships of dihydrofolate reductase inhibitors. *J. Med. Chem.*, 34:2824–2836, **1991**.

[35] R.W. Howard. On what intelligence is. *Br. J. Psychol.*, 84:27–37, **1993**.

[36] R. Penrose. *Las sombras de la mente*. Ed. Crítica, Madrid, **2007**.

[37] C. Eliasmith. How to build a brain: from function to implementation. *Synthese*, 159(3):373–388, **2007**.

[38] Laboratory of Neuro Imaging(UCLA) and Martinos Center for Biomedical Imaging (Massachusetts General Hospital). Human connectome project.

[39] H. Markram. The blue brain project. *Nature Reviews Neuroscience*, 7:153–160, **2006**.

[40] H. Aréchiga. Evolucion de los conceptos sobre el funcionamiento cerebral. *Revista de la Reial Acadèmia de Medicina de Catalunya*, 12(S1):7–30, **1998**.

[41] S. Russell, P. Norvig. *Inteligencia Artificial: Un enfoque moderno*. Prentice Hall, **1996**.

[42] J. Aubin. *Neural Networks and Qualitatuve Physics*. Cambridge University Press, New York, **1996**.

[43] M.T. Spining, J.A. Darsey, B.G. Sumpter, D.W. Noid. Opening up the black box of artificial neural networks. *J. Chem. Education*, 71(5):406–411, **1994**.

[44] L. Terfloth, J. Gasteiger. Neural networks and genetic algorithms in drug design. 6(15):S102–S108, **2001**.

[45] M. Jalali-Heravi, ParastarF. Use of artificial neural networks in a QSAR study of anti-HIV activity for a large group of HEPT derivatives. *J. Chem. Inf. Comput. Sci.*, 40:147–154, **2000**.

[46] J. Gasteiger , J. Zupan. Neural networks in chemistry. *Angew. Chem. Int. Ed. Engl.*, 32:503–552, **1993**.

[47] A.K. Jain, J. Mao. Artificial neural networks: A tutorial. *IEEE Computer Society*, pp. 31–44, **1996**.

[48] S. Haykin. *Neural Networks: A Comprehensive Foundation*. Prentice Hall, 2 ed., **1998**.

[49] K. Dasgupta, S. Bhattacharyya, P. Dutta. A three-dimensional self-organizing neural network architecture for three-dimensional object extraction from noisy perspective. *International Conference on Advanced Computing*, pp. 141–147, **2009**.

[50] J. Zupan, J. Gasteiger. Neural networks: A new method for solving chemical problems or just a passing phase? *Anal. Chim. Acta*, 248:1–30, **1991**.

[51] I.V. Tetko, D.J. Livingstone, A. Luik. Neural network studies. 1. Comparison of overfitting and overtraining. *J. Chem. Inf. Comput. Sci.*, 35:826–833, **1995**.

[52] S. Trenn. Multilayer perceptrons: Approximation order and necessary number of hidden units. *IEEE Trans. Neural Networks*, 19(5):836–844, **2008**.

[53] J. Sjöberg, L. Ljung. Overtraining regularization and searching for a minimum, with application to neural networks. *Int. J. of Control*, 62(6):1391–1407, **1995**.

[54] C.L. Giles, C.W. Omlin. Pruning recurrent neural networks for improving generalisation performance. *IEEE Transactions on Neural Networks*, 5:848–851, **1994**.

[55] J. Wu, J. Mei, S. Wen, LiaoS., J. Chen, Y. Shen. A self-adaptive genetic algorithm-artificial neural network algorithm with leave-one-out cross validation for descriptor selection in QSAR study. *J. Comput. Chem.*, 31(10):1957–1968, **2010**.

[56] T. Kohonen. *Self Organization and Associative Memory.* Springer-Verlag, New York, **1989**.

[57] J. Gasteiger, T. Engel. *Chemoinforatics.* Wiley-VCH, Weinheim, **2003**.

[58] D. Kaiser, L. Terfloth, S. Kopp, J. Schulz, R. de Laet, P. Chiba, G.F. Ecker, J. Gasteiger. Self-organizing maps for identification of new inhibitors of p-glycoprotein. *J. Med. Chem.*, 50:1698–1702, **2007**.

[59] Y. Xiao, R. Harris, E. Bayram, P. Santago, J.D. Schmidtt. Supervised self-organizing maps in drug discovery. 2. Improvements in descriptor selection and model validation. *J. Chem. Inf. Model.*, 46:137–144, **2006**.

[60] E. Arsuaga, F. Díaz. Topology preservation in SOM. *World Academy of Science Engineering and Technology*, 15:52–55, **2006**.

[61] J. Gola, O. Obrezanova, E. Champness, and M. Segall. ADMET property prediction: The state of art and current challenges. *QSAR Comb. Sci.*, 25(12):1172–1180, 2006.

[62] D.B. Fogel, R.W. Anderson. Revisiting Bremermann's genetic algorithm. Simultaneous mutation of all parameters. *Proc. 2000 Congress on Evolutionary Computation*, pp. 1204–1209, 2000.

[63] H.J. Bremermann. *The evolution of intelligence: The nervous system as a model of its environment*, vol. 477. Univ. Washington, Seattle, **1958**.

[64] D. Beasley, D.R. Bull, R.R. Martin. An overview of genetic algorithm: Part 1, fundamentals. *University Computing*, 15(2):58–69, **1993**.

[65] D.E. Goldberg. *Genetic Algorithms in Search, Optimization and Machine Learning*. Addison-Wesley, **1989**.

[66] R.E. Shaffer, G.W. Small. Learning optimization from nature. *Analytical Chemistry*, 69(7):236A–242A, **1997**.

[67] D.E. Goldberg. Not Your Grandmother's Genetic Algorithm, La Salle (URL), Barcelona, **2008**.

[68] R. Tejedor-Estrada. Implementació d'algorismes genètics en el programari PRALINS per a la selecció de quimioteques. *Treball final de carrera*, **2006**.

[69] Dopazo, J. Búsqueda de SNPs funcionales para estudios de genotipado de alto rendimiento, *II Reunión Nacional de Modelización Molecular y Quimioinformática (MMQ2005)*, Barcelona, **2005**.

[70] K.A. de Jong. An analysis of the behavior of a class of genetic adaptive systems. *College of Engineering, Technical Reports*, University of Michigan, **1975**.

[71] R. Pascual, J.I. Borrell, J. Teixidó. Analysis of selection methodologies for combinatorial library design. *Mol. Divers.*, 6:121–133, **2003**.

[72] S. Pettersson, V.I. Pérez-Nueno, L. Ros-Blanco, R. Puigdelabellacasa, O. Rabal, X. Batllori, B. Clotet, I. Clotet-Codina, M. Armand-Ugón, J.A. Esté, J.I. Borrell, J. Teixidó. Discovery of novel non-cyclam polynitrogenated CXCR4 coreceptor inhibitors. *Chem. Med. Chem.*, 3:1549–1557, **2008**.

[73] J.T. Souza, S. Matwin, N. Japkowicz. Evaluating data mining models: A pattern language. *9th Conference on Pattern Language of Programs*, **2002**.

[74] L. Douali, D. Villemin, D. Cherqaoui. Neural networks: Accurate nonlinear QSAR model for HEPT derivatives. *J. Chem. Inf. Comput. Sci.*, 43:1200–1207, **2003**.

[75] S. So, S.P. van Helden, V.J. vanGeerestein, M. Karplus. Quantitative structure-activity relationship studies of progesterone receptor binding steroids. *J. Chem. Inf. Comput. Sci.*, 40(1):762–772, **2000**.

[76] Microsoft Corporation. Visual studio 2010. v.10.0.30319.1, **2010**.

[77] Jmol: un visor java de código abierto para estructuras químicas en tres dimensiones. http://www.jmol.org/.

[78] C. Tumuluri, P.K. Varshney. An evidential extension of the MRII training algorithm for detecting erroneous MADALINE responses. *IEEE Transactions on Neural Networks*, 6(4):880–892, **1995**.

[79] J.A. Freeman, D.M. Skapura. *Neural Networks: Algorithms, Applications, and Programming Techniques*. Addison-Wesley, **1992**.

[80] R. Winter, B. Widrow MADALINE RULE II: A Training Algorithm for Neural Networks, *Proc. IEEE 2nd International Conference on Neural Networks*, vol. 1, San Diego, CA, **1988**.

[81] Inc. Chemical Computing Group. Molecular operating environment (MOE), v.2009.10, **2009**.

[82] I. Tetko, V. Tanchuk, N.P. Chentsova, S.V. Antonenko, G. Poda. HIV-1 reverse transcriptase inhibitor design using artificial neural networks. *J. Med. Chem.*, 37:2520–2526, **1994**.

[83] I. Gutman and M. Randic. Algebraic characterization of skeletal branch. *Chem. Phys. Lett.*, 47:15–21, 1977.

[84] J. Burns, D.F. Weaver. A mathematical model for prediction of drug molecule diffusion across the blood-brain barrier. *Can. J. Neurol. Sci.*, 31:520–527, **2004**.

[85] Fisher Scientific. Maybridge, http://www.maybridge.com, **1998**.

[86] Inc. Chemical Computing Group. Molecular operating environment (MOE), v.2007.09, **2007**.

[87] V. Sauri, L. Serrano-Andrés, A. Rehaman, L. Gagliardi, S. Vancoillie, K. Pierloot. Multiconfigurational second-order perturbation theory restricted active space (RASPT2) method for electronic excited states: A benchmark study. *J. Chem. Theory comput.*, 7:153–168, **2011**.

[88] A. Nordqvist, J. Nilsson, T. Lindmark, A. Eriksson, P. Garberg, M. Kihlén. A general model for prediction of CACO-2 cell permeability. *QSAR Comb. Sci.*, 23:303–310, **2004**.

[89] R. Reed. Pruning algorithms - a survey. *IEEE Transactions on Neural Networks*, 4(5):740–747, **1993**.

[90] S. Geman, E. Bienenstock, R. Doursat. Neural networks and the bias/variance dilemma. *Neural Computation*, 4:1–58, **1992**.

[91] S.J. Hanson, L.Y. Pratt. *Comparising biases for minimal network construction with back-propagation.* Advances in Neural Information Processing I. Morgan Kaufmann, **1989**.

[92] X. Yao, M. Islam. Evolving artificial neural networks ensembles. *IEEE Computational Intelligence Magazine*, 3(1):31–42, **2008**.

[93] Sung-Sau So, M. Karplus. Genetic neural networks for quantitative structure-activity relationships: Improvements and application of benzodiazepine affinity for benzodiazepine/GABA receptors. *J. Med. Chem.*, 39:5246–5256, **1996**.

[94] Sung-Sau So, M. Karplus. Three-dimensional quantitative structure-activity relationships from molecular similarity matrices and genetic neural networks. 1. Method and validations. *J. Med. Chem.*, 40:4347–4359, **1997**.

[95] Sung-Sau So, M. Karplus. Evolutionary optimization in quantitative structure-activity relationship: An application of genetic neural networks. *J. Med. Chem.*, 39:1521–1530, **1996**.

[96] M. Dam and D.N. Saraf. Design of neural networks using genetic algorithm for on-line property estimation of crude fractionator products. *Comput. Chem. Engineering*, 30:722–729, 2006.

[97] G. Oyro, L.K. Hansen. Fitness-functions of Generic Algorithms for Optimizing Neural Network topologies, *Proceedings of the Norwegian Signal Processing Symposium*, **1995**.

[98] A.C. Balfagón, A. Serrano-Hernanz, J. Teixidó, R. Tejedor-Estrada. Comparative study of neural networks and least mean square algorithm applied to the optimization of cosmetic formulations. *Int. J. Cosmetic Sci.*, 32(5):376–386, **2010**.

[99] Generalitat de Catalunya Departament d'Educació. Decret 142/2007, de 26 de juny, pel qual s'estableix l'ordenació dels ensenyaments de l'educació primària. *DOGC*, 4915:21822–21870, **2007**.

[100] Euclides. *Elementos. Libro I. Fundamentos de la Geometria: Teoria de los triangulos, paralelas y el área.* Biblioteca Clásica. Gredos, Madrid, 1a ed., **1991**.

[101] University of North Carolina (UNC). Poincaré's disk model for hyperbolic geometry *Math 6118 Non Euclidean Geometry Course*, 9, **2008**.

[102] G.A. Venema. *The Poincaré disk*, vol. 14, Prentice Hall, **2005**.

[103] J. Walter, H. Ritter. On Interactive Visualization of High-dimensional Data using the Hyperbolic Plane, *SIGKDD*, Edmonton, Canadà, **2002**.

[104] D. Bankston, A. Battles, D. Gurney, E.N. Reyes, and C. Steidley. Interfacing visual basic and mathematica to create an application for hyperbolic geometry. *Proc. 2003 American Society for Engineering Education Annual Conference and Exposition*, 2003.

[105] Ungar,A.A. Hyperbolic Trigonometry and its Application in the Poincaré Ball Model of Hyperbolic Geometry, *Proc. of the 4th European SGI/Cray MPP Workshop*, Garching, Germany, **1998**.

[106] J. Girbau. *Geometria Diferencial i Relativitat.* Manuals de la Universitat Autònoma de Barcelona. UAB, Bellaterra, **1993**.

[107] A. Wawrzynczyk. *Geometría de curvas y superfícies.* Anthropos, Mèxic, 1996.

[108] D.C. Royster. Poincaré's Disk Model for Hyperbolic Geometry, *Euclidean Geometry*, 9, **2008**.

[109] H. Liu, D. Song, S. Rüger, R. Hu, V. Uren. Comparing dissimilarity measures for content-based image retrieval. *AIRS*, 4993:44–50, **2008**.

[110] M.A. Johnson, G.M. Maggiora. *Concepts and Applications of Molecular Similarity.* Wiley, **1990**.

[111] J.W. Sammon. A non-linear mapping for data structure analysis. *IEEE Trans. Computers*, 18:401–409, **1969**.

[112] H. Klock, J.M. Buhmann. Multidimensional Scaling by Deterministic Annealing, *Proc. of the EMMCVPR*, Venice, Italy, **1997**.

[113] R.A. Fisher. The use of multiple measurements in taxonomic problems. *Annals of Eugenics*, 7(2):179–188, **1936**.

[114] C.A. Robertson, D. Hawkins, H. Abrahamse. Photodynamic therapy (PDT): A short review on cellular mechanisms and cancer research applications for PDT. *J. Photochem. Photobiol. B*, 96:1–8, **2009**.

[115] E.S. Nyman, P.H. Hynninen. Research advances in the use of tetrapyrrolic photosensitizers for photodynamic therapy. *J. Photochem. Photobiol. B*, 73:1–28, **2004**.

[116] N.L. Oleinick, R.L. Morris, I. Belichenko. The role of apoptosis in response to photodynamic therapy: what, where, why and how. *Photochem. Photobiol. Sci.*, 1:1–21, **2002**.

[117] A. Castano, T. Demidova, M. Hamblin. Mechanisms in photodynamic therapy: Part three - photosensitizer pharmacokinetics, biodistribution, tumor localization and modes of tumor destruction. *Photodiagnosis and Photodynamic Therapy*, 2(2):91–106, **2005**.

[118] J.C. Stockert, M. Cañete, A. Juarranz, A. Villanueva, R.W. Horobin, J.I. Borrell, J. Teixidó, S. Nonell. Porphycenes: Facts and prospects in photodynamic therapy of cancer. *Curr. Med. Chem.*, 14(9):997–1026, **2007**.

[119] T.J. Moan, Q. Peng. *Photodynamic Therapy: An outline of the history of PDT.* Ed. RSC, **2003**.

[120] A. Policard. Etude sur les aspects offerts par des tumeurs experimentales examinées a la lumière de wood. *C. R. Soc. Biol.*, 91:1423–1428, **1924**.

[121] D.S. Rasmussen-Taxdal, G.E. Ward, F.H. Figge. Fluorescence of human lymphatic and cancer tissues following high doses of intravenous hematoporphyrin. *Cancer*, 8:78–81, **1955**.

[122] R.L. Lipson, E.J. Baldes, A.M. Olsen. Hematoporphyrin derivative for detection and management of cancer. *Cancer*, 20:2255–2257, **1967**.

[123] J. Moan, T. Christensen, S. Sommer. The main photosensitizing components of hematoporphyrin derivative. *Cancer Lett.*, 15(2):161–166, **1982**.

[124] T.J. Dougherty. Photosensitizers: therapy and detection of malignant tumors. *Photochem. Photobiol.*, 45:879–889, **1987**.

[125] D. Kessel, P. Thompson. Purification and analysis of hematoporphyrin and hematoporphyrin derivative by gel exclusion and reverse phase chromatography. *Photochem. Photobiol.*, 46:1023–1026, **1987**.

[126] J. Moan, S. Sommer. Uptake of the components of hematoporphyrin derivative by cells and tumors. *Cancer Lett.*, 21:167–174, **1983**.

[127] B.W. Henderson, T.J. Dougherty. How does photodynamic therapy work? *Photochem. Photobiol.*, 55(1):145–157, **1992**.

[128] M. Tronconi, A. Colombo, M. de Cesare, R. Marchesini, K. Woodburn, J.A. Reiss, D.R. Phillips, F. Zunino. Biodistribution of haematoporphyrin analogues in a lung carcinoma model. *Cancer Lett.*, 88(1):41–48, **1995**.

[129] N. Rubio, F. Prat, N. Bou, J.I. Borrell, J. Teixidó, A. Villanueva, A. Juarranz, M. Cañete, J.C. Stockert, S. Nonell. A comparison between the photophysical and photosensitising properties of tetraphenyl porphycenes and porphyrins. *New J. Chem.*, 29:378–384, **2005**.

[130] N. Rubio, D. Sánchez-García, A. Jiménez-Banzo, O. Rey, J.I. Borrell, J. Teixidó, S. Nonell. Effect of aza substitution on the photophysical and electrochemical properties of porphycenes: Characterization of the near-IR-absorbing photosensitizers 2,7,12,17-tetrakis(*p*-substituted phenyl)-1,6,13,16-tetraazaporphycenes. *J. Phys. Chem. A*, 110:3480–3487, **2006**.

[131] S. Nonell, J.I. Borrell, S. Borràs, C. Colomines, O. Rey, N. Rubio, D. Sánchez-García, J. Teixidó. 2,7,12,17-tetra(*p*-butylphenyl)-3,6,13,16-tetraazaporphycene: The first example of a stright-forward synthetic approach to a new class of photosensitizing macrocycles. *Eur. J. Org. Chem.*, (9):1635–1640, **2003**.

[132] O. Rey. *Fototeràpia: Estudi teòric de sistemes d'interès per la Teràpia Fotodinàmica del Càncer i la Reacció de Bergman.* Tesi doctoral, Institut Químic de Sarrià, URL, **2005**.

[133] J. Linnanto, J. Korppi-Tomola. Quantum chemical simulation of excited states of chlorophylls, bacteriochlorophylls and their complexes. *Phys. Chem. Chem. Phys.*, 8(6):667–687, **2006**.

[134] A.C. Pelegrino, M.C. Gotardo, A.R. Simioni, M.D. Assis, A.C. Tedesco. Photophysical properties of crowed porphyrins. *Photochem. Photobiol.*, 81(4):771–776, **2005**.

[135] A.A. Rosenkranz, V.G. Lunin, O.V. Sergienko, D.G. Gilyazova, O.L. Voronina, D.E. Jans, A.A. Kofner, M.A. Shumiantseva, A.F. Mironov, A. Sobolev. Targeted intracellular site-specific drug delivery: Photosensitizer targeting to melanoma cell nuclei. *Russian Journal of genetics*, 39(2):198–206, **2003**.

[136] M. Qualls, D.H. Thompson. Chloroaluminium phtalocyanine tetrasulfonate delivered via acid-labile displasmenylcholine-folate liposomes: intracellular localization and synergistic phototoxicity. *Int. J. Cancer*, 93:384–392, **2001**.

[137] H. Toledano, R. Edrei, S. Kimel. Photodynamic damage by liposome-bound porphycenes : comparison between in vitro and in vivo models. *J. Photochem. Photobiol.B*, 42:20–27, **1998**.

[138] J.A. Hubble. Enchancing drug function. *Science*, 300:595–596, **2003**.

[139] C. Sawyers. Targeted cancer therapy. *Nature*, 432(18):294–297, **2004**.

[140] A.S. Sobolev, D.A. Jans, A.A. Rosenkranz. Targeted intracellular delivery of photosensitizers. *Progress in Biophysics & Molecular Biology*, 73:51–90, **2000**.

[141] C. Colominas, L. Eixarch, P. Fors, K. Lang, S. Nonell, J. Teixidó, F.R. Trull. Conformational folding induced by π-π interaction in a series of flexible dyads consisting of isomeric mesoporphyrin nitrobenzyl esters. *J. Chem. Soc. Perkin Trans. 2*, (5):993–1004, **1996**.

[142] K. Malsch, M. Roeb, V. Karuth, G. Hohlneicher. The importance of electron correlation for the ground state structure of porphycene and tetraoxaporphyrin-dication. *Chemical Physics*, 227(3):331–348, **1998**.

[143] M.J. Frisch, G.W. Trucks, H.B. Schlegel, G.E. Scuseria, M.A. Robb, J.R. Chesseman, J.A. Montgomery, T. Vreven, K.N. Kudin, J.C. Burant, J.M Millam, S.S. Iyengar, J. Tomasi, V. Barone, B. Mennucci, M. Cossi, G. Scalmani, N. Rega, G.A. Petersson, H. Nakatsuji, M. Hada, M. Ehara, K. Toyota, R. Fukuda, J. Hasegawa, M. Ishida, T. Nakajima, Y. Honda, O. Kitao, H. Nakai, M. Klene, X. Li, J.E. Knox, H.P. Hratchian, J.B. Cross, c. Adamo, J. Jaramillo, R. Gomperts, R.E. Stratmann, O. Yazyev, A.J. Austin, R. Cammi, C. Pomelli, J.W. Ochterski, P.Y. Ayala, K. Morokuma, G.A. Voth, P. Salvador, J.J. Dannenbeg, V.G. Zakrzewski, S. Dapprich, A.D. Daniels, M.C. Strain, O. Farkas, D.K. Malick, A.D. Rabuck, K. Raghavachari, J.B. Foresman, J.V. Ortiz, Q. Cui, A.G. Baboul, S. Clifford, J. Cioslowski, B.B. Stefanov, G. Liu, A. Liashenko, P. Piskorz, I. Komaromi, R.L. Martin, D.J. Fox, T. Keith, M.A. Al-Laham, C.Y. Peng, A. Nanayakkara, M. Challacombe, P.M.W. Gill, B. Johnson, W. Chen, M.W. Wong, C. Gonzalez, J.A. Pople. Gaussian 03 (rev.c.02), **2004**.

[144] O. Rey, D. Sánchez-García, S. Nonell, C. Colomines, J. Teixidó, N. Rubio, J.I. Borrell. Estudio teórico de las transiciones electrónicas de sistemas porficénicos y azaporficénicos de interés para la terapia fotodinámica (PDT). *Afinidad*, 62(519):439–447, **2005**.

[145] J.D. Xidos, J. Li, T. Zhu, G.D. Hawkins, S.D. Thompson, Y.Y. Chuang, P.L. Fast, D.A. Liotard, D. Rinaldi, C.J. Cramer, D.G. Truhlar. Gamesol: A module incorporating the SM5.42 solvation models, the CM2 and CM3 charge models, and Löwdin and redistributed Löwdin population analysis in GAMESS, **1998**.

[146] M.W. Schmidt, K.K. Baldridge, J.A. Boatz, S.T. Elbert, M.S. Gordon, J.H. Jensen, S. Koseki, N. Matsunaga, K.A. Nguyen, S. Su, T.L. Windus, M. Dupuis, J.A. Montgomery. General atomic and molecular electronic structure system. *J. Comput. Chem.*, 14:1347–1363, **1993**.

[147] D.A. Case, T.A. Darden, T.E. Cheatham, C.L. Simmerling, J. Wang, R.E. Duke, R. Luo, K.M. Merz, B. Wang, D.A. Pearlman, M. Crowley, S. Brozell, V. Tsui, H. Gohlke, J. Mongan, V. Hornak, G. Cui, P. Beroza, C. Schafmeister, J.W. Caldwell, W.S. Ross, P.A. Kollman. AMBER8, **2004**.

[148] R.H. Hastings, J.R. Wright, K.H. Albertine, R. Ciriales, M.A. Matthay. Effect of endocytosis inhibitors on alveolar clearance of albumin, immunogrobulin GAMMA, and SP-A in rabbits. *Am. J. Physiol.*, 266:L544–L552, **1994**.

[149] L. Petit, A. Quartarolo, C. Adamo, N. Russo. Spectroscopic properties of porphyrin-like photosensitizers: Insights from theory. *J.Phys. Chem B*, 110:2398–2404, **2006**.

[150] A. Domenico, N. Russo, E. Sicilia. Structures and electronic absorption spectra of a recently synthesised class of photodynamic therapy agents. *Chem. Eur. J.*, 12:6797–6803, **2006**.

[151] H.F. Ji, L. Shen. Triplet excited state characters and photosensitization mechanisms of α-terthienyl: A theoretical study. *J. Photochem. Photobiol.B*, 94:51–53, **2009**.

[152] T. Tsuji, M. Onoda, Y. Otani, T. Ohwada, T. Nakajima, K. Hirao. Theoretical study on the excited states of heteroarene chromophores: Comparison of calculated and experimental values. *Chem. Phys. Lett.*, 473(3):196–200, **2009**.

[153] J. Hasegawa, K. Takata, T. Miyahara, S. Neya, M.J. Frisch, H. Nakatsuji. Excited states of porphyrin isomers and porphycene derivatives: A SAC-CI study. *J. Phys. Chem. A*, 109:3187–3200, **2005**.

[154] K. Toyota, J. Hasegawa, H. Nakatsuji. Excited states of free base phtalocyanine studies by the SAC-CI method. *J. Phys. Chem. A*, 101:446–451, **1997**.

[155] P. Cronstrand, O. Christiansen, P. Normann, H. Agren. Theoretical calculations of excited state absorption. *Phys. Chem. Chem. Phys.*, 2:5357–5363, **2000**.

[156] J. Linnato, J. Korppi-Tommola. Semiempirical pm5 molecular orbital study on chlorophylls and bacteriochlorophylls: Comparison of semiempirical, ab initio, and density functional results. *J. Comput. Chem.*, 25(1):123–138, 2004.

[157] I. Baraldi, A. Carnevali, G. Ponterini, and D. Vanossi. Electronic spectrum of porphyrins. CS INDO CI study. *THEOCHEM*, 333(2):121–133, **1995**.

[158] M.C. Zerner, G.H. Loew, R.F. Kirchner, U.T. Mueller-Westerhoff. An intermediate neglect of differential overlap technique for spectroscopy of transition-metal complexes. Ferrocene. *J. Am. Chem. Soc.*, 102(2):589–599, **1980**.

[159] A. Ellervee, J. Linnato, A. Freiberg. Spectroscopic and quantum chemical study of pressure effects on solvated chlorophyll. *Chem. Phys. Lett.*, 394(1):80–84, **2004**.

[160] I. Kövesdi, M.F. Dominguez-Rodriguez, L. Orfi, G. Náray-Szabó, A. Varró, J. Papp, P. Mátyus. Application of neural networks in structure-activity relationships. *Med. Res. Rev.*, 19(3):249–269, **1999**.

[161] B. Buttingsrud, B.K. Alsberg, P. Astrand. Quantitative prediction of the absorption maxima of azobenzene dyes from bond lengths and critical points in the electron density. *Phys. Chem. Chem. Phys.*, 9:2226–2233, **2007**.

[162] S. Banfi, E. Caruso, L. Buccafurni, R. Murano, E. Monti, M. Gariboldi, E. Papa, P. Gramatica. Comparison between 5,10,15,20-tetraaryl- and 5,15-diarylporphyrins as photosensitizers: Synthesis, photodynamic activity and quantitative structure-activity relationship modeling. *J. Med. Chem.*, 49:3293–3304, **2006**.

[163] A.R. Katritzky, A.H. Slavov, D.A. Dobchev, M. Karelson. QSPR modeling of UV absorption intensities. *J. Comput. Aided Mol. Des.*, 21(7):371–377, 2007.

[164] J. Wan, Y. Ren, J. Wu, X. Xu. Time-dependent density functional theory investigation of electronic excited states of tetraoxaporphyrin dictation and porphycene. *J. Phys. Chem. A*, 108:9453–9460, **2004**.

[165] A.L. Sobolewski, M. Gil, J. Dobkowski, J. Waluk. On the origin of radiationless transitions in porphycenes. *J. Phys. Chem. A*, 113(27):7714–7716, **2009**.

[166] S.E. Braslavsky, M. Müller, D.O. Mártire, S. Pörting, S.G. Bertolotti, S. Chakravorti, G. Koç-Weier, B. Knipp, K. Schaffner. Photophysical properties of porphycene derivatices (18π pophyrinoids). *J. Photochem. Photobiol. B*, 40:191–198, **1997**.

[167] C. Richert, J.M. Wessels, M. Müller, M. Kisters, T. Benninghaus, A.E. Goetz. Photodynamic antitumor agents: β-methoxyethyl groups give access to functionalized porphycenes and enhance cellular uptake and activity. *J. Med. Chem.*, 37:2797–2807, **1994**.

[168] C. Abels, S. Karrer, C. Abels, W. Bäumler, M. Landthaler, F. Hofstädter, R. Szeimies. Photosensitization of human skin cell lines by ATMPn (9-acetoxy-2,7,12,17-tetrakis-(β-methoxyethyl)-porphycene) in vitro: mechanism of action. *J. Photochem. Photobiol. B*, 48:27–35, **1999**.

[169] J.J.P. Stewart. *MOPAC Manual.* 7 ed., 1993.

[170] *CRC Handbook of Chemistry and Physics.* CRC Press, 1994.

[171] S. Wildman, G. Crippen. Prediction of physicochemical parameters by atomic contributions. *J. Chem. Inf. Comput. Sci.*, 39:868–873, **1999**.

[172] G. Zheng, W.R. Potter, S.H. Camacho, J.R. Missert, G. Wang, D.A. Bellnier, B.W. Henderson, M.A.J. Rodgers, T.J. Dougherty, R.K. Pandey. Synthesis, photophysial properties, tumor uptake, and preliminary in vivo photosensitizing efficacy of homologous series of 3-(1'-alkyloxy)ethyl-3-devinylpurpurin-18-*n*-alkylimides with variable lipophilicity. *J. Med. Chem.*, 44:1540–1559, **2001**.

[173] G. Li, A. Graham, Y. Chen, M.P. Dobhal, J. Morgan, G. Zheng, A. Kozyrev, A. Oseroff, T.J. Dougherty, R.K. Pandey. Synthesis, comparative photosensitizing efficacy, human serum albumin (site II) binding ability, and intracellular localization characteristics of novel benzobacteriochlorins derived from *vic*-dihydroxybacteriochlorins. *J. Med. Chem.*, 46:5349–5359, **2003**.

[174] M.A. Grin, I.S. Lonin, A.A. Lakhina, E.S. Ol'shanskaya, A.I. Makarov, Y.L. Sebyakin, L.Y. Guryeva, P.V. Toukach, A.S. Kononikhin, V.A. Kuzmin, A.F. Mironov. 1,3-dipolar cycloaddition in the synthesis of glyconconjugates of natural chlorins and bacteriochlorins. *J. Porph. Phthaloc.*, 13:336–345, **2009**.

[175] A. Rocha, A. Serra, M. Pineiro. The small stones of coimbra in the huge tetrapyrrolic chemistry building. *J. Porph. Phthaloc.*, 13:429–445, **2009**.

[176] F. Postigo-Mariscal. *Vehiculización de fotosensibilizadores mediante liposomas. Aplicación a la esterilización fotodinámica de la sangre y a la terapia fotodinámica del cáncer.* Tesi doctoral, Facultat de biologia, Universitat de Barcelona, **2010**.

[177] M. Sibrian-Marquez, J.J. Timothy, H. Vicente. Synthesis and cellular studies of PEG-functionalized meso-tetraphenylporphyrins. *J. Photochem. Photobiol. B*, 86:9–21, 2007.

[178] A. Ofir. Mesures experimentals de l'espectre d'absorció del 9-amino-2,7,12,17-tetrafenilporficè. *Comunicació personal*, **2009**.

[179] Y. You, S.L. Gibson, R. Hilf, S.R. Davies, A. Oseroff, I. Roy, T.Y. Ohulchanskyy, E.J. Bergey, M.R. Detty. Water soluble, core-modified porphyrins. 3. Synthesis, photophysical properties, and in vitro studies of photosensitization, uptake, and localization with carboxylic acid-substituted derivatives. *J. Med. Chem.*, 46:3734–3747, **2003**.

[180] I. Burgés. Síntesi de 2,7,12,17-tetrakis(*m*-hidroxifenil)porficè i compostos relacionats. *Comunicació personal*, **2009**.

[181] M. Duran. Abnormal spectroscopic properties of 9-amino-2,7,12,17-tetraphenylporphycene. *Comunicació personal*, **2010**.

[182] M.J. Frisch, G.W. Trucks, H.B. Schlegel, G.E. Scuseria, M.A. Robb, J.R. Cheeseman, G. Scalmani, V. Barone, B. Mennucci, G.A. Petersson, H. Nakatsuji, M. Caricato, X. Li, H.P. Hratchian, A.F. Izmaylov, J. Bloino, G. Zheng, J.L. Sonnenberg, M. Hada, M. Ehara, K. Toyota, R. Fukuda, J. Hasegawa, M. Ishida, T. Nakajima, Y. Honda, O. Kitao, H. Nakai, T. Vreven, J.A. Montgomery, Jr., J.E. Peralta, F. Ogliaro, M. Bearpark, J.J. Heyd, E. Brothers, K.N. Kudin, V. Staroverov, R. Kobayashi, J. Normand, K. Raghavachari, A. Rendell, J.C. Burant, S.S. Iyengar, J. Tomasi, M. Cossi, N. Rega, N.J. Millam, M. Klene, J.E. Knox, J.B. Cross, V. Bakken, C. Adamo, J. Jaramillo, R. Gomperts, R.E. Stratmann, O. Yazyev, A.J. Austin, R. Cammi, C. Pomelli, J.W. Ochterski, R.L. Martin, K. Morokuma, V.G. Zakrzewski, G.A. Voth, P. Salvador, J.J. Dannenberg, S. Dapprich, A.D. Daniels, Ö. Farkas, J.B. Foresman, J.V. Ortiz, J. Cioslowski, D.J. Fox. Gaussian 09 (rev.b.01), **2009**.

[183] Inc. Hypercube. Hyperchem(TM) professional 7.

[184] P. Labute. Low mode MD - implicit low mode velocity filtering applied to conformational search of macrocycles and protein loops. *J. Chem. Inf. Model.*, 50:792–800, 2010.

[185] H. Shimakoshi, T. Baba, Y. Iseki, I. Aritome, A. Endo, C. Adachi, Y. Hisaeda. Photophysical and photosensitizing properties of brominated porphycenes. *Chem. Comm.*, 2882–2884, **2008**.

[186] T. Sarma, P.K. Panda, P.T. Anusha, S.V. Rao. Dinaphthoporphycenes: synthesis and nonlinear optical studies. *Organic Letters*, 13(2):188–191, **2011**.

[187] D. Kuzuhara, H. Yamada, K. Yano, T. Okujima, S. Mori, H. Uno. First synthesis of dodecasubstituted porphycenes. *Chemistry*, 17(12):3376–3383, **2011**.

[188] K.S. Anju, S. Ramakrishnan, A.P. Thomas, E. Suresh, A. Srinivasan. 9,10,19,20-tetraarylporphycenes. *Organic Letters*, 10(24):5545–5548, **2008**.

[189] D. Sánchez-García, J.I. Borrell, S. Nonell. One-pot synthesis of substituted 2,2'-bipyrroles. A straightforward route to aryl porphycenes. *Organic Letters*, 11(1):77–79, **2009**.

[190] M. Duran-Frigola, R. Tejedor-Estrada, D. Sánchez-García, and S. Nonell. Dual fluorescence in 9-amino-2,7,12,17-tetraphenylporphycene. *Phys. Chem. Chem. Phys.*, 13:10326–10332, **2011**.

[191] M. Gil, J. Jasny, E. Vogel, J. Waluk. Ground and excited state tautomerization in 9-acetoxy-2,7,12,17-tetra-*n*-propylporphycene. *Chem. Phys. Lett.*, 323:534–541, **2000**.

[192] H. Piwonski, C. Stupperich, A. Hartschuh, J. Sepiol, A. Meixner, J. Waluk. Imaging of tautomerism in a single molecule. *J. Am. Chem. Soc.*, 127:5302–5303, **2005**.

[193] A. Vdovin, J. Sepiol, N. Urbanska, M. Pietraszkiewicz, A. Mordzinski, J. Waluk. Evidence for two forms, double hydrogen tunneling, and proximity of excited states in bridge-substituted porphycenes: Supersonic jet studies. *J. Am. Chem. Soc.*, 128:2577–2586, **2006**.

[194] M. Gouterman, G.H. Wagnière, L.C. Snyder. Spectra of porphyrins: Part II. four orbital model. *J. Molecular Spectroscopy*, 11(6):108–127, **1963**.

[195] K. Woodburn, N.J. Vardaxis, J.S. Hill, A.H. Kaye, D.R. Phillips. Subcellular localization of porphyrins using confocal laser scanning microscopy. *Photochem. Photobiol.*, 54(5):725–732, **1991**.

[196] L. Rao, D. Perez, E. White. Lamin proteolysis facilitates nuclear events during apoptosis. *J. Cell Biol.*, 135(6):1441–1455, **1996**.

[197] P. Margaron, M. Grégoire, V. Scasnár, H. Ali, J.E. Lier. Structure-photodynamic activity relationships of a series of 4-substituted zinc phthalocyanines. *Photochem. Photobiol.*, 63(2):217–223, **1996**.

[198] B.W. Henderson, D.A. Bellnier, W.R. Greco, A. Sharma, R.K. Pandey, L.A. Vaughan, K.R. Weishaupt, T.J. Dougherty. An in vivo quantitative structure-activity relationship for a congeneric series of pyropheophorbide derivatives as photosensitizers for photodynamic therapy. *Cancer Res.*, 57:4000–4007, **1997**.

[199] R. Vanyúr, K. Héberger, I. Kövesdi, J. Jakus. Prediction of tumoricidal activity and accumulation of photosensitizers in photodynamic therapy using multiple linear regression and artificial neural networks. *Photochem. Photobiol.*, 75(5):471–478, **2002**.

[200] P. Gramatica, E. Papa, S. Banfi, E. Caruso. QSAR Modeling and Prediction of Tumoricidal Activity of Aryl-Porphyrins in Photodynamic Therapy *11th Congress of the European Society for Photobiology*,Aix-les-Bains, France 2005.

[201] C. Hansch, A. Leo. *Exploring QSAR, Fundamentals and Applications in Chemistry and Biology*. ACS, Washington, **1995**.

[202] R. Todeschini, V. Consonni. *Handbook of Molecular Descriptors.* Wiley-VCH,Weinheim, Germany, **2000**.

[203] T. Fujita, J. Iwasa, C. Hansch. A new substituent constant derived from partition coefficients. *J. Am. Chem. Soc.*, 86:5175–5180, **1964**.

[204] P. Broto, G. Moreau, C. Vandycke. Molecular structures: Perception, autocorrelation descriptor and SAR studies. *Eur.J. Med. Chem.*, 19:71–78, **1984**.

[205] V.N. Viswanadhan, A.K. Ghose, G.R. Revankar, R.K. Robins. Atomic physicochemical parameters for three dimensional structure directed quantitative structure-activity relationships. 4. Additional parameters for hydrophobic and dispersive interactions and their application for an automated superposition of certain naturally occurring nucleoside antibiotics. *J. Chem. Inf. Comput. Sci.*, 29(3):163–172, **1989**.

[206] I.V. Tetko, G.I. Poda. *Prediction of logP with property-based methods.* Drug Properties - Measurement and Prediction. Wiley-VCH, Weinheim, Germany, **2008**.

[207] Y. Sakuratani, K. Kasai, Y. Noguchi, J. Yamada. Comparison of predictivities of logP calculation models based on experimental data for 134 simple organic compounds. *QSAR Comb. Sci.*, 26(1):109–116, **2007**.

[208] I.V. Tetko, V.Y. Tanchuk, A.E. Villa. Prediction of n-octanol/water partition coefficients from PHYSPROP database using artificial neural networks and e-state indices. *J. Chem. Inf. Comput. Sci.*, 41(5):1407–1421, **2001**.

[209] T. Cheng, Y. Zhao, X. Li, F. Lin, Y. Xu, X. Zhang, Y. Li, R. Wang, L.Lai. Computation of octanol-water partition coefficients by guiding an additive model with knowledge. *J. Chem. Inf. Model.*, 47(6):2140–2148, **2007**.

[210] G. Kellogg, D. Abraham. Hydrophobicity: is logP(o/w) more than the sum of its parts? *Eur. J. Med. Chem.*, 35:651–661, **2000**.

[211] S. Ben-Dror, I. Bronshtein, A. Wiehe, B. Röder, M.O. Senge, B. Ehrenberg. On the correlation between hydrophobicity, liposome binding and cellular uptake of porphyrin sensitizers. *Photochem. Photobiol.*, 82:695–701, **2006**.

[212] A. Sholto, B. Ehrenberg. Hydrophobicity, topography in membranes and photosensitization of silicon phthalocyanines with axial ligands of varying lengths. *Photochem. Photobiol. Sci.*, 7(3):344–351, **2008**.

[213] N. Sabaté. Mesures experimentals del logP mitjançant mètodes cromatogràfics. *Comunicació personal*, **2008**.

[214] OECD Guide line for Testing of Chemicals. Partition coefficient (n-octanol/water), high performance liquid chromatography (HPLC) method. *Council on 30th March*, 117, **1989**.

[215] R. Put, Y. Van der Heyden. Review on modelling aspects in reversed-phase liquid chromatographic quantitative structure-retention relationships. *Anal. Chim. Acta*, 602(2):164–172, **2007**.

[216] Inc. StatPoint Technologies. Statgraphics 5.1.

[217] I.V. Tetko, J. Gasteiger, R. Todeschini, A. Mauri, D. Livingstone, P. Ertl, V.A. Paluyulin, E.V. Radchenko, N.S. Zefirov, A.S. Makarenko, V.Y. Tanchuk, V.V. Prokopenko. Virtual computational chemistry laboratory - design and description. *J. Comput. Aid. Mol. Des.*, 19:453–463, **2005**.

[218] Virtual Computational Chemistry Laboratory. VCCLAB, http://www.vcclab.org, **2005**.

[219] V. Consonni, D. Ballabio, R. Todeschini. Comments on the definition of the Q^2 parameter for QSAR validation. *J. Chem. Inf. Model.*, 49:1669–1678, **2009**.

[220] G. Meng, B.R. James, M. Korbelik, K.A. Skov. Porphyrin chemistry pertaining to the design of anticancer drugs. Part 2, the synthesis and in vitro tests of water-soluble porphyrins containing, in the meso positions, the functional groups: 4-mehtylpyridinium, or 4-sulfonatophenyl, in combination with phenyl, 4-pyridyl, 4-nitrophenyl, or 4-aminophenyl. *Cancer J. Chem.*, 72:2447–2457, **1994**.

[221] C. Drain, X. Gong, V. Ruta, C. Soll, P. Chiccoineau. Combinatorial synthesis and modification of functional porphyrin libraries; identification of new, amphipatic motifs for biomolecule binding. *J. Comb. Chem.*, 1(4):286–290, **1991**.

[222] H. Li, Z. Cao, H. Xiao. Synthesis of lactosylated piperazinyl porphyrins and their hepatocyte-selective targeting. *Med. Chem. Res.*, 16:28–38, **2007**.

[223] E. Milanesio, G. Alvarez, S. Bertolotti, E. Durantini. Photophysical characterization and photodynamic activity of metallo 5-(4-(trimethylammonium)phenyl)-10, 15,20-tris(2,4,6-trimethoxyphenyl)porphyrin in homogeneous and biomimetic media. *Photochem. Photobiol. Sci.*, 7:963–972, **2008**.

[224] D. Lazzeri, M. Rovera, L. Pascual, E. Durantini. Photodynamic studies and photoinactivation of *Escherichia Coli* using *meso*-substituted cationic porphyrin derivatives with assymetric charge distribution. *Photochem. Photobiol.*, 80:286–293, **2004**.

[225] M. Kepczynski, R. Pandian, K. Smith, B. Ehrenberg. Do liposome-binding constants of porphyrins correlate with their measured and predicted partitionig between octanol and water? *Photochem. Photobiol.*, 76(2):127–134, **2002**.

[226] P.K. Frederiksen, S.P. McIlroy, C.B. Nielsen, L. Nikolajsen, E. Skovsen, M. Jorgensen, K.V. Mikkelsen, P.R. Ogilby. Two-photon photosensitized production of siglet oxygen in water. *J. Am. Chem. Soc.*, 127:255–269, **2005**.

[227] J. Arnbjerg, A. Jiménez-Banzo, M.J. Paterson, S. Nonell, J.I. Borrell, O. Christiansen, P.R. Ogilby. Two-photon absorption in tetraphenylporphycenes: Are porphycenes better candidates than

porphyrins for providing optimal optical properties for two-photon photodynamic therapy? *J. Am. Chem. Soc.*, 129(16):5188–5199, **2007**.

[228] A.M. Jiménez. *New Insights in Photodynamic Therapy: Production, Diffusion and Reactivity of Singlet Oxygen in Biological Systems.* Tesi doctoral, Institut Químic de Sarrià, URL, **2008**.

[229] T. Poulsen, P.K. Frederiksen, M. Jorgensen, K.V. Mikkelsen. Two-photon singlet oxygen sensitizers: Quantifying, modeling and optimizing the two-photon absorption cross section. *J. Phys. Chem. A*, 105:11488–11495, **2001**.

[230] J. Olsen, P. Jorgensen. Linear and nonlinear response function for an exact state and for an MCSCF state. *J. Chem. Phys.*, 82:3235, **1985**.

[231] DALTON. A molecular electronic structure program. *http://www.daltonprogram.org*, **2009**.

[232] A.S. Huss, T. Pappenfus, J. Bohnsack, M. Burand, K.R. Mann, D.A. Blank. The influence of internal charge transfer on nonradiative decay in substituted terthiophenes. *J. Phys. Chem. A*, 13(38):10202–10210, **2009**.

[233] J. Moan, K. Berg, E. Kwam, A. Western, Z. Malik, A. Rück, H. Schneckenburger. Intracellular localization of photosensitizers. *Ciba Found. Symp.*, 146:95–111, **1989**.

[234] A.A. Rosenkranz, D.A. Jans, A. Sobolev. Targeted intracellular delivery of photosensitizers to enhance photodynamic efficiency. *Immunol. Cell Biol.*, 78(4):452–464, **2000**.

[235] D. Kessel. Correlation between subcellular localization and photodynamic efficacy. *J. Porph. Phthaloc.*, 8:1009–1014, **2004**.

[236] J.W. Snyder, E. Skovsen, J. Lambert, P.R. Ogilby. Subcellular, time-resolved studies of singlet oxygen in single cells. *J. Am. Chem. Soc.*, 127(42):14558–14559, **2005**.

[237] D. Kessel, Y. Luo, Y. Deng, and C.K. Chang. The role of subcellular localization in initialization of apoptosis by photodynamic therapy. *Photochem. Photobiol.*, 65(3):422–426, **1997**.

[238] R.J.B. King. *Cancer Biology.* Ed. Longman, Essex, **1996**.

[239] T.J. Dougherty, C. Gomer, B.W. Henderson, G. Jori, D. Kessel, M. Korbelik, J. Moan, Q. Peng. Photodynamic therapy. *J. Natl. Cancer Inst.*, 90(12):889–905, **1998**.

[240] A. Ashkenazi, V.M. Dixit. Death receptors: Signaling and modulation. *Science*, 281(5381):1305–1308, **1998**.

[241] M.L. Argawal, M.E. Clay, E.J. Harvey, H.H. Evans. Photodynamic therapy induces rapid cell death by apoptosis in L5178Y mouse lymphoma cells. *Cancer Res.*, 51(21):5993–5996, **1991**.

[242] S.W. Lowe, E. Cepero, G. Evan. Intrinsic tumour suppression. *Nature*, 432(18):307–315, **2004**.

[243] C. Fumarola, G.G. Guindotti. Stress-induced apoptosis: Toward a symmetry with receptor-mediated cell death. *Apoptosis*, 9:77–82, **2004**.

[244] N.N. Danial, S.J. Korsmeyer. Cell death: Critical control points. *Cell*, 116(2):205–219, **2004**.

[245] M.A. Seyed, O. Malini. Bio-distribution and subcellular localization of hypericin and its role in PDT induced apoptosis in cancer cells. *Int. J. Oncol.*, 21:531–540, **2002**.

[246] D. Kessel, N.L. Oleinick. Initiation of autophagy by photodynamic therapy. *Methods Enzimol.*, 453:1–16, **2009**.

[247] P. Agostinis, K. Berg, K.A. Cengel, T.H. Foster, A.W. Girotti, S.O. Gollnick, S.M. Hahn, M.R. Hamblin, A. Juzeniene, D. Kessel, M. Korbelik, J. Moan, P. Mroz, D. Nowis, J. Piette, B.C. Wilson, J. Golab. Photodynamic therapy of cancer: An update. *CA Cancer J. Clin.*, 61:250–281, **2011**.

[248] E. Bergamini, G. Cavallini, A. Donati, Z. Gori. The role of autophagy in aging: Its essential part in the anti-aging mechanism of caloric restriction. *Ann. N. Y. Acad. Sci.*, 1114:69–78, **2007**.

[249] J.D. Rabinowitz, E. White. Autophagy and metabolism. *Science*, 330(6009):1344–1348, **2010**.

[250] R.R. Allison, C.H. Sibata, G.H. Downie, R.E. Cuenca. A clinical review of PDT for cutaneous malignancies. 3:214–226, **2006**.

[251] Michel Pagé, editor. *Tumor targeting in cancer therapy*. Cancer drug discovery and development. Humana Press, Totowa, New Jersey, 1a ed., **2002**.

[252] K. Berg, J. Moan. Lysosomes and microtubules as targets for photochemotherapy of cancer. *Photochem. Photobiol.*, 65(3):403–409, **1997**.

[253] A. Ertel, A. Verghese, S.W. Byers, M. Ochs, A. Tozeren. Pathways-specific differences between tumor cell lines and normal and tumor tissue cells. *Mol. Cancer*, 5(1):55, **2006**.

[254] N. Gueddari, N. Favre, H. Hachem, E. Marek, F. LeGaillard, G. Soula. Evidence for up-regulated low density lipoprotein receptor in human lung adenocarcinoma cell line. *Biochimie*, 75:811–819, **1993**.

[255] A.R. Hilgenbrink, P.S. Low. Folate receptors-mediated drug targeting: From therapeutics to diagnostics. *J. Pharm. Sci.*, 94(10):2135–2146, **2005**.

[256] G. Zheng, J. Chen, H. Li, J.D. Glickson. Rerouting lipoprotein nanoparticles to selected alternate receptors for the targeted delivery of cancer diagnostic and therapeutic agents. *Proc. Natl. Acad. Sci.*, 102(49):17757–17762, **2005**.

[257] K. Malinowsky, C. Wolff, S. Gündisch, D. Berg, K.F. Becker. Targeted therapies in cancer - challenges and chances offered by newly developed techniques for protein analysis in clinical tissues. *J. of Cancer*, 2:26–35, **2011**.

[258] A.M. Douglas, G.A. Goss, R.L. Sutherland, D.J. Hilton, M.C. Berndt, N.A. Nicola, C.G. Begley. Expression and function of members of the cytokine receptor superfamily on breast cancer cells. *Oncogene*, 14:661–669, **1997**.

[259] F. Balkwill. Cancer and the chemokine network. *Nat. Cancer Rev.*, 4:540–550, **2004**.

[260] I. Belostotsky, S.M. da Silva, M.G. Paez, G.L. Indig. Mitochondrial targeting for photochemotherapy. Can selective tumor cell killing be predicted based on n-octanol/water distribution coefficients? *Biotech. Histochem.*, 86(5):302-314, **2011**.

[261] J.S. Modica-Napolitano, J.R. Aprille. Delocalized lipophilic cations selectively target the mitochondria of carcinoma cells. *Adv. Drug Deliv. Rev.*, 49(1):63–70, **2001**.

[262] G.R. Martin, R.K. Jain. Non invasive measurement of interstitial pH profiles in normal and neoplastic tissue using fluorescence ratio imaging microscopy. *Cancer Res.*, 54:5670–5674, **1994**.

[263] N. Raghunand, X. He, R. vanSluis, B. Mahoney, B. Baggett, C.W. Taylor, G. Paine-Murrieta, D. Roe, Z.M. Bhujwalla, R.J. Gillies. Enhancement of chemotherapy by manipulation of tumour pH. *Br. J. Cancer*, 80(7):1005–1011, **1999**.

[264] R.A. Gatenby, R.J. Gillies. Why do cancers have high aerobic glycolysis? *Nat. Rev. Cancer*, 4:891–899, **2004**.

[265] J. Moan, K. Berg. Photochemotherapy of cancer: Experimental research. *Photochem. Photobiol.*, 55(6):931–948, **1992**.

[266] G. Jori. Photosensitized processes in vivo: Proposed phototherapeutic applications. *Photochem. Photobiol.*, 52(2):439–443, **1990**.

[267] A. Gabizon, D. Goren, A.T. Horowitz, D. Tzemach, A. Lossos, T. Siegal. Long-circulating liposomes for drug delivery in cancer therapy: a review of biodistribution studies in tumor-bearing animals. *Adv. Drug Deliv. Rev.*, 24(3):337–344, **1997**.

[268] C. Abels, R. Szeimies, P. Steinbach, C. Richert, A.E. Goetz. Targeting of the tumor microcirculation by photodynamic therapy with a synthetic porphycene. *J. Photochem. Photobiol. B*, 40(3):305–312, **1997**.

[269] B.A. Goff, U. Hermanto, J. Rumbaugh, J. Blake, M. Bamberg, T. Hasan. Photoimmunotherapy and biodistribution with an OC125-chlorin immunoconjugate in an in vivo murine ovarian cancer model. *Br. J. Cancer*, 70:474–480, **1994**.

[270] M. Governatore, M.R. Hamblin, E.E. Piccinini, G. Ugolini, T. Hasan. Targeted photodestruction of human colon cancer cells using charged 17.1A chlorin e6 immunoconjugates. *Br. J. Cancer*, 82(1):56–64, **2000**.

[271] G.A.M.S. van Dongen, G.W.M. Visser, M.B. Vrouenraets. Photosensitizer-antibody conjugates for detection and therapy of cancer. *Adv. Drug Deliv. Rev.*, 56:31–52, **2004**.

[272] W.P. Thorpe, M. Toner, R.M. Ezzell, R.G. Tompkins, M.L. Yarmush. Dynamics of photoinduced cell plasma membrane injury. *Biophys. J.*, 68:2198–2206, **1995**.

[273] M. Monsigny, A.C. Roche, P. Midoux, R. Mayer. Glycoconjugates as carriers for specific delivery of therapeutic drugs and genes. *Adv. Drug Deliv. Rev.*, 14(1):1–24, 1994.

[274] R.K. Jain. The next frontier of molecular medicine: Delivery of therapeutics. *Nature Medicine*, 4:655–657, **1998**.

[275] E. Reddi, C. Zhou, R. Biolo, E. Menegaldo, G. Jori. Liposome- or LDL-administered in (II)-phthalocyanine as a photodynamic agent for tumours. I. Pharmacokinetic properties and phototherapeutic efficiency. *Br. J. Cancer*, 61:407–411, **1990**.

[276] V. Omelyanenko, C. Gentry, P. Kopecková, J. Kopecek. HPMA copolymer-anticancer drug-OV-Tl16 antibody conjugates. II. processing in epithelial ovarian carcinoma cells in vitro. *Int. J. Cancer*, 75:600–608, **1998**.

[277] J. Morgan, H. Lottman, C.C. Abbou, D.K. Chopin. A comparison of direct and liposomal antibody conjugates of sulfonated aluminum phthalocyanines for selective photoimmunotherapy of human bladder carcinoma. *Photochem. Photobiol.*, 60:486–496, **1994**.

[278] L.C. Bergstrom, I. Vucenik, I.K. Hagen, S.A. Chernomorsky, R.D. Poretz. In-vitro photocytotoxicity of lysosomotropic immunoliposomes containing pheophorbide a with human bladder carcinoma cells. *J. Photochem. Photobiol. B*, 24:17–23, **1994**.

[279] G. Jori, L. Schindl, A. Schindl, L. Polo. Novel approaches towards a detailed control of the mechanism and efficiency of photosensitized processes in vivo. *J. Photochem. Photobiol. A.*, 102:101–107, **1996**.

[280] G. Jori, E. Reddi. The role of lipopropteins in the delivery of tumor-targeting photosensitizers. *Intl. J. Biochem.*, 25:1369–1375, **1993**.

[281] O. Bourdon, V. Mosqueira, P.H. Legrand, J. Blais. A comparative study of the cellular uptake, localization and phototoxicity of meta-tetra(hydroxyphenyl)chlorin encapsulated in surface-modified submicronic oil/water carriers in HT29 tumor cells. *J. Photochem. Photobiol. B*, 55:164–171, **2000**.

[282] A. Ruebner, Z. Yang, D. Leung, R. Breslow. A cyclodextrin dimer with a photocleavable linker as a possible carrier for the photosensitizer in photodynamic tumor therapy. *Proc. Natl. Acad. Sci.*, 96(26):14692–14693, **1999**.

[283] X. Zhang, K. Shedden, G. Rosania. A cell-based molecular transport simulator for pharmacokinetic prediction and chemoinformatic exploration. *Mol. Pharm.*, 3(6):704–716, **2006**.

[284] A.J. Versluis, P.J. Geel, H. Oppelaar, T.J. Berkel, M.K. Bijsterbosch. Receptor-mediated uptake of low-density lipoprotein by B16 melanoma cells in vitro and in vivo in mice. *Br. J. Cancer*, 74:525–532, **1996**.

[285] C.P. Brangwynne, G.H. Koenderink, F.C. MacKintosh, D.A. Weitz. Cytoplasmic diffusion: molecular motors mix it up. *J. Cell. Biol.*, 183(4):583–587, **2008**.

[286] L.B. Chen. Mithocondrial membrane potential in living cells. *Ann. Rev. Cell Biol.*, 4:155–181, **1988**.

[287] W. Becker, L.J. Kleinsmith, J. Hardin. *The World of the Cell.* Addison Wesley Longman Inc., 4 ed., **2000**.

[288] J.W. Winkelman, G.H. Collins. Neurotoxicity of tetraphenylporphinesulfonate $TPPS_4$ and its relation to photodynamic therapy. *Photochem. Photobiol.*, 46(5):801–807, **1987**.

[289] A. Juarranz, A. Villanueva, V. Díaz, M. Cañete. Photodynamic effects of the cationic porphyrin, mesotetra(4N-methylpyridyl)porphine, on microtubules of HeLa cells. *J. Photochem. Photobiol. B*, 27(1):47–53, **1995**.

[290] D.J. Ball, S. Mayhew, S.R. Wood, J. Griffiths, D.I. Vernon, S.B. Brown. A comparative study of the cellular uptake and photodynamic efficacy of three novel zinc phtalocyanines of differing charge. *Photochem. Photobiol.*, 69(3):390–396, **1999**.

[291] R.W. Boyle, D. Dolphin. Structure and biodistribution relationships of photodynamic sensitizers. *Photochem. Photobiol.*, 64(3):469–485, **1996**.

[292] A. Oseroff, D. Ohuoha, G. Ara, D. McAuliffe, J.W. Foley, L. Cincotta. Intramitochondrial dyes allow selective in vitro photolysis of carcinoma cells. *Proc. Natl. Acad. Sci.*, 83:9729–9733, **1986**.

[293] K. Woodburn, N.J. Vardaxis, J.S. Hill, A.H. Kaye, J.A. Reiss, D.R. Phillips. Evaluation of porphyrin characteristics required for photodynamic therapy. *Photochem. Photobiol.*, 55(5):697–704, **1992**.

[294] S.M. Sharkey, B.C. Wilson, R. Moorehead, G. Singh. Mitochondrial alterations in photodynamic therapy-resistant cells. *Cancer Res.*, 53(20):4994–4999, **1993**.

[295] Usuda,J.; Xue,L.Y.; Chiu,S.M.; Azizuddin,K.; Morris,R.L.; Mulvihill,J.; Oleinick,N.L. From molecular PDT damage to cellular PDT response: Attempts at bridging the gap on the role of Bcl-2 *Proc. SPIE*,4952 , **2003**.

[296] D.H. Lee, T. Park, H.W. Kim. Induction of apoptosis by disturbing mithocondrial-membrane potential and cleaving PARP in Jurkat T cells through treatment with acetoxyscirpenol mycotoxins. *Biol. Pharm. Bull.*, 29(4):648–654, **2006**.

[297] R.A. Smith, C. Porteous, A.M. Gane, M.P. Murphy. Delivery of bioactive molecules to mithocondria in vivo. *Proc. Natl. Acad. Sci.*, 100(9):5407–5412, **2003**.

[298] S.H.D. Lacerda, B. Abraham, T.C. Stringfellow, G. Indig. Photophysical, photochemical, and tumor-selectivity properties of bromine derivatives of rhodamine-123. *Photochem. Photobiol.*, 81:1430–1438, **2005**.

[299] C. Lin, R. Shulok, S.D. Kirley, L. Cincotta, J.W. Foley. Lysosomal localization and mechanism of uptake of nile blue photosensitizers in tumor cells. *Cancer Res.*, 51:2710–2719, **1991**.

[300] D. Kessel. Delivery of photosensitiz agents. *Adv. Drug Deliv. Rev.*, 56:7–8, **2004**.

[301] C.J. Gomer. Preclinical examination of first and second generation photosensitizers used in photodynamic therapy. *Photochem. Photobiol.*, 54(6):1093–1107, **1991**.

[302] D. Kessel, M. Conley, H. Vicente, and H. Antoni. Studies on the subcellular localization of the porphycene CPO. *Photochem. Photobiol.*, 81(3):569–572, **2005**.

[303] D. Kessel, R. Luguya, H. Vicente. Localization and photodynamic efficacy of two cationic porphyrins varying in charge distribution. *Photochem. Photobiol.*, 78(5):431–435, **2003**.

[304] Y. Huang, P. Mroz, T. Zhiyentayev, S.K. Sharma, T. Balasubramanian, C. Ruzié, M. Krayer, D. Fan, K.E. Borbas, E. Yang, H.L. Kee, C. Kirmaier, J.R. Diers, D.F. Bocian, D. Holten, J.S. Lindsay, M. Hamblin. In vitro photodynamic therapy and quantitative structure-activity relationship studies with stable synthetic near-infrared-absorbing bacteriochlorin photosensitizers. *J. Med. Chem.*, 53(10):4018–4027, **2010**.

[305] I.J. MacDonald, J. Morgan, D.A. Bellnier, G.M. Paszkiewicz, J.E. Whitaker, D.J. Litchfield, T.J. Dougherty. Subcellular localization patterns and their relationship to photodynamic activity of pyropheophorbide-a derivatives. *Photochem. Photobiol.*, 70(5):789–797, **1999**.

[306] F. Rashid, R.W. Horobin. Interaction of molecular probes with living cells and tissues. part 2. A structure-activity analysis of mitochondrial staining by cationic probes, and a discussion of the synergistic nature of image-based and biochemical approaches. *Histochemistry*, 94(3):303–308, **1990**.

[307] R. Szeimies, S. Karrer, C. Abels, P. Steinbach, S. Fickweiler, H. Messmann, W. Bäumler, M. Landthaler. 9-acetoxy-2,7,12,17-tetrakis-(β-methoxyethyl)-porphycene (ATMPn), a novel photosensitizer for photodynamic therapy: uptake kinetics and intracellular localization. *J. Photochem. Photobiol. B*, 34:67–72, **1996**.

[308] K. Berg, A. Western, J.C. Bommer, J. Moan. Intracellular localization of sulfonated meso-tetraphenylporphines in a human carcinoma cell line. *Photochem. Photobiol.*, 52:481–487, **1990**.

[309] B. Paquette, H. Ali, R. Langlois, J.E. Lier. Biological activities of phthalocyanines. VIII. Cellular distribution in V-79 chinese hamster cells and phototoxicityof selective sulfonated aluminum phthalocyanines. *Photochem. Photobiol.*, 47:215–220, **1988**.

[310] K. Berg, J.C. Bommer, J. Moan. Evaluation of sulfonated aluminium phthalocyanines for use in photochemotherapy. A stufy on the relative efficiencies of photoinactivation. *Photochem. Photobiol.*, 49:587–594, **1989**.

[311] X. Sun, W.N. Leung. Photodynamic therapy with pyropheophorbide-a methyl ester in human lung carcinoma cancer cell: Efficacy, localization and apoptosis. *Photochem. Photobiol.*, 75(6):644–651, **2002**.

[312] V.Y. Chen, S.M. Khersonsky, K. Shedden, Y.T. Chan, G. Rosania. System dynamics of subcellular transport. *Mol.Pharm.*, 1(6):414–425, **2004**.

[313] G.N. Georgiou, M.T. Ahmet, A. Houlton, J. Silver, R.J. Cherry. Measurement of the rate of uptake and subcellular localization of porphyrins in cells using fluorescence digital imaging microscopy. *Photochem. Photobiol.*, 59:419–422, **1994**.

[314] M. Duvvuri, S. Konkar, R.S. Funk, J.M. Krise, J.P. Krise. A chemical strategy to manipulate the intracellular localization of drugs in resistant cancer cells. 44:15743–15749, **2005**.

[315] M. Duvvuri, Y. Gong, D. Chatterji, J.P. Krise. Weak base permeability characteristics influence the intracellular sequestration site in the multidrug-resistant human leukemic cell line HL-60. *J. Biol. Chem.*, 279:32367–32372, **2004**.

[316] J. Roding, A. Naujok, H.W. Zimmermann. Effects of ethidium bromide, tetramethylethidium bromide and betaine B on the ultrastructure of HeLa cell mitochondria. *Histochemistry*, 85(3):215–222, **1986**.

[317] D. Kessel, K. Woodburn, B.W. Henderson, C.K. Chang. Sites of photodamage in vivo and in vitro by a cationic porphyrin. *Photochem. Photobiol.*, 62(5):875–881, **1995**.

[318] G. Rosania. Supertargeted chemistry: Identifying relationships between molecular structures and their sub-cellular distribution. *Curr. Top. Med. Chem.*, 3:659–685, **2003**.

[319] R.K. Pandey, F.Y. Shiau, A.B. Sumlin, T.J. Dougherty. Structure/activity relationships among photosensitizers related to pheophorbides and bacteriopheophorbides. *Bioorg. Med. Chem. Lett.*, 2:491–496, **1992**.

[320] H. Dummin, T. Cernay, H.W. Zimmermann. Selective photosensitization of mitochondria in HeLa cells by cationic Zn(II) phthalocyanines with lipophilic side-chains. *J. Photochem. Photobiol. B*, 37:219–229, **1997**.

[321] S. Hirohara, M. Obata, H. Alitomo, K. Sharyo, S. Ogata, C. Ohtsuki, S. Yano, T. Ando, M. Tanihara. Structure-photodynamic effect relationships of 24 glycoconjugated photosensitizers in HeLa cells. *Biol. Pharm. Bull.*, 31(12):2265–2272, **2008**.

[322] Y. Cai, L. Lu, L. Chen, J. He. Predicting subcellular location of proteins using integrated-algorithm method. *Mol. Divers.*, 14(3):551–558, **2010**.

[323] Z. Szafron, R. Greiner, P. Lu, D. Wishart, B. Poulin, J. Anvik, C. Macdonell, R. Eisner. Predicting subcellular localization of proteins using machine-learned classifiers. *Bioinformatics*, 20(4):547–556, **2004**.

[324] A. Garg, M. Bhasin, G.P.S. Raghava. Support vector machine-based method for subcellular localization of human proteins using amino acid compositions, their order, and similarity search. *J. Biol. Chem.*, 280(15):14427–14432, **2005**.

[325] J. Guo, Y. Lin. TSSub: eukaryotic protein subcellular localization by extracting features from profiles. *Bioinformatics*, 22(14):1784–1785, **2006**.

[326] S. Trapp, R.W. Horobin. A predictive model for the selective accumulation of chemicals in tumor cells. *Eur. Biophys. J.*, 34:959–966, **2005**.

[327] F. Rashid, R.W. Horobin, M.A. Williams. Predicting the behaviour and selectivity of fluorescent probes for lysosomes and related structures by means of structure-activity models. *Histochem. J.*, 23:450–459, **1991**.

[328] R.W. Horobin, J.C. Stockert, F. Rashid-Doubell. Fluorescent cationic probes for nuclei of living cells: why are they selective? A quantitative structure-activity relations analysis. *Histochem. Cell Biol.*, 126:165–175, **2006**.

[329] J.J. Sutherland, L.A. O'Brien, D.F. Weaver. A comparison of methods for modeling quantitative structure-activity relationships. *J. Med. Chem.*, 47:5541–5554, **2004**.

[330] D. Kessel, K. Woodburn, C. Gomer, N. Jagerovic, K.M. Smith. Photosensitization with derivatives of chlorin p6. *J. Photochem. Photobiol. B*, 28:13–18, **1995**.

[331] J. Cristóbal, J.C. Stockert, A. Villanueva, S. Rello-Varona, A. Juarranz, M. Cañete. Caspase-2: A possible trigger of apoptosis induced in A-549 tumor cells by znpc photodynamic treatment. *Int. J. Oncol.*, 28:1057–1063, **2006**.

[332] GmbH Rapid-I. Rapidminer 5.1, 2009.

[333] I. Aizenberg. Multilayer feedforward neural network based on multi-valued neurons (MLMVN) and back-propagation learning algorithm. *Soft. Comput.*, 11:169–183, **2007**.

[334] I. Guyon, A. Elisseeff. An introduction to variable and feature selection. *J. Machine Learning Research*, 3:1157–1182, **2003**.

[335] J.R.M. Smits, L.W. Breedveld, M.W.J. Derksen, G. Kateman. Pattern classification with artificial neural networks: classification of algae, based upon flow cytometer data. *Anal. Chim. Acta*, 258:11–25, **1992**.

[336] J. Gasteiger, M. Marsili. Iterative partial equalization of orbital electronegativity - a rapid access to atomic charges. *Tetrahedron*, 36:3219–3228, **1980**.

[337] R.S. Pearlman, K.M. Smith. Novel software tools for chemical diversity. *Perspect. Drug Discov. Des.*, 9/10/11:339–353, **1998**.

[338] S. Baláz. Lipophilicity in trans-bilayer transport and subcellular pharmacokinetics. *Perspect. Drug Discov. Des.*, 19:157–177, **2000**.

[339] G. Siboni, H. Weitman, D. Freeman, Y. Mazur, Z. Malik, B. Ehrenberg. The correlation between hydrophilicity of hypericins and helianthrone: internalazation mechanisms, subcellular distribution and photodynamic action in colon carcinoma cells. *Photochem. Photobiol. Sci.*, 1:483–491, **2002**.

[340] I.V. Tetko, J. Gasteiger, R. Todeschini, A. Mauri, D. Livingstone, P. Ertl, V.A. Palyulin, E.V. Radchenko, N.S. Zefirov, A.S. Makarenko, V.Y. Tanchuk, V.V. Prokopenko. Virtual computational chemistry laboratory - design and description. *J. Comput. Aid. Mol. Des.*, 19:453–463, **2005**.

[341] R. Mannhold, editor. *Molecular Drug Properties in Methods and Principles in Medicial Chemistry Series.* Wiley, **2007**.

[342] N.K. Mak, T.W. Kok, R.N.S. Wong, S.W. Lam, Y.K. Lau, W.N. Leung, N.H. Cheung, D.P. Huang, L.L. Yeung, C.K. Chang. Photoynamic activities of sulfonamide derivatives of porphycene on nasopharyngeal carcinoma cells. *J. Biomed. Sci.*, 10:418–429, **2003**.

[343] D. Kessel, Y. Luo. Photodynamic therapy: a mitochondrial inducer of apoptosis. *Cell Death Differ.*, 6:28–35, **1999**.

[344] D. Kessel, M. Castelli, J.J. Reiners. Ruthenium red-mediated suppression of Bcl-2 loss and Ca^{2+} release initiated by photodamage to the endoplasmatic reticulum: scavenging of reactive oxygen species. *Cell Death Differ.*, 12(5):502–511, **2005**.

[345] K. Scherer, C. Abels, W. Bäumler, G. Ackermann, R. Szeimies. Structure-activity relationships of three differently substituted 2,7,12,17-tetrakis-(β-metrhoxyethyl)porphycene derivatives in vitro. *Arch. Dermatol. Res.*, 295(12):535–541, **2004**.

[346] D. Kessel, Y. Luo, P. Mathieu, J.J. Reiners. Determinants of the apoptotic response to lysosomal photodamage. *Photochem. Photobiol.*, 71(2):196–200, **2000**.

[347] S. Fickweiler, C. Abels, S. Karrer, W. Baumler, M. Landthaler, F. Hofstadter, R.M. Szeimies. Photosensitization of human skin cell lines by AMPn in vitro: mechanism of action. *J. Photochem. Photobiol. B*, 48:27–35, **1999**.

[348] M. Cañete, M. Lapeña, A. Juarranz, V. Vendrell, J.I. Borrell, J. Teixidó, S. Nonell, A. Villanueva. Uptake of tetraphenylporphycene and its photoeffects on actin and cytokeratin elements of HeLa cells. *Anticancer Drug Des.*, 12:543–554, **1997**.

[349] A. Villanueva, M. Cañete, S. Nonell, J.I Borrell, J. Teixidó, A. Juarranz. Photodamaging effects of tetraphenylporphycene in a human carcinoma cell line. *Anticancer Drug Des.*, 11:89–99, **1996**.

[350] D. Kessel, Y. Luo. Mithocondrial photodamage and PDT-induced apoptosis. *J. Photochem. Photobiol. B*, 42:89–95, **1998**.

[351] J.R. Shulok, M.H. Wade, and C.W. Lin. Subcellular localization of hematoporphyrin derivative in bladder tumor cells in culture. *Photochem. Photobiol.*, 51:451–457, **1990**.

[352] J.M. Gaullier, A. Gèze, R. Santus, T. Melo, J.C. Mazière, M. Bazin, R. Morlière, L. Dubertret. Subcellular localization and photosensitization by protoporphyrin IX in human keratinocytes and fibroblasts cultivated with 5-aminolevulinic acid. *Photochem. Photobiol.*, 62:114–122, **1995**.

[353] Z. Malik, M. Dishi, Y. Garini. Fourier transform multipixel spectroscopy and spectral imaging of protoporphyrin in single melanoma cells. *Photochem. Photobiol.*, 63:608–614, **1996**.

[354] B. Li, E.H. Moriyamal, F. Li, M.T. Jarvil, C. Allen, B.C. Wilson. Diblock copolymer micelles deliver hydrophobic proptoporphyrin IX for photodynamic therapy. *Photochem. Photobiol.*, 83:1505–1512, **2007**.

[355] J.S. Hill, S.B. Kahl, A.H. Kaye. Selective tumor uptake of a boronated porphyrin in an animal model of cerebral glioma. *Proc. Natl. Acad. Sci.*, 89:1785–1789, **1992**.

[356] T. Cernay, H.W. Zimmermann. Selective photosensitization of mitochondria by the lipophilic cationic porphyrin POR10. *J. Photochem. Photobiol. B*, 34:191–196, **1996**.

[357] I.A. Patito, C. Rothmann, Z. Malik. Nuclear transport of photosensitizers during photosensitization and oxidative stress. *Biol.Cell.*, 93:285–291, **2001**.

[358] A. Villanueva, J.C. Stockert, M. Cañete, P. Acedo. A new protocol in photodynamic therapy: enhanced tumour cell death by combining two different photosensitizers. *Photochem. Photobiol. Sci.*, pages 295–297, **2010**.

[359] A. Villanueva, A. Juarranz, V. Díaz, J. Gómez, M. Cañete. Photodynamic effects of a cationic *meso*-substituted porphyrin in cell cultures. *Anticancer Drug Des.*, 7:297–303, **1992**.

[360] M. Gèze, P. Morlière, J.C. Mazière, K.M. Smith, J. Santus. Lysosomes, a key target of hydrophobic photosensitizers proposed for photochemotherapeutic applications. *J. Photochem. Photobiol. B*, 20(1):23–35, **1993**.

[361] A.J. Ward, E.K. Matthews. Cytotoxic, nuclear, and growth inhibitory effects of photodynamic drugs on pancreatic carcinoma cells. *Cancer Lett.*, 102:39–47, **1996**.

[362] P. Morliere, M. Momenteau, C. Candide, V. Simonin, J. Santus, J.C. Maziere. Synthesis, cellular uptake of, and cell photosensitization by a porphyrin bearing a quinoline group. *J. Photochem. Photobiol. B*, 5:49–67, **1990**.

[363] D.S. Lawrence, S.L. Gibson, M.L. Nguyen, K.R. Whittemore, D.G. Whitten, R. Hilf. Photosensitization and tissue distribution studies of the picket fence porphyrin, 3,1-TPRO, a candidate for photodynamic therapy. *Photochem. Photobiol.*, 61:90–98, **1995**.

[364] Y. Luo, C.K. Chang, D. Kessel. Rapid initiation of apoptosis by photodynamic therapy. *Photochem. Photobiol.*, 63(4):528–534, **1996**.

[365] D. Kessel. Relocalization of cationic porphyrins during photodynamic therapy. *Photochem. Photobiol. Sci.*, 1:837–840, **2002**.

[366] B.B. Noodt, T. Stokke, K. Berg, J.M. Nesland. Different apoptotic parthways are induced from various intracellular sites by tetraphenylporphyrins and light. *Br.J.Cancer*, 79(1):72–81, **1999**.

[367] Z. Malik, I. Amit, C. Rothmann. Subcellular localization of sulfonated tetraphenyl porphines in colon carcinoma cells by spectrally resolved imaging. *Photochem. Photobiol.*, 65:389–396, **1997**.

[368] K. Woodburn, Q. Fan, D.R. Miles, D. Kessel, Y. Luo, S.W. Young. Localization and efficacy analysis of the therapeutic Lutetium texaphyrin (PCI-0123) in the murine EMT6 sarcoma model. *Photochem. Photobiol.*, 65:410–415, **1997**.

[369] A. Ambroz, A. MacRobert, J. Morgan, G. Rumbles, M.J. Foley, D.R. Phillips. Time-resolved fluorescence spectroscopy and intracellular imaging of disulphonated aluminium phtalocyanine. *J. Photochem. Photobiol. B*, 22:105–117, **1994**.

[370] A. Rück, G. Beck, R. Bachor, N. Akgün, M.H. Gschwend, R. Steiner. Dynamic fluorescence changes during photodynamic therapy in vivo and in vitro of hydrophilic Al(III) phthalocyanine tetrasulphonate and lipophilic Zn(II) phthalocyanine administered in liposomes. *J. Photochem. Photobiol. B*, 36:127–133, **1996**.

[371] J. Moan, K. Berg, J.C. Bommer, A. Western. Action spectra of phtalocyanines with respect to photosensitization of cells. *Photochem. Photobiol.*, 56:171–175, **1992**.

[372] C. Fabris, G. Valduga, G. Miotto, L. Borsetto, G. Jori, S. Garbisa, E. Reddi. Photosensitization with Zinc (II) phthalocyanine as a switch in the decision berween apoptosis and necrosis. *Cancer Res.*, 61:7495–7500, **2001**.

[373] S. Galaz, J. Espada, J.C. Stockert, M. Pacheco, F. Sanz-Rodríguez, R. Arranz, S. Rello, M. Cañete, A. Villanueva, M. Esteller, A. Juarranz. Loss of E-cadherin mediated cell–cell adhesion as an early trigger of apoptosis induced by photodynamic treatment. *J. Cell. Physiol.*, 205:86–96, **2005**.

[374] J. Soriano, J.C. Stockert, A. Villanueva, M. Cañete. Cell uptake of Zn(II)-phthalocyanine-containing liposomes by clathrin-mediated endocytosis. *Histochem. Cell. Biol.*, 133:449–454, **2010**.

[375] S. Rello-Varona, J.C. Stockert, M. Cañete, P. Acedo, A. Villanueva. Mitotic catastrophe induced in hela cells by photodynamic treatment with Zn(II)-phthalocyanine. *Int. J. Oncol.*, 32:1189–1196, **2008**.

[376] A. Villanueva, E.N. Durantini, J.C. Stockert, S. Rello, R. Vidania, M. Cañete, A. Juarranz, R. Arranz, V. Rivarola. Photokilling of cultured tumour cells by the porphyrin derivative CF3. *Anticancer Drug Des.*, 16:279–290, **2001**.

[377] N.S. Trivedi, H.W. Wang, A. Nieminen, N.L. Oleinick, J.A. Izatt. Quantitative analysis of pc 4 localization in mouse lymphoma (LY-R) cells via double-label confocal fluorescence microscopy. *Photochem. Photobiol.*, 71(5):634–639, **2000**.

[378] R.L. Morris, M.E. Varnes, M.E. Kenney, Y.S Li, K. Azizuddin, M.W. McEnery, N.L. Oleinick. The peripheral benzodiazepine receptor in photodynamic therapy with the phthalocyanine photosensitizer Pc4. *Photochem. Photobiol.*, 75(6):652–661, **2002**.

[379] M. Lam, N.L. Oleinick, A. Nieminen. Photodynamic therapy-induced apoptosis in epidermoid carcinoma cells. *J. Biol. Chem.*, 276(50):47379–47386, **2001**.

[380] S.R. Wood, J.A. Holroyd, S.B. Brown. The subcellular localization of Zn(II) phthalocyanines and their redistribution on exposure to light. *Photochem. Photobiol.*, 65:397–402, 1997**.**

[381] N. Cauchon, H. Tian, R. Langlois, C. LaMadeleine, S. Martin, H. Ali, D. Hunting, J.E. vanLier. Structure-photodynamic activity relationships of substituted zinc trisulfophtalocyanines. *Bioconjugate Chem.*, 16:80–89, **2005**.

[382] D. Kessel,A. Morgan. Photosensitization with etiobenzochlorins and octaethylbenzochlorins. *Photochem. Photobiol.*, 58(4):521–526, **1993**.

[383] W.G. Roberts, M.W. Berns. Cellular uptake and subcellular localization of mono-l-aspartyl chlorin e6, chloro-aluminium sulfonated phthalocyanine, and photofrin II. *Laser Surg. Med.*, 9:90–101, **1989**.

[384] G.P. Gurinovich, T.E. Zorina, S.B. Melnov, N.I. Melnova, I.F. Gurinovich, L.A. Gruvina, M.V. Sarzhevskaya, S.N. Cherenkevich. Photodynamic activity of chlorin e6 and chlorin e6 ethylenediamine in vitro and in vivo. *J. Photochem. Photobiol. B*, 13:51–57, **1992**.

[385] D. Kessel, M. Castelli. Evidence that Bcl-2 is the target of three photosensitizers that induce a rapid apoptotic response. *Photochem. Photobiol.*, 74:318–322, **2001**.

[386] C.M. Yow, J.Y. Chen, N.K. Mak, N.H. Cheung, W.N. Leung. Cellular uptake, subcellular localization and photodamaging effect of temoporfin (mTHPC) in nasopharyngeal carcinoma cells: comparison with hematoporphyrin derivative. *Cancer Lett.*, 157:123–131, **2000**.

[387] V.O. Melnikova, L.N. Bezdetnaya, C. Bour. Subcellular localization of meta-tetra(hydroxyhenyl)chlorin in human tumor cells subjected to photodynamic treatment. *J. Photochem. Photobiol. B*, 49:96–103, **1999**.

[388] J. Chen, N.K. Mak, C.M. Yow, M.C. Fung, L.C. Chiu, W.N. Leung, N.H. Cheung. The binding characteristics and intracellular localization of temoporfin (mTHPC) in myeloid leukemia cells: phototoxicity and mitochondrial damage. *Photochem. Photobiol.*, 72:541–547, **2000**.

[389] W.N. Leung, X. Sun, N.K. Mak, C.M. Yow. Photodynamic effects of the mTHPC on human colon adenocarcinoma cells: Photocytotoxicity, subcellular localization and apoptosis. *Photochem. Photobiol.*, 75(4):406–411, **2002**.

[390] S. Marchal, A. François, D. Dumas, F. Guillemin, L. Bezdetnaya. Relationship between subcellular localisation of Foscan(R) and caspase activation in hotosensitised MCF-7 cells. *Br. J. Cancer*, online publication(27):1–8, **2007**.

[391] R. Bachor, CR Shea, R. Gillies, T. Hasan. Photosensitized destruction of human bladder carcinoma cells treated with chlorin e6-conjugated microspheres. *Proc. Natl. Acad. Sci.*, 88:1580–1584, **1991**.

[392] M.W. Leach, R.J. Higgins, S. Autry, J. Boggan, S.J. Lee, and K.M. Smith. R. Bachor, CR Shea, R. Gillies, T. Hasan. In vitro photodynamic effects of lysyl chlorin p6: Cell survival, localization and ultrastructural changes. *Photochem. Photobiol.*, 58:653–660, **1993**.